The Role of Chiral Symmetry in Extrapolations of Lattice QCD Results to the Physical Regime

E. J. Hackett-Jones

Supervisors: Dr. D. B. Leinweber and Prof. A. W. Thomas

Department of Physics and Mathematical Physics
and Special Research Centre for the Subatomic Structure of Matter,
University of Adelaide, Australia 5005

Thesis submitted for the degree of Master of Science

Date Submitted: 10 September, 2001

Contents

Abstract

In this thesis we explore new methods of extrapolating lattice QCD results to the physical regime. In particular, we extrapolate lattice results for octet baryon magnetic moments and electric charge radii as a function of the pion mass, m_π. The results are compared with experiment at the physical pion mass. The extrapolation procedures developed here are guided by the predictions of a successful phenomenological model for baryons – the Cloudy Bag Model (CBM). It has been found that the predictions of the CBM for nucleon magnetic moments may be encapsulated by a simple extrapolation formula – the Padé approximant. This approximant enables us to build in the correct asymptotic behaviour of the nucleon magnetic moments in both the chiral and heavy quark limits. Here we extend the formalism to extrapolate lattice results for magnetic moments of the entire baryon octet. Successful predictions are obtained for the nucleon and Σ baryon magnetic moments. Motivated by this success we develop similar procedures to extrapolate lattice calculations of octet baryon charge radii. These extrapolation formulae include the leading non-analytic logarithmic terms predicted by chiral perturbation theory and respect the constraints of heavy quark effective theory. Good agreement with experiment is obtained for the predicted nucleon and Σ^- charge radii. Predictions for the remaining octet baryon charge radii are made in anticipation of future experimental measurements.

This work contains no material which has been accepted for the award of any other degree or diploma in any university or other tertiary institution and, to the best of my knowledge and belief, contains no material previously published or written by another person, except where due reference has been made in the text.

I consent to this copy of my thesis, when deposited in the University Library, being available for loan and photocopying.

Emily Hackett-Jones

$\frac{c\,(A)}{m^2}$

Acknowledgements

I would like to thank my supervisors, Dr. D. B. Leinweber and Prof. A. W. Thomas, for the considerable time and effort they have invested in this project. I am also very grateful for the helpful comments they have made on this thesis. This project has been a very rewarding experience for me, and I thank them very much for making this opportunity available.

I am also most grateful for the financial assistance provided by the Special Research Centre for the Subatomic Structure of Matter. The Department of Physics and Mathematical Physics has also been most accommodating in allowing me to enrol in the M.Sc. degree.

Finally I would like to thank Mark, my parents, and particularly my sister, Mary, who have all been very helpful, and also insisted in being included in the acknowledgements!

Chapter 1

Introduction

The currently accepted model of the strong interactions is the theory of Quantum Chromodynamics (QCD). This theory was originally formulated in the 1960s and 70s. It began with the proposal of Gell-Mann [1] and Zweig [2] that hadrons consisted of elementary particles known as "quarks". This idea was based on the realization that all low-mass hadrons could be classified into low dimensional representations of SU(3) which suggested that hadrons consisted of more elementary constituents – the quarks – belonging to the fundamental representation of SU(3). The three types (or "flavours") of quarks were named "up" (u), "down" (d) and "strange" (s), with each quark possessing spin $\frac{1}{2}$ and fractional charge: $+\frac{2}{3}$ for u and $-\frac{1}{3}$ for d and s (all charges are in units of $e = |e|$). In terms of quarks, baryons could be constructed as quark triplets (qqq), while mesons consisted of quark anti-quark pairs ($q\bar{q}$). Since the 1960s more hadrons have been observed, necessitating the introduction of 3 more quark flavours: "charm" (c) and "top" (t) with charge $+\frac{2}{3}$, and "bottom" (b) with charge $-\frac{1}{3}$.

Soon after the introduction of the quark model, it was realized that there were observed hadrons whose naive quark model description violated Fermi-Dirac statistics. For example, the quark model description of the spin-$\frac{3}{2}$ baryon, Δ^{++}, is a bound state of 3 u quarks, with their spins parallel, in the $l = 0$ angular momentum state. This description of the Δ^{++} clearly violates Fermi-Dirac statistics, since the 3 quarks are in identical states. To rectify this problem an additional quantum number, known as "colour", was introduced. By allowing the quarks to carry this quantum number the anti-symmetry of the Δ^{++} wavefunction could be produced via anti-symmetry in the colour part of the wavefunction. Thus it was postulated that quarks came in 3 different colours (red, green and blue). More technically, quarks belong to the fundamental representation of $SU(3)_{\text{colour}}$. The introduction of colour was sufficient to overcome the major problems with the quark model and it soon became widely accepted by the physics community.

With the quark model well established, interest soon turned to describing the dynamics of quarks. Given the success of the Abelian gauge theory of Quantum Electrodynamics (QED), it was postulated that a gauge principle could also be used to formulate a field theory for the quarks to describe the strong interactions. This resulted in the birth of Quantum Chromodynamics (QCD) – a non-Abelian gauge theory with gauge symmetry group $SU(3)_{\text{colour}}$ [3, 4]. The theory of QCD is described by a Lagrangian (see Eq. (1.1) below) which is constructed to be invariant under local $SU(3)_{\text{colour}}$ transformations. The gauge bosons of QCD, which mediate all strong interactions, are known as "gluons". In analogy to the gauge bosons of QED, the photons, which mediate all electromagnetic interactions and couple to electrically charged particles, gluons couple to fermions and bosons which carry a "colour charge". Like photons, gluons are massless and have spin 1. However unlike photons, which couple to electric charge but are electrically neutral, gluons carry a colour charge themselves. This means that gluons interact with each other and undergo self-interactions. Gluons belong to the adjoint representation of $SU(3)_{\text{colour}}$ and are represented in the QCD Lagrangian by the fields A^a_μ, where $a = 1, \ldots 8$.

The fact that QCD is a non-Abelian gauge theory leads to several fundamental differences between QCD and the Abelian gauge theory of QED. Firstly, it has been observed experimentally that strong interactions become weaker at short distances – a phenomenon known as "asymptotic freedom". This is in total contrast to QED, where the electromagnetic interactions grow stronger at short distances. Historically it was the experimental evidence for asymptotic freedom which suggested that the theory of the strong interactions was non-Abelian, since it had earlier been shown that non-Abelian gauge theories in 4 dimensions exhibit asymptotic freedom, while Abelian theories do not. Asymptotic freedom allows perturbation theory to be used at short distances (e.g. in high momentum transfer reactions). Perturbative calculations for decay rates, cross sections and other observables in high momentum transfer reactions have been very successful (e.g. Refs. [5, 6]). This success is a good indication that QCD is the correct theory of the strong interactions.

The second major difference between QCD and QED is that in QCD the interaction does not become weaker at large distances. This phenomenon is thought to produce the observed colour confinement. It has been found experimentally that all observed particles are colour singlets, or "colourless". This is thought to be a fundamental property of QCD. If this is the case, then it is easy to explain why free quarks are not observed in nature since quarks carry a colour quantum number, and hence must be confined to colour singlet objects, such as baryons and mesons. Despite the fact that free quarks have never been observed, there is very strong evidence to support their existence.

The Lagrangian density of QCD has a particularly simple form. It is given by

$$\mathcal{L} = -\frac{1}{4} F_a^{\mu\nu} F^a_{\mu\nu} + \bar{q}(i\not{D} - \mathbf{m})q \ , \tag{1.1}$$

where the quark covariant derivative is given by

$$i\not{D}\, q = i\gamma^\mu D_\mu q = \gamma^\mu \left(i\,\partial_\mu - g A^a_\mu \frac{\lambda^a}{2} \right) q \ , \tag{1.2}$$

A^a_μ are the gluon fields and λ^a are the 8 Gell-Mann matrices (given explicitly in Ref. [7]). We use the same conventions as Ref. [7] for the γ matrices. The quark mass matrix, $\mathbf{m}$, is given by $\mathbf{m} = \mathrm{diag}(m_u, m_d, \ldots)$, where m_q is the mass of quark q. The gluon field strength tensor is given in components by

$$F^a_{\mu\nu} = \partial_\mu A^a_\nu - \partial_\nu A^a_\mu - g\, f^{abc} A^b_\mu A^c_\nu \ , \tag{1.3}$$

where g is the SU(3) gauge coupling parameter and f^{abc} are the structure constants of SU(3). In principle, one could extract all the properties of strongly interacting particles from the QCD Lagrangian, Eq. (1.1). However, in practice this is very difficult to do in the low energy sector. In the low energy sector, the observed participants in strong interactions are hadrons. Since the QCD Lagrangian is formulated in terms of the more fundamental quarks and gluons, and the mechanism of confinement is not fully understood, it is very difficult to make predictions about hadronic observables from the QCD Lagrangian. In fact, so far it has been impossible to extract non-perturbative information about hadronic observables from first principle, analytic studies of the QCD Lagrangian. As a result, numerical methods must be used to calculate properties of hadronic observables.

The most successful method of extracting the properties of hadrons from the theory of QCD is via the numerical method of lattice QCD. In lattice QCD the 4-D space-time continuum is discretized, and QCD is formulated on the space-time grid. Each quark field in the QCD Lagrangian is specified at every grid-point on the lattice, while the gluon fields are defined on the links between grid-points. The Feynman path integral approach is used to calculate physical

observables. For example, the expectation value of an observable $\mathcal{O}$ (where $\mathcal{O}$ is any combination of operators, expressed as a time-ordered product of quark and gluon fields) is given by

$$\langle \mathcal{O} \rangle = \frac{1}{Z} \int \mathcal{D}A_\mu \mathcal{D}\psi \mathcal{D}\bar{\psi}\ \mathcal{O}\, e^{iS[A_\mu,\psi,\bar{\psi}]} \ , \tag{1.4}$$

where the integral extends over all possible field configurations of ψ, $\bar{\psi}$ and A_μ. The quantity $S[A_\mu, \psi, \bar{\psi}]$ is the QCD action, given by

$$S[A_\mu, \psi, \bar{\psi}] = \int d^4x \left(-\frac{1}{4} F_{\mu\nu} F^{\mu\nu} + \bar{\psi} M \psi \right) = S_G + S_F \ , \tag{1.5}$$

where $M = \not{D} - \mathbf{m}$ is the Dirac operator and S_G and S_F are the gauge field and fermion actions respectively. The partition function, Z, which appears in the expectation value, Eq. (1.4), is given explicitly by

$$Z \equiv \int \mathcal{D}A_\mu \mathcal{D}\psi \mathcal{D}\bar{\psi}\ e^{iS} \ . \tag{1.6}$$

To evaluate the expectation value $\langle \mathcal{O} \rangle$ numerically, an analytic continuation to imaginary time is performed, i.e., $t \to -i\tau$. Then $\langle \mathcal{O} \rangle$ becomes

$$\langle \mathcal{O} \rangle = \frac{\int \mathcal{D}A_\mu \mathcal{D}\psi \mathcal{D}\bar{\psi}\ \mathcal{O}\, e^{-S_E}}{\int \mathcal{D}A_\mu \mathcal{D}\psi \mathcal{D}\bar{\psi}\ e^{-S_E}} \ , \tag{1.7}$$

where S_E is the Euclidean action. To evaluate such an expression on the lattice, the integral must be discretized and the action expressed in terms of quantities defined on the lattice. The expression for $\langle \mathcal{O} \rangle$, given in Eq. (1.7), closely resembles a correlation function in statistical mechanics. Hence computational methods founded in statistical mechanics can be used to numerically simulate the path integrals.

In Euclidean space-time, the fermionic part of the partition function can be integrated out, to obtain

$$Z = \int \mathcal{D}A_\mu \det M\, e^{-F_{\mu\nu}F^{\mu\nu}/4} \ . \tag{1.8}$$

In this form the entire fermionic contribution to the partition function is contained in the determinant, $\det M$. Setting $\det M$ to be constant is known as the *quenched approximation*. It is equivalent to removing vacuum polarization effects from the QCD vacuum. The lattice results that we consider in this thesis are all obtained from quenched lattice QCD simulations. At this point, full QCD simulations which include vacuum polarization effects (i.e. $\det M \neq$ const) are in their infancy. Results for electromagnetic form factors are not yet available.

In the standard model there are several parameters which are not specified by the theory itself, but must be determined from experiment. (It has been postulated that these parameters are specified by a more fundamental theory, but this underlying theory has not yet been discovered.) For QCD these parameters are the strong coupling constant, g, and the bare quark masses. In any lattice simulation of QCD these independent parameters become input parameters of the simulation. Clearly for the lattice results to match experimental measurements, the input parameters must be fixed to their experimental values. However, they can also be explored within the lattice simulation to establish the dependence of the physical observable on the input parameters. Of particular interest in this thesis is establishing the dependence of hadronic observables on the input quark mass. The reason for this is as follows. Computational limitations force lattice simulations of hadronic observables to be performed at quark masses much larger than their physical values. This means that results from lattice simulations cannot be directly compared with experimental measurements, but must be extrapolated to the physical regime. Although improvements in actions, algorithms and computer speed will allow lattice calculations

to be performed much closer to the physical regime, these improvements will proceed over many years. In the meantime it is imperative to understand how to extrapolate lattice results from the large quark masses where they are obtained to the physical regime.

In early lattice calculations the problem of extrapolating lattice results to the physical regime was not given a high priority. In exploratory calculations, lattice results were usually extrapolated as simple linear functions of the squared pion mass, m_π^2. With the advent of chiral perturbation theory, it was discovered that hadronic observables, such as electric charge radii and magnetic moments, exhibit certain non-analytic behaviour in the quark mass, m_q, near the chiral limit. As we will see, this non-analytic behaviour can give rise to dramatic deviations from the predictions of simple linear fits. The non-analytic behaviour in chiral expansions originates from Goldstone boson loops, as we now explain.

The QCD Lagrangian exhibits (approximate) invariance under chiral transformations. However, this symmetry of the theory is not realized in the conventional manner. In particular, chiral symmetry is dynamically broken, resulting in the formation of an octet of very light particles known as (pseudo-) Goldstone bosons. This octet of Goldstone bosons corresponds to the ground state pseudo-scalar meson octet, which contains the pions, kaons and η_8 meson. Since Goldstone bosons are very light compared to other hadrons in the spectrum, at low energies (≤ 1 GeV) these particles are the most important dynamical degrees of freedom in strong interactions. Goldstone boson loops are responsible for the non-analytic behaviour of hadronic observables. As we will discuss in Chapter 2, an effective field theory – Chiral Perturbation Theory – can be formulated to describe the system of light Goldstone bosons and the other (heavier) hadrons with which they interact. Chiral perturbation theory can be used to predict the behaviour of hadronic observables near the chiral limit. For example, the chiral expansion of the nucleon magnetic moment is given as follows

$$\mu_N = c_0 + c_1 m_\pi + c_2 m_\pi^2 \log(m_\pi^2) + c_3 m_\pi^2 + \dots \ , \tag{1.9}$$

where c_1 and c_2 are fully determined by chiral perturbation theory, whilst c_0 and c_3 must be determined phenomenologically. The leading non-analytic behaviour of μ_N is contained in the $c_1 m_\pi$ term, since $m_\pi \propto \sqrt{m_q}$ in the chiral limit. Since the coefficient c_1 is quite large ($c_1 = \mp 4.41\ \mu_N GeV^{-1}$ for $N = p/n$ respectively), this non-analytic behaviour is significant near the physical pion mass and must be taken into account in *any* extrapolation to the physical regime [8] – [16].

Since chiral perturbation theory gives expansions of hadronic observables as a function of m_π, it would be tempting to use these expansions directly to extrapolate lattice QCD results for the observable. However, since the radius of convergence of chiral perturbation theory is unknown and lattice results are obtained far from the chiral limit, it would be inappropriate to use expansions such as Eq. (1.9), which are valid in the chiral limit, to extrapolate the results. In fact, attempts using the first four terms in the chiral expansion, Eq. (1.9), to extrapolate nucleon magnetic moment lattice results have not been successful. The major problem is that the $c_2 m_\pi^2 \log(m_\pi^2)$ term dominates at large pion masses and prohibits contact with the lattice results. From this we conclude that lattice results obtained at large pion masses simply cannot be accessed directly via chiral perturbation theory expansions.

In order to access the heavy quark mass regime of the lattice results, we consider a successful phenomenological model of baryons – the Cloudy Bag Model (CBM) [17, 18] – which includes the underlying quark structure. The CBM builds in the phenomenon of pion emission in such a way that the leading non-analytic behaviour predicted in chiral perturbation theory is contained within the model. The reason for using the CBM to extrapolate lattice results is that this model contains additional physics which is not present in chiral perturbation theory. For example, in the CBM baryons have a finite size, in contrast to chiral perturbation theory where they are

considered point-like. As a result the non-analytic behaviour in chiral expansions in the CBM is suppressed at large pion masses due to the presence of form factors which regulate the pion loops. This gives a much more realistic description of hadronic observables at large pion masses. In practice this means that the lattice results at large pion masses can be accessed in a convergent way.

The CBM extrapolation procedure involves an algorithm which updates the properties of the CBM as the pion mass is changed. However, as we will see, the predictions of the CBM for the nucleon magnetic moments can be encapsulated in a simple analytic extrapolation formula. This extrapolation formula agrees with chiral perturbation theory in the small m_π limit, while it maintains the expected Dirac moment behaviour in the heavy quark mass regime. In Chapter 5 this extrapolation formula will be applied to magnetic moment lattice data of the entire spin-1/2 octet. We will apply a similar extrapolation procedure to the electric charge radius lattice results in Chapter 6.

The main aim of this thesis is to develop extrapolation schemes for lattice QCD results of hadronic observables. Here we focus on extrapolating the results for the electric charge radii and magnetic moments of octet baryons. By extrapolating the lattice results, one may directly confront experiment with the predictions of QCD, thereby testing the theory as a valid description of the strong interactions. Therefore, wherever possible our predictions are compared with experimental results. We also hope that work of this type will lead to a better understanding of the theory of QCD, so that it may be possible understand how the theory works in terms of simple ideas and models.

Chapter 2

Chiral Perturbation Theory

In this thesis we are interested in the low energy sector of QCD (≤ 1 GeV) where the observed particles which participate in the strong interactions are hadrons. As we have already remarked, since the QCD Lagrangian, Eq. (1.1), is formulated in terms of quarks and gluons, it is very difficult to extract information about hadrons directly. Chiral perturbation theory is an alternative means of making predictions for hadronic observables. In chiral perturbation theory one constructs an effective Lagrangian for the low energy sector which has hadronic degrees of freedom, but respects the same symmetry properties as the original QCD Lagrangian. In particular, the effective Lagrangian must be invariant under chiral transformations. In this chapter we construct the chiral effective Lagrangian and use it to make predictions for various hadronic observables. Eventually (in Chapters 3 – 5) we will use expansions from chiral perturbation theory to guide extrapolations of lattice results to the physical regime.

2.1 Chiral symmetry in the QCD Lagrangian

Recall the QCD Lagrangian of Eq. (1.1):

$$\mathcal{L} = -\frac{1}{4} F_a^{\mu\nu} F^a_{\mu\nu} + \bar{q}(i\not{D} - \mathrm{m})q \ . \tag{2.1}$$

This Lagrangian can be rewritten in terms of left- and right-handed quark wavefunctions, q_L and q_R, where

$$q_L = \frac{1}{2}(1-\gamma_5)\, q \qquad \text{and} \qquad q_R = \frac{1}{2}(1+\gamma_5)\, q \ , \tag{2.2}$$

to obtain

$$\mathcal{L} = -\frac{1}{4} F_a^{\mu\nu} F^a_{\mu\nu} + \bar{q}_L\, i\not{D} q_L + \bar{q}_R\, i\not{D} q_R - \bar{q}_L\, \mathrm{m}\, q_R - \bar{q}_R\, \mathrm{m}\, q_L \ . \tag{2.3}$$

Note that the left- and right-handed fields are mixed only in the terms proportional to the quark mass matrix, m. Therefore in the case of massless quarks the Lagrangian is invariant under global $SU(N_f)_L \otimes SU(N_f)_R$ transformations, where N_f is the number of flavours being considered. That is, the massless QCD Lagrangian is invariant under the following transformations

$$q_L \to g_L\, q_L \qquad \text{and} \qquad q_R \to g_R\, q_R \ , \tag{2.4}$$

where (g_L, g_R) is an element of the group $SU(N_f)_L \otimes SU(N_f)_R$. As an example we give the general form of an element of this transformation group in the case $N_f = 2$:

$$(g_L, g_R) = \left(e^{-i\alpha_L \cdot \tau/2}, e^{-i\alpha_R \cdot \tau/2} \right) \in SU(2)_L \otimes SU(2)_R \ . \tag{2.5}$$

Here α_L and α_R are 3-vectors with constant entries and $\tau = (\tau_1, \tau_2, \tau_3)$ is the triplet of Pauli matrices. The invariance of the massless Lagrangian under the transformations given in Eq. (2.4)

is known as **chiral symmetry**. In the physical case of non-zero quark masses, chiral symmetry is an approximate symmetry of the QCD Lagrangian, provided that the quark masses are small. This is certainly reasonable in 2-flavour QCD, since $m_{u,d} << \Lambda_{\rm QCD}$. It is also common to use 3-flavour chiral symmetry to make SU(3) chiral expansions. However, these expansions must be treated with caution since m_s is comparable to $\Lambda_{\rm QCD}$.

In 3-flavour QCD, chiral symmetry of the massless QCD Lagrangian gives rise to 16 conserved Noether currents, namely

$$J_X^{\mu a} = \bar{q}_X \gamma^\mu \frac{\lambda^a}{2} q_X \ ,$$

where $a = 1, \ldots 8$ and $X = L, R$. Each current satisfies $\partial_\mu J_X^{\mu a} = 0$. Alternatively, the currents can be written in terms of the conserved vector and axial currents, $J_V^{\mu a}$ and $J_A^{\mu a}$, where $J_V^{\mu a} = J_L^{\mu a} + J_R^{\mu a}$ and $J_A^{\mu a} = J_R^{\mu a} - J_L^{\mu a}$. There are 16 conserved charges, Q_V^a and Q_A^a, corresponding to the conserved vector and axial currents. They are given by

$$Q_V^a = \int d^3x \ J_V^{0a} \qquad \text{and} \qquad Q_A^a = \int d^3x \ J_A^{0a} \ . \tag{2.6}$$

These charges are the generators of the vector and axial symmetries of the QCD Lagrangian.

Since chiral symmetry is an approximate symmetry of the QCD Lagrangian, we expect that this symmetry is replicated in the light quark sector of the hadronic spectrum. If chiral symmetry is realized in the conventional way each observed hadron will have an opposite parity partner. For example, if $|N^+\rangle$ is an eigenstate of the QCD Hamiltonian with mass m we expect $Q_A |N^+\rangle$ also to be an eigenstate of the Hamiltonian with mass m since the axial charge, Q_A, commutes with the Hamiltonian, i.e. $[H, Q_A] = 0$ (since Q_A is a constant of the motion, $\partial_0 Q_A = 0$). However, experimentally opposite parity partners are not observed in the hadronic spectrum. For example, there are no particles with the same mass as the proton but opposite parity.

The explanation for the lack of parity partners in the hadronic spectrum is that the vacuum is not chirally symmetric – i.e. the state $Q_A |0\rangle$ is not identical to the vacuum state, $|0\rangle$, but it contains an arbitrary number of massless pseudo-scalar particles known as Goldstone bosons. In other words, the $SU(N_f)_L \otimes SU(N_f)_R$ symmetry of the QCD Lagrangian is dynamically broken to $SU(N_f)_V$ by the vacuum state $|0\rangle$. This produces massless Goldstone bosons in accordance with Goldstone's theorem which states that for every spontaneously broken symmetry a massless particle is produced. In the case $N_f = 3$ there are 16 generators of the chiral symmetry, 8 of which are broken in the dynamical breaking to $SU(3)_V$. Hence an octet of (almost) massless pseudo-scalar Goldstone bosons appears (comprising the pions, kaons and η_8 meson). These eight particles are created by the axial currents, $J_A^{\mu a}$, and obey the following relationship

$$\left\langle 0 \left| J_A^{\mu a}(0) \right| \pi_b(\vec{p}) \right\rangle = i f_\pi p^\mu \delta_b^a \ , \tag{2.7}$$

where π_a is the $a^{\rm th}$ Goldstone boson field and f_π is the pseudoscalar decay constant, which has dimensions of mass. Experimentally f_π is found to be 93 MeV [19].

The Goldstone bosons produced by chiral symmetry breaking would be completely massless if chiral symmetry was an exact symmetry of the QCD Lagrangian – i.e, if quarks were massless. The reality of small quark masses means that the eight pseudo-Goldstone bosons acquire small masses. However, there is a gap of $\Delta \approx 0.5$ GeV between the Goldstone boson masses and all other hadron masses. This means that at energies small compared to Δ the Goldstone bosons are the main dynamical degrees of freedom in the system. This allows an effective field theory – Chiral Perturbation Theory – to be formulated for the low energy sector. We will see this formulation in the following sections. (Excellent accounts of chiral perturbation theory and the

construction of chiral effective Lagrangians can be found in Refs. [20] – [23].) However, before we construct the chiral perturbation theory Lagrangian, we consider a simple model, the σ-model, to demonstrate the process of spontaneous chiral symmetry breaking and the associated production of Goldstone bosons.

2.2 The σ-model and spontaneous chiral symmetry breaking

The σ-model is a simple model describing a system of nucleons and pions. It is formulated in terms of a fermion field, $\psi = (p, n)^{\mathrm{T}}$, a pion triplet, π, and a scalar field, σ. The Lagrangian of the σ-model is chirally symmetric. As we will demonstrate, masses for the nucleons and σ particle arise through spontaneous chiral symmetry breaking. The σ-model will be helpful in understanding the nature of meson-baryon interactions before we move to the more general formalism of chiral perturbation theory. Moreover, it motivates chiral quark models such as the Cloudy Bag Model (see Chapter 3) where the underlying quark structure of baryons is included.

The Lagrangian of the σ-model is given by

$$\mathcal{L} = \bar{\psi} i \partial\!\!\!/ \psi + \frac{1}{2}\partial_\mu \boldsymbol{\pi} \cdot \partial^\mu \boldsymbol{\pi} + \frac{1}{2}\partial_\mu \sigma \partial^\mu \sigma - g \bar{\psi} \left(\sigma - i \boldsymbol{\tau} \cdot \boldsymbol{\pi} \gamma_5\right) \psi + \frac{\mu^2}{2}\left(\sigma^2 + \boldsymbol{\pi}^2\right) - \frac{\lambda}{4}\left(\sigma^2 + \boldsymbol{\pi}^2\right)^2 \quad (2.8)$$

The first three terms are kinetic energy terms for the nucleon, pion and σ fields respectively. The fourth term contains the pseudoscalar nucleon-pion interaction and the Yukawa coupling of the nucleons with the σ-field. The last two terms form a potential energy term, $V(\sigma, \boldsymbol{\pi})$, where

$$V(\sigma, \boldsymbol{\pi}) = -\frac{\mu^2}{2}\left(\sigma^2 + \boldsymbol{\pi}^2\right) + \frac{\lambda}{4}\left(\sigma^2 + \boldsymbol{\pi}^2\right)^2 \ . \quad (2.9)$$

The above Lagrangian can be written in a number of different forms. One particularly useful form of the Lagrangian is obtained when the pion and scalar fields are combined in a matrix, Σ, where

$$\Sigma = \sigma + i \boldsymbol{\tau} \cdot \boldsymbol{\pi} \ . \quad (2.10)$$

This matrix has the property that

$$\frac{1}{2}\mathrm{Tr}(\Sigma^\dagger \Sigma) = \sigma^2 + \boldsymbol{\pi}^2 \quad (2.11)$$

which is easily proved using the Pauli matrix identities. This allows the σ-model Lagrangian, Eq. (2.8), to be written in the following way

$$\begin{aligned} \mathcal{L} \ &= \ \bar{\psi}_L i \partial\!\!\!/ \psi_L + \bar{\psi}_R i \partial\!\!\!/ \psi_R + \frac{1}{4}\mathrm{Tr}\left(\partial_\mu \Sigma^\dagger \partial^\mu \Sigma\right) - g\left(\bar{\psi}_L \Sigma \psi_R + \bar{\psi}_R \Sigma^\dagger \psi_L\right) \\ &\quad + \frac{\mu^2}{4}\mathrm{Tr}(\Sigma^\dagger \Sigma) - \frac{\lambda}{16}\left[\mathrm{Tr}(\Sigma^\dagger \Sigma)\right]^2 \ , \end{aligned} \quad (2.12)$$

where ψ_L and ψ_R are the left and right handed fermion fields, as defined in Eq. (2.2). In this form it is clear that the σ-model Lagrangian is invariant under the chiral transformations

$$\psi_L \ \rightarrow \ e^{-i\boldsymbol{\alpha}_L \cdot \boldsymbol{\tau}/2}\, \psi_L \quad (2.13)$$

$$\psi_R \ \rightarrow \ e^{-i\boldsymbol{\alpha}_R \cdot \boldsymbol{\tau}/2}\, \psi_R \quad (2.14)$$

provided that the matrix Σ transforms as

$$\Sigma \rightarrow e^{-i\boldsymbol{\alpha}_L \cdot \boldsymbol{\tau}/2}\, \Sigma\, e^{i\boldsymbol{\alpha}_R \cdot \boldsymbol{\tau}/2} \ . \quad (2.15)$$

Since the σ-model Lagrangian is chirally symmetric, it is clearly also invariant under isospin transformations, where $\boldsymbol{\alpha}_L = \boldsymbol{\alpha}_R$ in Eqs. (2.13) – (2.15).

The σ-model Lagrangian exhibits spontaneous chiral symmetry breaking. This can be seen by considering the potential energy term, $V(\sigma,\pi)$. Stationary points of $V(\sigma,\pi)$ occur at $(\sigma,\pi) = (0,\mathbf{0})$ and when (σ,π) satisfies

$$\sigma^2 + \pi^2 = \frac{\mu^2}{\lambda} \ . \tag{2.16}$$

Since the field configuration $(\sigma,\pi) = (0,\mathbf{0})$ is an unstable critical point, we cannot consider quantum fluctuations about this point. However, the degenerate ground states satisfying Eq. (2.16) are stable critical points, and the potential energy is minimized on the surface formed by these points. We now consider fluctuations about a particular degenerate ground state on the surface; $(\sigma,\pi)_0 = (v,\mathbf{0})$, where $v = (\mu^2/\lambda)^{1/2}$. Fluctuations about $(\sigma,\pi)_0$ are denoted by $(\bar{\sigma},\pi)$, where $\bar{\sigma} = \sigma - v$. Rewriting Eq. (2.8) in terms of the fluctuations we see that the Lagrangian becomes

$$\begin{aligned} \mathcal{L} \ &= \ \bar{\psi}\left(i\partial\!\!\!/ - gv\right)\psi + \frac{1}{2}\left[\partial_\mu\bar{\sigma}\partial^\mu\bar{\sigma} - 2\mu^2\bar{\sigma}^2\right] + \frac{1}{2}\partial_\mu\boldsymbol{\pi}\cdot\partial^\mu\boldsymbol{\pi} - g\bar{\psi}\left(\bar{\sigma} - i\boldsymbol{\tau}\cdot\boldsymbol{\pi}\gamma_5\right)\psi \\ &\quad -\lambda v\bar{\sigma}\left(\bar{\sigma}^2 + \boldsymbol{\pi}^2\right) - \frac{\lambda}{4}\left[\left(\bar{\sigma}^2 + \boldsymbol{\pi}^2\right)^2 - v^4\right] \ . \end{aligned} \tag{2.17}$$

Therefore the nucleon acquires a mass of gv, the σ field acquires a mass of $\sqrt{2}\mu$ and the pions are massless. The pions are the massless Goldstone bosons corresponding to the 3 broken axial generators, i.e. they arise from the spontaneous breaking of $SU(2)_L \otimes SU(2)_R$ to $SU(2)_V$.

The σ-model Lagrangian no longer looks chirally symmetric in Eq. (2.17). For example, the fermion field now has an explicit mass term, which does not suggest chiral symmetry. However, the Noether currents of the original σ-model Lagrangian are still conserved [18]. In particular, the axial current remains conserved. Thus the symmetry of the original Lagrangian has been "hidden" by the field transformation $\sigma \to \bar{\sigma}$. However, some of the original symmetry has been broken, since $m_\sigma \neq m_\pi$ in Eq. (2.17), whereas these masses were the same in the original Lagrangian, Eq. (2.8).

We now consider adding a small symmetry breaking term to the σ-model Lagrangian. This addition is motivated by the fact that the original QCD Lagrangian contains non-zero quark mass terms which explicitly break chiral symmetry. We add the following term to the σ-model Lagrangian,

$$\mathcal{L}_{\rm sb} = a\,\sigma = \frac{a}{4}\mathrm{Tr}(\Sigma + \Sigma^\dagger) \ . \tag{2.18}$$

This term is not invariant under chiral transformations. Moreover, the addition of this term shifts the position of the ground state, $(v,\mathbf{0})$, to $(v',\mathbf{0})$, where

$$v' = \sqrt{\frac{\mu^2}{\lambda}} + \frac{a}{2\mu^2} \ . \tag{2.19}$$

By considering fluctuations about this new ground state, we find that the pions acquire a mass

$$m_\pi^2 = \frac{a}{v'} \ . \tag{2.20}$$

This reduces to our previous result in the limit $a \to 0$ because clearly $m_\pi \to 0$ in this case. Note that by adding this symmetry breaking term we have explicitly broken the $SU(2)_L \otimes SU(2)_R$ symmetry of the σ-model Lagrangian, but $SU(2)_V$ remains an exact symmetry.

There is a third form of the σ-model Lagrangian which will be useful in § 2.4.1, when we consider including baryon fields in chiral perturbation theory. Consider writing the matrix Σ in the following way

$$\Sigma = \sigma + i\boldsymbol{\tau}\cdot\boldsymbol{\pi} = (v+S)U \ , \tag{2.21}$$

where the scalar field, S, is defined by the following relationship

$$(S+v)^2 = \sigma^2 + \pi^2 \ , \tag{2.22}$$

where $v = (\mu^2/\lambda)^{1/2}$ as before. In this form the scalar field, S, takes over the role of the σ field and the matrix U replaces Σ. The matrix U is unitary since

$$(S+v)^2 U^\dagger U = (\sigma - i\tau\cdot\pi)(\sigma + i\tau\cdot\pi) = \sigma^2 + \pi^2 = (S+v)^2 \ , \tag{2.23}$$

and hence $U^\dagger U = 1$. Taking the determinant on both sides of Eq. (2.21) we see that U has unit determinant, and thus $U \in SU(2)$. In fact, using Eq. (2.21) we find that U can be written as

$$U = e^{i\tau\cdot\pi'/v} \ , \tag{2.24}$$

where $\pi' = \left(1 - \frac{\bar{\sigma}}{v} + \frac{\bar{\sigma}^2}{v^2} + \ldots\right)\pi$ and $\bar{\sigma} = \sigma - v$. Under chiral transformations the matrix U transforms in the same way as Σ, given in Eq. (2.15). Rewriting the Lagrangian in terms of U and S we obtain

$$\begin{aligned} \mathcal{L} &= \frac{1}{2}\left[(\partial_\mu S)^2 - 2\mu^2 S^2\right] + \frac{(v+S)^2}{4}\mathrm{Tr}(\partial_\mu U \partial^\mu U^\dagger) - \lambda v S^3 - \frac{\lambda}{4}S^4 \\ &\quad + \bar{\psi} i\partial\!\!\!/ \psi - g(v+S)(\bar{\psi}_L U \psi_R + \bar{\psi}_R U^\dagger \psi_L) \ . \end{aligned} \tag{2.25}$$

Compared to the form of the Lagrangian given in Eq. (2.12), here we have reintroduced a scalar field into the Lagrangian while retaining the matrix formulation. The scalar field, S, is heavy compared to the Goldstone bosons. The advantage of writing the Lagrangian in terms of S and U is that at low energies we can integrate out the heavy S field and obtain an effective theory for the low energy sector in terms of the matrix U [23]. We will discuss this in the next section.

The σ-model is clearly a very useful model for demonstrating spontaneous chiral symmetry breaking. However, there is a more systematic approach for constructing chirally invariant Lagrangians, namely chiral perturbation theory. In the following sections we will discuss this systematic approach applied to the meson and baryon octets. We will refer to the results of this section frequently in the construction of the chiral perturbation theory Lagrangian.

2.3 The effective chiral Lagrangian for Goldstone bosons

In this section we wish to construct an effective Lagrangian for the low energy sector which describes the interactions of Goldstone bosons. To do this we introduce an SU(3) matrix, U, which contains the Goldstone boson fields. This is analogous to the SU(2) matrix, U, introduced for the σ-model in Eq. (2.24). The matrix U is defined by

$$U = e^{i\Phi/f} \ , \tag{2.26}$$

where f is a constant with dimensions of mass and

$$\Phi = \lambda_a \pi_a = \sqrt{2}\begin{pmatrix} \frac{\pi^0}{\sqrt{2}} + \frac{\eta_8}{\sqrt{6}} & \pi^+ & K^+ \\ \pi^- & -\frac{\pi^0}{\sqrt{2}} + \frac{\eta_8}{\sqrt{6}} & K^0 \\ K^- & \bar{K}^0 & -\frac{2\eta_8}{\sqrt{6}} \end{pmatrix} \tag{2.27}$$

Here λ_a are the Gell-Mann matrices and π_a are the 8 Goldstone boson fields ($a = 1, \ldots 8$). Under a chiral transformation of the fermion fields

$$\begin{aligned} \psi_L &\to e^{-i\alpha_L\cdot\lambda/2}\psi_L \ , \\ \psi_R &\to e^{-i\alpha_R\cdot\lambda/2}\psi_R \ , \end{aligned}$$

(here $\boldsymbol{\alpha}_L$ and $\boldsymbol{\alpha}_R$ are constant vectors with 8 components) we require that the matrix U transforms in the following way

$$U \to e^{-i\boldsymbol{\alpha}_L\cdot\boldsymbol{\lambda}/2} U e^{i\boldsymbol{\alpha}_R\cdot\boldsymbol{\lambda}/2} \,, \tag{2.28}$$

analogous to the transformation property of the SU(2) matrix, U, in the σ-model.

We now construct the most general, chirally symmetric Lagrangian in terms of the matrix U. Since there are infinitely many possible terms consistent with chiral symmetry, this Lagrangian must be constructed in a systematic way. We use an expansion in powers of derivatives of U. This is equivalent to an expansion in powers of the meson momenta. Lorentz invariance requires that only terms with an even number of derivatives are allowed in the Lagrangian. Therefore the effective Lagrangian can be expressed as follows

$$\mathcal{L}_{\text{eff}} = \mathcal{L}_{\text{eff}}^{(2)} + \mathcal{L}_{\text{eff}}^{(4)} + \mathcal{L}_{\text{eff}}^{(6)} + \dots \,, \tag{2.29}$$

where $\mathcal{L}_{\text{eff}}^{(n)}$ contains terms with n derivatives. The term with zero derivatives is not needed in the expansion since it would comprise terms proportional to $U^\dagger U = 1$. The first term in this expansion is given by

$$\mathcal{L}_{\text{eff}}^{(2)} = \frac{f^2}{4}\text{Tr}(\partial_\mu U \partial^\mu U^\dagger) \,, \tag{2.30}$$

where the coefficient has been chosen so that the kinetic energy terms for the Goldstone boson fields are properly normalized. This term is similar to the kinetic term for the Goldstone bosons in the σ-model (see Eq. (2.25)), except that here the heavy scalar field, S, does not appear. This is because we are considering a low energy effective field theory, where heavy fields such as S are integrated out of the action. The $\mathcal{L}_{\text{eff}}^{(4)}$ term in the expansion of $\mathcal{L}_{\text{eff}}$ is given by

$$\mathcal{L}_{\text{eff}}^{(4)} = \frac{L_1}{4}\left[\text{Tr}(\partial_\mu U \partial^\mu U^\dagger)\right]^2 + \frac{L_2}{4}\text{Tr}(\partial^\mu U \partial^\nu U^\dagger)\text{Tr}(\partial_\mu U \partial_\nu U^\dagger) \tag{2.31}$$

where L_1 and L_2 are independent constants which need to be determined phenomenologically. Terms such as

$$\text{Tr}(\partial^\mu U^\dagger \partial_\mu U \partial^\nu U^\dagger \partial_\nu U) \qquad \text{and} \qquad \text{Tr}(\partial^\mu U^\dagger \partial_\nu U \partial_\mu U^\dagger \partial^\nu U) \tag{2.32}$$

are not included in $\mathcal{L}_{\text{eff}}^{(4)}$ since they can be re-written as linear combinations of the terms in Eq. (2.31).

The advantage of expanding $\mathcal{L}_{\text{eff}}$ in powers of derivatives is that at low enough energies only a few orders of the expansion are needed. From dimensional analysis the coefficient of a term with n derivatives behaves as Λ^{4-n}, where Λ has dimensions of energy and is of the order 1 GeV. Hence an n-derivative vertex is of order $q^n\Lambda^{4-n}$, where q is the momentum scale. Therefore, at energies small compared to Λ, matrix elements involving terms with a large number of derivatives will be very small. Loop effects do not change this general conclusion [23]. Thus the expansion of the effective Lagrangian, Eq. (2.29), is very convenient for calculating matrix elements at low energies.

In parallel with our discussion of the σ-model, we now consider the effect of adding explicit chiral symmetry breaking terms to $\mathcal{L}_{\text{eff}}$. Here we only show the effect of adding such a term to second order in the effective Lagrangian. However, symmetry breaking terms should be included at each order in the expansion to produce the most general effective Lagrangian for the Goldstone bosons. The symmetry breaking term is added to $\mathcal{L}_{\text{eff}}^{(2)}$ in the following way

$$\mathcal{L}_{\text{eff}}^{(2)} = \frac{f^2}{4}\text{Tr}(\partial_\mu U \partial^\mu U^\dagger) + \frac{B}{2}f^2\text{Tr}[\mathbf{m}(U + U^\dagger)] \,, \tag{2.33}$$

where B is a constant and $\mathbf{m}$ is the quark mass matrix. As we will see, the matrix $\mathbf{m}$ is of order m_π^2 and hence the symmetry breaking term has the right dimensions for the second order effective Lagrangian. We can determine the constant B if we consider Eq. (2.33) in the 2-flavour case. In that case

$$U(x) = e^{i\pi(x)\cdot\tau/f} \tag{2.34}$$

and Eq. (2.33) can be expanded in the following way

$$\begin{aligned}\mathcal{L}_{\text{eff}}^{(2)} &= \frac{1}{2}\partial_\mu\pi\cdot\partial^\mu\pi + \frac{1}{6f^2}\left[(\pi\cdot\partial_\mu\pi)(\pi\cdot\partial^\mu\pi) - (\pi\cdot\pi)(\partial_\mu\pi\cdot\partial^\mu\pi)\right] \\ &\quad +(m_u+m_d)B\left[f^2 - \frac{1}{2}\pi\cdot\pi + \frac{1}{24f^2}(\pi\cdot\pi)^2\right] + \mathcal{O}(\pi^6)\ . \end{aligned} \tag{2.35}$$

This allows us to make the following identification immediately

$$(m_u+m_d)B = m_\pi^2\ . \tag{2.36}$$

There is also a constant vacuum contribution to the second order Lagrangian, Eq. (2.35), namely

$$(m_u+m_d)Bf^2\ . \tag{2.37}$$

This can be identified with the the constant vacuum contribution to the (2-flavour) QCD Lagrangian, $-(m_u+m_d)<\bar{q}q>$. Hence

$$B = \frac{m_\pi^2}{m_u+m_d} = -\frac{<\bar{q}q>}{f^2}\ . \tag{2.38}$$

We can also compute the (2-flavour) vector and axial vector currents from $\mathcal{L}_{\text{eff}}^{(2)}$ to find

$$J_V^{\mu a} = \epsilon^{abc}\pi^b\partial^\mu\pi^c + \ldots \tag{2.39}$$

$$J_A^{\mu a} = -f\partial^\mu\pi^a + \ldots \tag{2.40}$$

Thus, using Eq. (2.7), we see that f can be identified with the pseudo-scalar decay constant, f_π, and Eq. (2.38) reproduces the Gell Mann - Oakes - Renner (GOR) relation.

2.4 Including the baryons

The effective Lagrangian which was constructed in the previous section describes the interactions between Goldstone bosons alone. The next step is to incorporate the spin-1/2 baryon octet in the effective Lagrangian. These particles are not light compared to the QCD scale. Heavy particles exist in vectorial flavour multiplets. We will see that this vectorial flavour symmetry is important when constructing an effective Lagrangian which includes the baryon fields. However, first we consider how baryons enter the σ-model as motivation.

2.4.1 Fermions in the σ-model

In terms of the matrix U and scalar field S, the fermionic sector of the σ-model Lagrangian is given by

$$\mathcal{L}_f = \bar{\psi}i\partial\!\!\!/\psi - (M_0+gS)\left(\bar{\psi}_L U\psi_R + \bar{\psi}_R U^\dagger\psi_L\right)\ , \tag{2.41}$$

where $M_0 = gv$ is the fermion mass. At low energies the heavy scalar field, S, can be integrated out of the action to produce an effective Lagrangian for the low energy sector. To lowest order this integration corresponds to setting $S = 0$ in the Eq. (2.41) [23]. (To obtain higher order

effective Lagrangians one must perform the integration explicitly.) Thus we consider the following Lagrangian for the fermionic sector of the σ-model at low energies

$$\mathcal{L}_f = \bar{\psi}_L i\partial\!\!\!/ \psi_L + \bar{\psi}_R i\partial\!\!\!/ \psi_R - M_0 \left(\bar{\psi}_L U \psi_R + \bar{\psi}_R U^\dagger \psi_L\right) \ . \tag{2.42}$$

This Lagrangian is invariant under the following chiral transformations,

$$\psi_L \to L\psi_L \qquad \psi_R \to R\psi_R \qquad U \to LUR^\dagger \ , \tag{2.43}$$

where $L, R \in SU(2)_{L,R}$ respectively. We now make a change of variables:

$$U = \xi\xi \qquad N_L = \xi^\dagger \psi_L \qquad N_R = \xi\psi_R \tag{2.44}$$

where $\xi = e^{i\pi\cdot\tau/2f_\pi}$ to agree with the definition of U given in Eq. (2.34). Physically, this change of variables corresponds to 'dressing' the bare nucleon field, ψ, with a meson cloud which is contained in the matrix ξ. The fermionic Lagrangian, Eq. (2.42), then becomes

$$\mathcal{L}_f = \bar{N}\left(i\not{D} - \not{\bar{A}}\gamma_5 - M_0\right) N \ , \tag{2.45}$$

where $N = N_L + N_R$ and $\mathcal{D}_\mu N = (\partial_\mu + i\bar{V}_\mu)N$. In terms of the matrix ξ, the vector field, $\bar{V}_\mu$, is given by

$$\bar{V}_\mu = -\frac{i}{2}\left(\xi^\dagger\partial_\mu\xi + \xi\partial_\mu\xi^\dagger\right) \ , \tag{2.46}$$

and the axial field, $\bar{A}_\mu$, is defined as

$$\bar{A}_\mu = -\frac{i}{2}\left(\xi^\dagger\partial_\mu\xi - \xi\partial_\mu\xi^\dagger\right) \ . \tag{2.47}$$

We now consider the chiral behaviour of the new fields. Under the chiral transformations given in Eq. (2.43), the matrix ξ is defined to transform as follows

$$\xi \to L\xi V^\dagger = V\xi R^\dagger \ , \tag{2.48}$$

where V is an SU(2) matrix defined implicitly by Eq. (2.48) [1]. Clearly this transformation rule ensures that $U = \xi\xi$ transforms correctly as in Eq. (2.43). Using the transformation rule given for ξ, together with the transformation rules for the original fields, Eq. (2.43), we find the following transformation rules for all quantities in the Lagrangian, $\mathcal{L}_f$,

$$\begin{aligned} N_{L,R} &\to V N_{L,R} & \bar{V}_\mu &\to V\left[\bar{V}_\mu - i(\partial_\mu V^\dagger)V\right]V^\dagger \\ \bar{A}_\mu &\to V\bar{A}_\mu V^\dagger & \mathcal{D}_\mu N &\to V\mathcal{D}_\mu N \end{aligned} \tag{2.49}$$

Under purely vectorial transformations, where $L = R$, it can be seen from Eqs. (2.43), (2.48) and (2.49) that $V = L = R$. Otherwise the explicit form of V is much more complicated. In general V is a function of $\pi(x)$. Thus the transformation $N \to VN$ explicitly mixes nucleons with states consisting of nucleons and pions. This mixing is expected from spontaneous chiral symmetry breaking. From Eq. (2.49) we see that unlike the undressed fermion fields, the left- and right-handed dressed fermion fields, N_L and N_R, transform in exactly the same way under chiral transformations, i.e. both transform via the SU(2) matrix V. The covariant derivative for the dressed nucleon field also transforms in this simple vectorial manner. This is a manifestation of the vectorial flavour symmetry of baryons, which is made explicit by this parameterization of the fields.

[1] The unitary nature of V may be shown by noting that $L\xi V^\dagger = V\xi R^\dagger$ must also be unitary. Obviously V also has unit determinant.

From this example we can see how baryons should be added to chiral effective Lagrangians in general. First one assumes that the baryon multiplet transforms via the SU(n) matrix V, as in Eq. (2.49). The covariant derivative is then constructed for the baryon multiplet so that it also transforms under V. In general, this covariant derivative will include the ξ matrix. Pion coupling terms are included in the effective Lagrangian by constructing chirally invariant quantities which involve the ξ and U matrix fields. For example, the term $\bar{N}\not{A}\gamma_5 N$ in Eq. (2.45) is invariant under the chiral transformations Eqs. (2.48) - (2.49). In general, each pion coupling term will have a coefficient which must be determined by experiment. Finally, one may include explicit chiral symmetry breaking terms in the effective Lagrangian if the original theory contains terms of this nature.

2.4.2 Generalization to $SU(3)\otimes SU(3)$

In this section we construct an effective Lagrangian to describe the interactions of the spin-1/2 baryon octet with the Goldstone boson octet. We will use the results of the previous section, §2.4.1, as motivation. The main difference between this section and the last is that the dressed nucleon field, N, of the σ-model is generalized to a matrix, Ψ_B, in this case. This means that products such as $\bar{N}N$ become $\mathrm{Tr}(\bar{\Psi}_B\Psi_B)$ in this generalization. Here we will also consider the effect of including explicit chiral symmetry breaking terms in the effective Lagrangian. These terms correspond to the quark mass terms in the original QCD Lagrangian.

The SU(3) matrix, Ψ_B, which contains the octet baryon fields, is given by

$$\Psi_B(x) = \frac{1}{\sqrt{2}}\lambda_a\psi_B^a = \begin{pmatrix} \frac{\Lambda}{\sqrt{6}} + \frac{\Sigma^0}{\sqrt{2}} & \Sigma^+ & p \\ \Sigma^- & \frac{\Lambda}{\sqrt{6}} - \frac{\Sigma^0}{\sqrt{2}} & n \\ \Xi^- & \Xi^0 & -\frac{2}{\sqrt{6}}\Lambda \end{pmatrix}$$

where ψ_B^a are the 8 baryon fields and λ^a are the Gell-Mann matrices. The free field Lagrangian for the baryon fields is a simple generalization of the Dirac Lagrangian, namely

$$\mathcal{L} = \mathrm{Tr}\left[\bar{\Psi}_B(i\gamma_\mu\partial^\mu - M_0)\Psi_B\right] \tag{2.50}$$

where M_0 is the degenerate baryon mass in the chiral SU(3) limit. To include interactions with Goldstone bosons we generalize the results of the σ-model, Eq. (2.45), identifying the dressed nucleon field, N, with the matrix field, Ψ_B. This gives rise to the following leading order effective Lagrangian for the baryon-meson sector

$$\mathcal{L}_{\mathrm{MB}}^{(1)} = \mathrm{Tr}\left[\bar{\Psi}_B(i\gamma_\mu D^\mu - M_0)\Psi_B\right] + F\mathrm{Tr}\left(\bar{\Psi}_B\gamma_\mu\gamma_5[A^\mu,\Psi_B]\right) + D\mathrm{Tr}\left(\bar{\Psi}_B\gamma_\mu\gamma_5\{A^\mu,\Psi_B\}\right) \ , \tag{2.51}$$

where F and D are coupling constants which can be determined from neutron and hyperon beta decays. We use the one-loop corrected values $F = 0.4$ and $D = 0.61$ in this thesis [24]. The covariant derivative for the baryon fields is given by

$$\mathcal{D}_\mu\Psi_B = \partial_\mu\Psi_B + i\left[\bar{V}_\mu,\Psi_B\right] \ . \tag{2.52}$$

The vector and axial fields, $\bar{V}_\mu$ and $\bar{A}_\mu$, are given in Eq. (2.46). (N.B. The matrix ξ must now be generalized to three flavours in the definitions of $\bar{V}_\mu$ and $\bar{A}_\mu$ - i.e,

$$\xi = e^{i\Phi(x)/2f_\pi} \ , \tag{2.53}$$

where $\Phi(x)$ is given in Eq. (2.27).)

Explicit chiral symmetry breaking terms, corresponding to the quark mass terms in the QCD Lagrangian, are added to the effective Lagrangian at second order. These terms involve the

quark mass matrix, $\mathbf{m}$. For example, there will be terms proportional to $\mathrm{Tr}(\bar{\Psi}_B[\mathbf{m}, \Psi_B])$ and to $\mathrm{Tr}(\bar{\Psi}_B[\xi\mathbf{m}\xi + \xi^\dagger\mathbf{m}\xi^\dagger, \Psi_B])$ in the symmetry breaking piece of the second order effective Lagrangian. Once the symmetry breaking terms have been included in the Lagrangian, the baryon masses will be shifted and split so that they are no longer degenerate. This can be seen in Ref. [23] where the full second order Lagrangian for the meson-baryon sector is given and the mass splittings are discussed.

One can also construct higher order effective Lagrangians for the meson-baryon sector. Since only the low order Lagrangians are needed for calculations at low energies we will not give the explicit forms for these Lagrangians here. However, the full chiral perturbation theory expansion is given schematically as follows

$$\mathcal{L}_{\text{eff}} = \mathcal{L}_{\text{MB}}^{(1)} + \mathcal{L}_{\text{M}}^{(2)} + \mathcal{L}_{\text{MB}}^{(2)} + \mathcal{L}_{\text{MB}}^{(3)} + \dots \ , \tag{2.54}$$

where "MB" and "M" stand for meson-baryon sector and meson sector respectively. Explicit expressions for $\mathcal{L}_{\text{MB}}^{(1)}$ and $\mathcal{L}_{\text{M}}^{(2)}$ are given in Eqs. (2.51) and (2.33).

Electromagnetic interactions can be included in the effective Lagrangian by modifying all partial derivatives so that they include couplings to the photon field, $\mathcal{A}^\mu$. For example, the fermion covariant derivative would be modified as follows

$$D_\mu\Psi_B \equiv \partial_\mu\Psi_B + i\left[\bar{V}_\mu, \Psi_B\right] \to \partial_\mu\Psi_B - ie\mathcal{A}_\mu[Q, \Psi_B] + \frac{1}{8f_\pi^2}[[\Phi, \partial^\mu\Phi], \Psi_B] + \dots \ , \tag{2.55}$$

where the matrix Φ is defined in Eq. (2.27) and

$$Q = \begin{pmatrix} \frac{2}{3} & 0 & 0 \\ 0 & -\frac{1}{3} & 0 \\ 0 & 0 & -\frac{1}{3} \end{pmatrix} \tag{2.56}$$

Similarly for the meson sector, electromagnetic interactions are introduced by making the following substitution: $\partial_\mu U \to D_\mu U = \partial_\mu U + ie\mathcal{A}_\mu[Q, U]$. Once the electromagnetic interactions have been included in the effective Lagrangian one can determine the associated conserved electromagnetic current by calculating

$$J^\mu = -\frac{\partial\mathcal{L}_{\text{eff}}}{\partial(e\mathcal{A}_\mu)} \ . \tag{2.57}$$

This expression for the current can clearly be decomposed into a sum of contributions from each term in Eq. (2.54).

2.5 Electromagnetic form factors in chiral perturbation theory

In this section we show how the chiral perturbation theory Lagrangian can be used to make chiral expansions of electric charge radii and magnetic moments for octet baryons. Here we simply give a general overview of the method used to obtain these expansions, but do not include all the details. Precise details of the calculations can be found in Refs. [24] – [26]. The basic quantities we must compute for each baryon are the Sachs electric and magnetic form factors, $G_E(q^2)$ and $G_M(q^2)$. The 4-vector q is the momentum transfer vector; the difference in momentum of the outgoing and ingoing baryon state. This corresponds to the momentum brought into the vertex by the (virtual) photon. In the Breit frame, where the momentum transfer 4-vector, q, satisfies $q^0 = 0$, the Sachs form factors are related to the spatial electromagnetic current, $J^\mu(\vec{r})$, in the following way

$$\langle B\left|J^0(\vec{r})\right|B\rangle = \frac{e}{(2\pi)^3}\int d^3q\, G_E(q^2)e^{-i\vec{q}\cdot\vec{r}} \ , \tag{2.58}$$

$$\langle B, s_B|\,\vec{J}(\vec{r})\,|B, s_B\rangle = \frac{ie}{(2\pi)^3}\int d^3q\, G_M(q^2)\,\langle s_B\,|\vec{\sigma}\times\vec{q}|\,s_B\rangle\, e^{-i\vec{q}\cdot\vec{r}} \ , \tag{2.59}$$

Baryon	$\alpha_i^{(\pi)}$	$\alpha_i^{(K)}$	$\beta_i^{(\pi)}$	$\beta_i^{(K)}$
p	$-\frac{1}{6}-\frac{5}{6}(D+F)^2$	$-\frac{1}{3}-\frac{5}{3}(\frac{D^2}{3}+F^2)$	$-(D+F)^2$	$-\frac{2}{3}D^2-2F^2$
n	$\frac{1}{6}+\frac{5}{6}(D+F)^2$	$-\frac{1}{6}-\frac{5}{6}(D-F)^2$	$(D+F)^2$	$-(D-F)^2$
Λ	0	$\frac{5}{3}DF$	0	$2DF$
Σ^+	$-\frac{1}{3}-\frac{5}{3}\left(\frac{D^2}{3}+F^2\right)$	$-\frac{1}{6}-\frac{5}{6}(D+F)^2$	$-\frac{2}{3}D^2-2F^2$	$-(D+F)^2$
Σ^0	0	$-\frac{5}{3}DF$	0	$-2DF$
Σ^-	$\frac{1}{3}+\frac{5}{3}\left(\frac{D^2}{3}+F^2\right)$	$\frac{1}{6}+\frac{5}{6}(D-F)^2$	$\frac{2}{3}D^2+2F^2$	$(D-F)^2$
Ξ^0	$-\frac{1}{6}-\frac{5}{6}(D-F)^2$	$\frac{1}{6}+\frac{5}{6}(D+F)^2$	$-(D-F)^2$	$(D+F)^2$
Ξ^-	$\frac{1}{6}+\frac{5}{6}(D-F)^2$	$\frac{1}{3}+\frac{5}{3}(\frac{D^2}{3}+F^2)$	$(D-F)^2$	$\frac{2}{3}D^2+2F^2$

Table 2.1: Table of coefficients for the chiral expansions Eqs. (2.62) and (2.63) in terms of the axial vector coupling constants F and D.

where $|s_B\rangle$ contains the spin information of the baryon state $|B\rangle$. The Breit frame is chosen because in this frame the expressions relating $G_E(q^2)$ and $G_M(q^2)$ to the electromagnetic current are decoupled, with $G_E(q^2)$ related to the time component of the current and $G_M(q^2)$ related to the spatial components. This significantly simplifies the calculation of the Sachs form factors. Physically, the Sachs form factors measure the interaction of the baryon B with weak, static electric and magnetic fields. The electric charge radius and magnetic moment of baryon B can be extracted from the Sachs form factors as follows

$$r_B^2 = -6\left.\frac{dG_E(q^2)}{dq^2}\right|_{q^2=0} \tag{2.60}$$

$$\vec{\mu}_B = e\,G_M(0)\left\langle B(\vec{p}=\vec{0}),s_B\right|\vec{\sigma}\left|B(\vec{p}=\vec{0}),s_B\right\rangle \tag{2.61}$$

These relations are easily proven from the definitions

$$r_B^2 = \left\langle B(\vec{p}=\vec{0})\left|\int d^3r\; r^2 j_B^0(\vec{r})\right|B(\vec{p}=\vec{0})\right\rangle ,$$

$$\vec{\mu}_B = \left\langle B(\vec{p}=\vec{0}),s_B\left|\frac{1}{2}\int d^3r\;\vec{r}\times\vec{j}_B(\vec{r})\right|B(\vec{p}=\vec{0}),s_B\right\rangle ,$$

and using Eqs. (2.58) and (2.59) also.

Therefore, to determine the charge radius and magnetic moment chiral expansions, one must first compute the electromagnetic current from the effective Lagrangian. This involves computing $\partial\mathcal{L}_{\rm eff}/\partial(e\mathcal{A}_\mu)$ as in Eq. (2.57). Realistically, one would use the first few terms in the expansion of $\mathcal{L}_{\rm eff}$, Eq. (2.54), since this is a good approximation at low energies. Next one would compute the left hand sides of Eqs. (2.58) and (2.59) and hence determine $G_E(q^2)$ and $G_M(q^2)$. Details of these calculations can be found in Refs. [24, 27, 28]. Once the Sachs form factors have been determined, it is then simple to compute the squared charge radius and magnetic moment expansion for each octet baryon using Eqs (2.60) and (2.61). One finds the following SU(3) chiral expansions,

$$\langle {r_i}^2\rangle = \delta_i + \sum_{X=\pi,K}\frac{6\alpha_i^{(X)}}{(4\pi f_\pi)^2}\ln\left(\frac{m_X}{\lambda}\right)+\cdots , \tag{2.62}$$

$$\mu_i = \gamma_i + \sum_{X=\pi,K}\beta_i^{(X)}\frac{m_N}{8\pi f_\pi^2}m_X+\cdots , \tag{2.63}$$

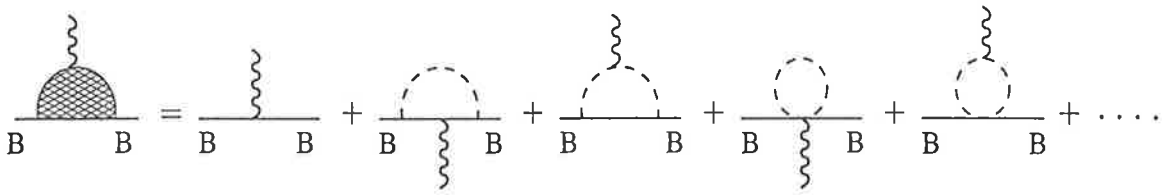

Figure 2.1: The lowest order processes contributing to the charge radius and magnetic moment expansions for an octet baryon, B. The shaded diagram on the left-hand side of the equation represents the sum of contributing diagrams. Unspecified internal fermion lines are intermediate baryon states, which do not necessarily have the same quantum numbers as B.

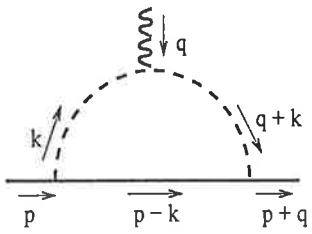

Figure 2.2: The Goldstone boson loop which produces the leading order non-analytic term in the expansions of baryon magnetic moments. The momenta are indicated.

where "i" labels the octet baryon, λ is the scale of the dimensional regularization, m_N is the nucleon mass, the coefficients $\alpha_i^{(X)}$ and $\beta_i^{(X)}$ are listed in Table 2.1 and the values for δ_i and γ_i are given in Refs. [24, 25]. The terms δ_i and γ_i are constant and thus are analytic functions of the quark mass, m_q. It can be shown [27, 29] that all coefficients of analytic terms are model dependent (they depend on the cutoff value), while coefficients of non-analytic terms are model independent. Therefore we will not be interested in the values of the coefficients δ_i and γ_i, since they depend on the cutoff value. However, the coefficients $\alpha_i^{(X)}$ and $\beta_i^{(X)}$ are model independent, since the terms $\ln(m_X/\lambda)$ and m_X are non-analytic in the quark mass. (Recall that $m_\pi \propto m_q^{1/2}$ and $m_K \propto (m_q + m_s)^{1/2}$.) For this reason we will be interested in the values of these coefficients. Eventually (in Chapters 3 – 5) we will use the non-analytic terms together with their coefficients in extrapolation formulae for electric charge radii and magnetic moments.

We have seen that the electric charge radius and magnetic moment expansions contain both analytic and non-analytic terms as a function of the quark mass, m_q. To see how each term arises one must calculate the relevant Feynman diagram. The lowest order processes contributing to the magnetic moment and electric charge radius expansions for an octet baryon, B, are shown in Fig. 2.1. The 3$^{\text{rd}}$ diagram in this expansion (which is enlarged in Fig. 2.2, where the momentum conventions are chosen) gives rise to the leading non-analytic term in the magnetic moment chiral expansion when the intermediate baryon state has the same quantum numbers as the external state, B. In the following paragraphs we will explicitly show how this leading non-analytic term arises from the process shown in Fig. 2.2. However, first we discuss the expected form of the amplitude for the "full" process (i.e. the sum of all contributing processes), depicted by the shaded diagram on the left-hand side of Fig. 2.1.

The amplitude for the full process in Fig. 2.1 can be written as $\bar{u}(p')\epsilon_\mu \Gamma^\mu u(p)$, where $\epsilon_\mu \equiv \epsilon_\mu(q)$ is the polarization vector for the incoming photon, Γ^μ contains a sum of contributing processes and $u(p)$ and $\bar{u}(p')$ are the Dirac spinors for the baryon, where $p' = p + q$ is the outgoing baryon momentum. Note that the amplitude will also include a factor involving the isospin components

of the Dirac spinors. However, the isospin part of the amplitude can be calculated separately because it factors out from the full expression, and can be recovered at the end of the calculation. Using general properties, such as Lorentz invariance and the Ward identity, it can be shown [7] that Γ^μ must take the form

$$\Gamma^\mu = F_1(q^2)\gamma^\mu + F_2(q^2)\frac{i\sigma^{\mu\nu}q_\nu}{2m} \ , \tag{2.64}$$

where m is the mass of the baryon and $F_1(q^2)$ and $F_2(q^2)$ are real functions. $F_1(q^2)$ and $F_2(q^2)$ are related to the Sachs form factors, defined in Eqs. (2.58) and (2.59), in the following way

$$G_E(q^2) = F_1(q^2) - \frac{|q^2|}{4m^2}F_2(q^2) \ , \tag{2.65}$$

$$G_M(q^2) = F_1(q^2) + F_2(q^2) \ . \tag{2.66}$$

We will now sketch the calculation of the leading non-analytic contribution to the nucleon magnetic moment from the process shown in Fig. 2.2. This contribution is labelled $\delta\Gamma^\mu$.

The Feynman rules for fermions and pseudoscalar particles allow us to write down the following expression for the amplitude of the process shown in Fig. 2.2 in the case where the intermediate state has the same quantum numbers as the external nucleon,

$$\epsilon_\mu \delta\Gamma^\mu = g_{\pi N}^2 \ \epsilon_\mu \int \frac{d^4k}{(2\pi)^4}(i\gamma_5)\left[\frac{i^3(2k^\mu + q^\mu)(\not{p} - \not{k} + m)}{(k^2 - m_\pi^2 + i\epsilon)((p-k)^2 - m^2 + i\epsilon)((k+q)^2 - m_\pi^2 + i\epsilon)}\right](-i\gamma_5) \ . \tag{2.67}$$

The factor of $2k^\mu + q^\mu = k^\mu + (k^\mu + q^\mu)$ comes from the photon coupling to the pion. The factors of $i\, g_{\pi N}\, \gamma_5$ arise from the vertices where the pion is emitted and absorbed ($g_{\pi N}$ is the pion-nucleon coupling). Using the fact that $\{\gamma_5, \gamma^\mu\} = 0$, $\epsilon_\mu q^\mu = 0$ and $\not{p}u(p) = mu(p)$, this amplitude can be written

$$\epsilon_\mu \delta\Gamma^\mu = -2\, i\, g_{\pi N}^2\, \epsilon_\mu \gamma_\lambda \int \frac{d^4k}{(2\pi)^4} \frac{k^\mu k^\lambda}{(k^2 - m_\pi^2 + i\epsilon)((p-k)^2 - m^2 + i\epsilon)((k+q)^2 - m_\pi^2 + i\epsilon)} \ . \tag{2.68}$$

Working in the Breit frame, where $q^0 = 0$, this amplitude becomes

$$\epsilon_\mu \delta\Gamma^\mu = -2\, i\, g_{\pi N}^2\, \epsilon_\mu \gamma_\lambda \int \frac{d^4k}{(2\pi)^4} \frac{k^\mu k^\lambda}{((k^0)^2 - \omega_k^2 + i\epsilon)(k^2 - 2p^0k^0 + 2\vec{p}\cdot\vec{k} + i\epsilon)((k^0)^2 - w_{k+q}^2 + i\epsilon)} \ , \tag{2.69}$$

where $\omega_k^2 \equiv |\vec{k}|^2 + m_\pi^2$. Taking the heavy baryon limit, where $p^0 = \sqrt{|\vec{p}|^2 + m^2} >> |\vec{p}|, k^0, |\vec{k}|$ and $p^0 \approx m$, the following factor in the denominator can be simplified,

$$k^2 - 2p^0k^0 + 2\vec{p}\cdot\vec{k} + i\epsilon \to -2p^0(k^0 - i\epsilon + \mathcal{O}(1/m)) \approx -2m(k^0 - i\epsilon + \mathcal{O}(1/m)) \ , \tag{2.70}$$

and the $\mathcal{O}(1/m)$ term can be disregarded. Using this simplification, the denominator can be fully factorised as follows

$$\epsilon_\mu \delta\Gamma^\mu = i\, g_{\pi N}^2\, \epsilon_\mu \gamma_\lambda \int \frac{d^4k}{(2\pi)^4} \frac{k^\mu k^\lambda}{m(k^0 - i\epsilon)(k^0 - \omega_k + i\epsilon)(k^0 + \omega_k - i\epsilon)(k^0 - \omega_{k+q} + i\epsilon)(k^0 + \omega_{k+q} - i\epsilon)} \ . \tag{2.71}$$

We now perform the k^0 integral by contour integration, closing the contour in the lower half of the k^0 complex plane so that only the poles in this half plane contribute. The integration over k^0 produces a number of terms. The term which gives rise to the leading non-analytic behaviour in the chiral expansions has k^ik^j in the numerator $(i, j = 1, 2, 3)$, i.e. the term,

$$\frac{g_{\pi N}^2}{(2\pi)^3}\ \epsilon_i\, \gamma_j \int d^3k\ k^ik^j \left[\frac{1}{2\omega_k^2 m(\omega_k^2 - \omega_{k+q}^2)} + \frac{1}{2\omega_{k+q}^2 m(\omega_{k+q}^2 - \omega_k^2)}\right] \ , \tag{2.72}$$

where the first term in square brackets is the residue from the pole at $k^0 = \omega_k - i\epsilon$ and the second term is the residue at $k^0 = \omega_{k+q} - i\epsilon$. There will be other terms arising from the k^0 integration involving k^0 in the numerator, but we are not interested in these terms here since they do not give rise to the leading non-analytic behaviour. Now simplifying the above term gives

$$-\frac{g_{\pi N}^2}{2m(2\pi)^3}\,\epsilon_i\,\gamma_j \int d^3k\,\frac{k^i k^j}{\omega_k^2 \omega_{k+q}^2} \tag{2.73}$$

Since the leading non-analytic contribution to the magnetic moment arises from the anomalous part of the magnetic moment we use the Gordon identity, namely

$$\bar{u}(p')\gamma^\mu u(p) = \bar{u}(p')\left[\frac{p'^\mu + p^\mu}{2m} + \frac{i\sigma^{\mu\nu}q_\nu}{2m}\right] u(p)\ , \tag{2.74}$$

to replace γ_j in Eq. (2.73) by $\sigma_{j\mu}q^\mu$ (As before, we neglect other terms which do not contribute to the leading non-analytic piece.) to obtain

$$-\frac{g_{\pi N}^2}{2m(2\pi)^3}\,\frac{i\,\epsilon_i\,\sigma_{j\mu}q^\mu}{2m} \int d^3k\,\frac{k^i k^j}{\omega_k^2 \omega_{k+q}^2} \tag{2.75}$$

This substitution allows $\vec{q}$ to be set to zero in the denominator since the leading non-analytic piece comes from the term linear in q. With $\vec{q}$ set to zero in the denominator, the symmetry properties of the integrand then allow $k^i k^j$ to be replaced with $\delta^{ij}|\vec{k}|^2/3$ and we obtain

$$\frac{g_{\pi N}^2}{6m(2\pi)^3}\,\frac{i\epsilon_j\,\sigma^{j\mu}q_\mu}{2m} \int d^3k\,\frac{k^2}{\omega_k^4}\ . \tag{2.76}$$

Therefore, using Eqs. (2.64) and (2.66), the contribution to $G_M(0)$ is

$$\frac{g_{\pi N}^2}{3m(2\pi)^2}\int_0^\infty dk\,\frac{k^4}{\omega_k^4}\ , \tag{2.77}$$

performing the trivial angular integration. Writing $\omega_k^4 = (k^2 + m_\pi^2)^2 = (k + im_\pi)^2(k - im_\pi)^2$ allows the model independent part of this expression to be extracted by contour integration. One obtains

$$-\frac{g_{\pi N}^2 m_\pi}{16\pi m}\ . \tag{2.78}$$

If we now include the factor arising from the isospin part of the amplitude this will give an extra factor of 2 in the numerator for each of the processes $p \to n\pi^+ \to p$ and $n \to p\pi^- \to n$ which are relevant here. There will also be a factor of ± 1 due to the respective charges of the pion in these processes. Using the Goldberger-Treiman relation, i.e. $g_{\pi N} = g_A m/f_\pi$, where $g_A = (F + D)$ is the axial-vector coupling constant, one then arrives at the following leading non-analytic term,

$$\mp\frac{(F+D)^2 m}{8\pi f_\pi^2} m_\pi\ , \tag{2.79}$$

which contributes to the chiral expansions for the magnetic moments of the proton and neutron respectively. This agrees exactly with the leading non-analytic term in Eq. (2.63) for the proton and neutron. Similar calculations may be performed for the entire baryon octet to obtain the leading non-analytic term in each magnetic moment expansion. A similar calculation could also be used to derive the leading non-analytic logarithmic terms which are present in electric charge radius expansions. The leading non-analytic terms in both the magnetic moment and charge radius expansions will be important in the remaining chapters, because we will use these terms in designing functions to extrapolate lattice results to the physical regime.

Chapter 3

The Cloudy Bag Model

In Chapter 2 we saw that chiral perturbation theory could be used to make expansions of hadronic observables. Our goal in this thesis is to extrapolate lattice results of hadronic observables obtained at large pion masses to the physical regime. It would be ideal to use chiral perturbation theory expansions directly to extrapolate the lattice results. However, the lattice results are obtained at large pion masses where chiral perturbation theory is not applicable. Thus these chiral expansions cannot be used directly. We must therefore find an alternative means to access the results obtained at large quark masses.

This leads us to consider a successful phenomenological model of baryons – the Cloudy Bag Model (CBM) [17, 18]. The CBM is a relativistic quark model of baryons which builds in the phenomena of quark confinement and pion emission. It is an extension of a simpler model, the MIT bag model, which describes baryons in terms of a system of relativistic quarks confined to a volume known as a "bag". The CBM Lagrangian consists of the MIT bag model Lagrangian coupled to a pion field in such a way that the resulting Lagrangian is invariant under chiral transformations. Unlike chiral perturbation theory, where baryons are considered as elementary, both the CBM and MIT bag model build in the underlying quark structure of baryons. This allows important considerations such as the finite size of baryons to be included in calculations.

The CBM can be used to explore the quark mass dependence of physical observables. One finds that the pion loop contributions to physical observables predicted in the CBM match those given by chiral perturbation theory in the chiral limit. This is expected since both models are based on chiral symmetry. However, in the CBM these contributions are suppressed at large pion masses by the form factors associated with the finite size of the hadron under study. Thus the CBM might be expected to provide a good guide to the behaviour of physical observables over a wide range of pion masses. This is a major improvement on chiral perturbation theory, which is only applicable near the chiral limit. In chiral perturbation theory the form factor suppression of pion loop contributions does not occur since the hadrons are treated as pointlike in canonical field theory. In practice the suppression of pion loop corrections in the CBM allows lattice results at large pion masses to be accessed in a convergent way. We will see this in § 3.4.

Our first task in this chapter is to introduce the MIT bag model and discuss its properties. The CBM will then be introduced and we will show how it improves on the MIT bag model. Since the CBM will eventually be used to extrapolate lattice results for magnetic moments, we will then discuss the electromagnetic properties of the CBM. Next we will show how lattice results for nucleon magnetic moments can be extrapolated within the CBM. Finally a simple extrapolation formula will be proposed for the nucleon magnetic moments which encompasses the CBM predictions, as well as agreeing with chiral perturbation theory and heavy quark effective theory in the appropriate limits. Eventually (in Chapter 4) this simple extrapolation formula will be extended to extrapolate lattice results for magnetic moments of the entire baryon octet.

3.1 The MIT bag model

The MIT bag model was one of the first attempts to model hadrons in terms of their underlying quark structure. This model builds in the observed quark confinement by permanently confining the quarks to a bag (a volume denoted by V). We now construct the MIT bag model Lagrangian and discuss the consequences and limitations of this model.

Consider a system of 3 massless, relativistic quarks moving freely in a volume, V. Inside this confining volume the quarks will move according to the Dirac equation. Hence, we consider the following Lagrangian

$$\mathcal{L}(x) = \sum_{i=1}^{3} i\,\bar{q}_i(x)\partial\!\!\!/ q_i(x)\,\theta_V \tag{3.1}$$

where $q_i(x)$ is the i^{th} quark field and

$$\theta_V = \begin{cases} 1 & \text{inside } V \\ 0 & \text{outside } V \end{cases} \tag{3.2}$$

is the step function for the confining region, V. From now on we use the Einstein summation convention, where repeated indices (such as "i" in Eq. (3.1)) are summed over. This Lagrangian is simply the Dirac Lagrangian for the quark fields, restricted to the volume V. In addition, there must be a boundary condition to ensure that there is no current flow through the surface of the confining region, S. We require that $n \cdot j \equiv n^\mu j_\mu = 0$ on S, where $j^\mu = \bar{q}_i\gamma^\mu q_i$ is the electromagnetic current and n^μ are the components of the unit vector normal to the confining region. In the MIT bag model this boundary condition is imposed via the following linear boundary condition

$$i\gamma \cdot n\; q_i \equiv i\gamma^\mu n_\mu\; q_i = q_i \tag{3.3}$$

which must be satisfied on S. Taking the Hermitian conjugate of Eq. (3.3), we see that

$$\bar{q}_i = -i\;\bar{q}_i\;\gamma \cdot n \tag{3.4}$$

on S also. Hence

$$i\,n \cdot j = i\,n^\mu\,\bar{q}_i\gamma_\mu q_i = \bar{q}_i q_i = -\bar{q}_i q_i = 0 \tag{3.5}$$

on S as required, where we have used Eqs. (3.3) and (3.4). Therefore we see that $\bar{q}_i q_i = 0$ on the surface of the confining region also.

The energy momentum tensor for the above Lagrangian, Eq. (3.1), is given by

$$T^{\mu\nu} = i\,\bar{q}_i\gamma^\mu\partial^\nu q_i\,\theta_V\ . \tag{3.6}$$

Energy momentum conservation requires that $\partial_\mu T^{\mu\nu} = 0$. However, this is not satisfied here since

$$\partial_\mu T^{\mu\nu} = i\,\bar{q}_i\gamma^\mu\partial^\nu q_i\,\partial_\mu\theta_V = i\,\bar{q}_i\gamma\cdot n\,\partial^\nu q_i\,\Delta_S = -\frac{1}{2}\partial^\nu\left[\bar{q}_i q_i\right]\Delta_S\ , \tag{3.7}$$

where Δ_S is the surface delta function defined by $\partial_\mu\theta_V = n_\mu\Delta_S$. Therefore, clearly $\partial_\mu T^{\mu\nu}$ is non-zero on S, and we do not have energy momentum conservation. This problem can be avoided if the Lagrangian contains an extra term as follows

$$\mathcal{L}(x) = (i\bar{q}_i(x)\partial\!\!\!/ q_i(x) - B)\,\theta_V\ , \tag{3.8}$$

where B is a constant given by

$$B = -\frac{1}{2}n\cdot\partial\left[\bar{q}_i(x)q_i(x)\right]\Big|_S\ . \tag{3.9}$$

The term $-B\theta_V$ is a phenomenological term describing the difference in the energy density of the vacuum inside and outside the bag. It is an assumption of the MIT bag model that B is the same constant for each hadron (B is known as the bag constant). The full MIT bag model Lagrangian is given by

$$\mathcal{L}_{MIT}(x) = i\bar{q}_i(x)\partial\!\!\!/ q_i(x)\theta_V - B\theta_V - \frac{1}{2}\bar{q}_i(x)q_i(x)\Delta_S \ , \tag{3.10}$$

where the final term is a Lagrange multiplier which ensures that $\bar{q}_i(x)q_i(x) = 0$ on the surface of the confining region, S. The equations of motion of the MIT Lagrangian are generated by demanding that the MIT action, $S_{MIT} = \int d^4x \mathcal{L}_{MIT}(x)$, is stationary under arbitrary variations of the fields and bag surface. As expected we recover the massless Dirac equation

$$i\partial\!\!\!/ q_i(x) = 0 \qquad \forall x \in V \ , \tag{3.11}$$

as well as the linear boundary condition, Eq. (3.3), and the bag stability condition (or non-linear boundary condition), Eq. (3.9).

In the case of a static, spherical confining region of radius R, exact solutions of the MIT bag model equations can be found. The exact solution for the case $l = 0$ is given by

$$q_i(r) = N_i \begin{bmatrix} j_0(\omega_i r/R) \\ i\sigma \cdot \hat{r} j_1(\omega_i r/R) \end{bmatrix} b_i \theta(R-r) \ , \tag{3.12}$$

where N_i is a normalization constant, b_i contains the spin and isospin information for the wavefunction and $j_l(z)$ are spherical Bessel functions. (Since the non-linear boundary condition of Eq. (3.9) is angle independent, only quark wavefunctions with $j = 1/2$ can satisfy this condition. Hence only $l = 0, 1$ are allowed.) The quark frequency, ω_i, for the solution Eq. (3.12) can be found from the linear boundary condition, Eq. (3.3), which amounts to

$$j_0(\omega_i) = j_1(\omega_i) \ . \tag{3.13}$$

Solving this condition gives a ground state frequency of $\omega_0 = 2.04$. The energy of this (single quark) ground state is given by

$$E = \frac{\omega_0}{R} = \frac{2.04}{R} \ . \tag{3.14}$$

Thus the total mass of a baryon with all quarks in the ground state is given by

$$M(R) = \frac{3\omega_0}{R} + \frac{4}{3}\pi R^3 B - \frac{Z_0}{R} \ , \tag{3.15}$$

where the second term arises from the phenomenological energy density term in the MIT Lagrangian and the last term is the zero point energy contribution, arising from quantization (Z_0 is a constant phenomenological parameter). It can be shown that the non-linear boundary condition, Eq. (3.9), is equivalent to requiring that

$$\frac{\partial M}{\partial R} = 0 \ . \tag{3.16}$$

This condition, together with Eq. (3.15), allows the bag radius to be calculated as a function of the ground state frequency, ω_0, and phenomenological parameters, Z_0 and B, as follows

$$R^4 = \frac{3\omega_0 - Z_0}{4\pi B} \ . \tag{3.17}$$

Note that the full mass formula should also include a contribution from the one-gluon exchange. We have neglected this term for simplicity, but it is easily included.

Clearly the approximation of massless quarks in the MIT bag model Lagrangian leads to degenerate masses for all members of the baryon octet. This situation can be rectified by adding explicit quark mass terms to the MIT Lagrangian. That is, one adds the term $m_i\bar{q}_i(x)q_i(x)$ to Eq. (3.10). The analysis with non-zero quark masses proceeds in exactly the same way as the massless case, with exact solutions for the spherical, static case given by

$$q_i(r) = N_i \begin{bmatrix} \left(\frac{E_i+m_i}{E_i}\right)^{1/2} j_0\left(\omega_i r/R\right) \\ \left(\frac{E_i-m_i}{E_i}\right)^{1/2} i\boldsymbol{\sigma}\cdot\hat{\mathbf{r}} j_1\left(\omega_i r/R\right) \end{bmatrix} b_i\theta(R-r) \ , \tag{3.18}$$

where

$$E_i(m_i,R) = \frac{1}{R}\left[w_i^2 + (m_i R)^2\right]^{1/2} \ . \tag{3.19}$$

Since our examples deal primarily with nucleon wavefunctions (and nucleons are made up of light quarks), we will neglect this subtlety in the following and use the massless MIT Lagrangian, Eq. (3.10), and its solutions, Eq. (3.12), for simplicity.

Notice that so far we have not mentioned the colour degree of freedom in this discussion of the MIT bag model. To introduce colour interactions between quarks we would modify the MIT Lagrangian by making the following substitution: $i\partial\!\!\!/ q \rightarrow i\not{D} q$, where $i\not{D} q$ includes couplings to the gluon fields. One would also need to include a kinetic energy term for the gluon fields, $F^a_{\mu\nu}F^{\mu\nu}_a$, in the modified Lagrangian. The details of making these substitutions can be found in Ref. [17]. By considering the conserved charges associated with the modified Lagrangian, it can be shown [17] that all finite energy solutions of the MIT bag model equations are colour singlets. This shows that the MIT bag model produces the observed confinement of colour.

Historically, one of the most important successes of the MIT bag model was the prediction of the axial coupling constant, g_A. The MIT bag model predicts $g_A = 1.27$ (including centre of mass corrections) [18], compared with the experimental value $g_A = 1.26$. The model also provides a much improved prediction for the proton magnetic moment compared to the naive quark model expectation. However, the MIT bag model produces disappointing results for the neutron charge radius; it predicts that the neutron mean square charge radius is exactly zero [18], in contrast to the experimental value of $-0.113(4)$ fm^2 [30]. Also the model does not describe interactions between hadrons, and therefore is not useful for nuclear physics problems. These problems with the MIT bag model originate from the lack of chiral symmetry in the model.

The MIT bag model Lagrangian is not invariant under chiral transformations. This is due to the $\bar{q}q\Delta_S$ term in Eq. (3.10) which is not chirally invariant. This violation of chiral symmetry can be illustrated by the schematic diagram in Fig. 3.1 together with the following explanation. Because of confinement, all quarks impinging on the interior bag surface must be reflected. However, since the MIT Lagrangian does not contain a spin-flipping mechanism, the quark's spin is not affected by this reflection, even though it now travels in the opposite direction. This means that the quark has changed its chirality by striking the boundary. Hence chiral symmetry is violated.

Lack of chiral symmetry means that the axial current of the MIT Lagrangian is not conserved. This conflicts with strong experimental evidence to support the partially conserved axial current (PCAC) hypothesis in the strong interactions. Moreover, as discussed in § 2.1, chiral symmetry is a fundamental property of QCD, and is expected in any reasonable model of the strong interactions.

We now present a bag model for baryons, the Cloudy Bag Model (CBM), which incorporates the MIT bag model, but improves on it by building in chiral symmetry. This involves the introduction of pions into the model and thus provides a mechanism by which baryons can interact.

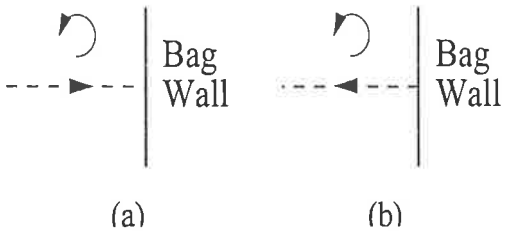

Figure 3.1: Schematic illustration of chiral symmetry breaking in the MIT bag model. In (a) the quark travels towards the bag surface. The upper arrow indicates the quark's spin. In (b) the quark is reflected from the bag wall without changing its spin. Clearly the chirality (or "handedness") of the quark is changed in this interaction. Hence chiral symmetry is broken.

3.2 The Cloudy Bag Model

The linearized Lagrangian of the Cloudy Bag Model (CBM) is given very simply by

$$\mathcal{L}_{CBM}(x) = \mathcal{L}_{\rm MIT}(x) + \mathcal{L}_{\pi}(x) + \mathcal{L}_{\rm int}(x) \ , \tag{3.20}$$

where $\mathcal{L}_{\rm MIT}$ is given in Eq. (3.10), $\mathcal{L}_{\pi}$ is given by

$$\mathcal{L}_{\pi} = \frac{1}{2}(\partial_{\mu}\pi)^2 - \frac{1}{2}m_{\pi}^2\pi^2 \ , \tag{3.21}$$

and $\mathcal{L}_{\rm int}$, which describes the pseudoscalar interactions of nucleons and pions, is given by

$$\mathcal{L}_{\rm int} = -\frac{i}{2f_{\pi}}\bar{q}\gamma_5\tau\cdot\pi q\Delta_S \ . \tag{3.22}$$

Note that without this interaction term, the theory would describe free pions and stable MIT bag configurations. Thus the linearized CBM Lagrangian is given explicitly by

$$\mathcal{L}_{CBM} = (i\bar{q}\partial\!\!\!/ q - B)\theta_V - \frac{1}{2}\bar{q}q\Delta_S + \frac{1}{2}(\partial_{\mu}\pi)^2 - \frac{1}{2}m_{\pi}^2\pi^2 - \frac{i}{2f_{\pi}}\bar{q}\gamma_5\tau\cdot\pi q\Delta_S \ . \tag{3.23}$$

Notice that although the CBM includes the constituent quark structure of baryons, it does not include the underlying quark structure of the pions, i.e. the pion is treated as an elementary field. This is an assumption of the model. In the CBM a long wavelength approximation is made such that the internal structure of the pion can be neglected. It has been shown in Refs. [17, 18] that this is a good approximation in many situations involving low momentum transfer.

A further simplification is made when calculating physical observables in the CBM. One assumes that the quark wavefunction is unperturbed by the presence of the pion field, i.e., one takes the first order approximation for the quark wavefunctions. This allows the exact MIT bag model solutions, Eqs.(3.12) and (3.18), to be used in calculations of physical observables. A final assumption made in CBM calculations is that the linearized Lagrangian, Eq. (3.23), is a sufficient approximation to the full, non-linear CBM Lagrangian. (We do not show the full, non-linear CBM Lagrangian here, but it can be found in Refs. [17, 18].)

The CBM Lagrangian is invariant under chiral symmetry [17, 18]. It also includes pions which mediate the interactions of the baryons. Thus the CBM overcomes the major problems of the MIT bag model. It also retains the good features of the MIT bag model. For example, the axial coupling constant prediction in the CBM is $g_A = 1.27$ (with centre of mass corrections)[17, 18], just as in the MIT bag model (and in very good agreement with the experimental value).

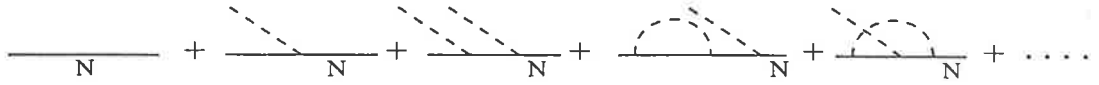

Figure 3.2: The first terms in the expansion of the nucleon state $|N\rangle$ in Eq. (3.30), where the unspecified internal lines are either N or Δ.

The CBM Hamiltonian, H, is obtained from the CBM Lagrangian in the canonical way: $H = \int d^3x T^{00}_{CBM}(x)$, where $T^{\mu\nu}_{CBM}$ is the energy-momentum tensor corresponding to the (linearized) CBM Lagrangian, Eq. (3.23). This Hamiltonian can be decomposed as

$$H = H_0 + H_{\rm int} \ , \tag{3.24}$$

where the bare Hamiltonian, H_0, describes free pions and stable MIT bag configurations and the interaction Hamiltonian, $H_{\rm int}$, describes the quark-pion interactions. The explicit expressions for H_0 and $H_{\rm int}$ can be found in Ref. [17, 18]. There are two types of baryonic eigenstates for the bare Hamiltonian, H_0. Firstly there are eigenstates which are simply bare MIT bag states (i.e. no pions); for example, the bare nucleon state, $|N_0\rangle$. The second type consists of bare bag states with n pions, such as the state $|N_0, n\rangle$ (where $|n\rangle$ represents the state with n pions). These states are obtained from the bare bag states by repeated applications of the pion creation operators. From this point we restrict the discussion to non-strange baryons for simplicity.

The physical nucleon state, $|N\rangle$, is an eigenstate of the full CBM Hamiltonian, H. That is, $H|N\rangle = E_N|N\rangle$. We now wish to express $|N\rangle$ in terms of eigenstates of the bare Hamiltonian, H_0. It is clear that $|N\rangle$ can be written in the form

$$|N\rangle = Z_2^N(E_N)^{1/2}|N_0\rangle + \Lambda|N\rangle \ , \tag{3.25}$$

where $Z_2^N(E_N)$ is the probability of the physical nucleon state being bare and Λ is a projection operator which projects out all components of $|N\rangle$ containing at least one pion. Λ is given explicitly by

$$\Lambda = 1 - \sum_{B=N,\,\Delta} |B_0\rangle\langle B_0| \tag{3.26}$$

where the sum extends only over N and Δ since we have restricted to non-strange baryons and the lowest mass intermediate states. Now since $[\Lambda, H_0] = 0$ (this can be seen easily from the explicit expression for H_0, see Refs. [17, 18]) we are free to write

$$\Lambda|N\rangle = (E_N - H_0)^{-1}\Lambda(E_N - H_0)|N\rangle \ , \tag{3.27}$$

and hence

$$|N\rangle = Z_2^N(E_N)^{1/2}|N_0\rangle + G_0(E_N)\Lambda H_{\rm int}|N\rangle \ , \tag{3.28}$$

where

$$G_0(E_N) = (E_N - H_0)^{-1} \tag{3.29}$$

is the bare bag propagator. Using this recursive expression for $|N\rangle$ we find

$$|N\rangle = Z_2^N(E_N)^{1/2}(1 + G_0(E_N)\Lambda H_{\rm int} + G_0(E_N)\Lambda H_{\rm int}G_0(E_N)\Lambda H_{\rm int} + \ldots)|N_0\rangle \tag{3.30}$$

This relation for $|N\rangle$ can be conveniently expressed as a sum of diagrams, shown in Fig. (3.2). Note that the solid lines represent the baryon and dashed lines denote the pion. The complete set of rules and conventions for these diagrams can be found in Ref. [17].

3.3 Electromagnetic Properties of Baryons in the CBM

In this section we use the CBM to make predictions for the electric charge radii and magnetic moments of baryons. To do this we must first derive formal expressions for the Sachs electric and magnetic form factors, $G_E(q^2)$ and $G_M(q^2)$, which were introduced in § 2.5. The electric charge radius and magnetic moment of the baryon can then be extracted from these form factors using the relations given in Eqs. (2.60) and (2.61). Recall from § 2.5 that in the Breit frame, where the momentum transfer 4-vector satisfies $q^0 = 0$, the Sachs form factors for a baryon, B, are related to the spatial electromagnetic current, $J^\mu(\vec{r})$, by

$$\langle B \left| J^0(\vec{r}) \right| B \rangle = \frac{e}{(2\pi)^3} \int d^3q \; G_E(q^2) e^{-i\vec{q}\cdot\vec{r}} \tag{3.31}$$

$$\left\langle B, s_B \left| \vec{J}(\vec{r}) \right| B, s_B \right\rangle = \frac{ie}{(2\pi)^3} \int d^3q \; G_M(q^2) \, \langle s_B \left| \vec{\sigma}\times\vec{q} \right| s_B \rangle \, e^{-i\vec{q}\cdot\vec{r}} \tag{3.32}$$

where all quantities are defined in § 2.5. Thus the first step in the derivation of the CBM Sachs form factors is calculating the electromagnetic current.

Electromagnetic interactions are introduced into the CBM Lagrangian in the standard way: the substitution $\partial_\mu \to \partial_\mu + iqA_\mu$ is made, where q is the charge of the field that the derivative acts on in each case. The following Lagrangian is obtained ($e = |e|$ everywhere)

$$\begin{aligned} \mathcal{L}_{CBM}(x) = & \sum_{i=1}^{3} \bar{q}_i \, i \, (\partial\!\!\!/ + i \, e_i \, \bar{A}\!\!\!/) \, q_i \, \theta_V - B\theta_V - \frac{1}{2} \sum_{i=1}^{3} \bar{q}_i \, q_i \, \Delta_s \\ & - \frac{i}{2f_\pi} \sum_{i=1}^{3} \bar{q}_i \, \tau \cdot \pi \, q_i \, \Delta_s + \frac{1}{2}((\partial_\mu \pi_3)^2 - m_\pi^2 \pi_3^2) \\ & + [(\partial^\mu + i \, e \, A^\mu) \, \pi^\dagger] \cdot [(\partial_\mu - i \, e \, A_\mu) \, \pi] - m_\pi^2 \pi^\dagger \pi - \frac{1}{4} F_{\mu\nu} F^{\mu\nu} \end{aligned} \tag{3.33}$$

where

$$\pi(x) = \frac{1}{\sqrt{2}} [\pi_1(x) + i\pi_2(x)] \tag{3.34}$$

is the charged pion field. After quantization of the fields, the π operator will destroy π^- and create π^+ particles. The Lagrangian in Eq. (3.33) is invariant under the following local infinitesimal transformations

$$q_i(x) \to q_i(x) - i \, e_i \, \epsilon(x) q_i(x) \; , \tag{3.35}$$

$$\pi(x) \to \pi(x) - i \, e \, \epsilon(x) \pi(x) \; , \tag{3.36}$$

$$A^\mu(x) \to A^\mu(x) - \frac{1}{e} \partial^\mu \epsilon(x) \; . \tag{3.37}$$

The conserved current associated with these transformations is the electromagnetic current, $J^\mu(x)$, which is given by

$$J^\mu(x) = j^{\mu(\mathrm{Q})}(x) + j^{\mu(\pi)}(x) \tag{3.38}$$

where

$$j^{\mu(\mathrm{Q})}(x) = \sum_{i=1}^{3} e_i \, \bar{q}_i(x) \gamma^\mu q_i(x) \, \theta_V \tag{3.39}$$

$$j^{\mu(\pi)}(x) = -ie(\pi^\dagger(x)\partial^\mu \pi(x) - \pi(x)\partial^\mu \pi^\dagger(x)) \tag{3.40}$$

Since the total electromagnetic current can be decomposed into a sum of contributions from the quark core and pion cloud, it can be seen from Eqs. (3.31) and (3.32) that the Sachs form factors

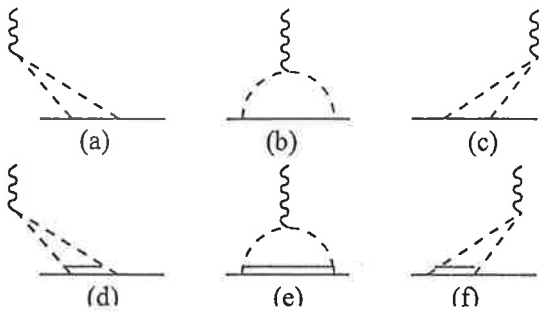

Figure 3.3: Lowest order time-ordered diagrams contributing to the pion part of the electromagnetic form factors for the nucleon. Double lines represent the Δ resonance and wiggly lines denote the photon. The complete set of rules for these diagrams can be found in Ref. [17].

also undergo this decomposition, i.e., $G_X(q^2) = G_X^{(Q)}(q^2) + G_X^{(\pi)}(q^2)$, where $X = E, M$. Thus we determine the Sachs form factors by calculating the quark core and pion cloud contributions separately.

First we calculate the pion cloud contribution to the form factors. This involves calculating the expectation value $\langle B | j^{\mu(\pi)}(\vec{r}) | B \rangle$, where the classical pion current, $j^{\mu(\pi)}(x)$, is given in Eq. (3.40). Thus we begin by quantizing the pion fields, π_i, as follows

$$\pi_i(\vec{r}, t=0) = \int d^3k \frac{1}{\sqrt{2w_k(2\pi)^3}} \left\{ a_i(\vec{k}) e^{i\vec{k}\cdot\vec{r}} + a_i^\dagger(\vec{k}) e^{-i\vec{k}\cdot\vec{r}} \right\} \tag{3.41}$$

where the operators $a_i(\vec{k})$ and $a_i^\dagger(\vec{k})$ obey the usual bosonic commutation relations:

$$\left[a_i(\vec{k}), a_j(\vec{k'}) \right] = \left[a_i^\dagger(\vec{k}), a_j^\dagger(\vec{k'}) \right] = 0 \ , \tag{3.42}$$

$$\left[a_i(\vec{k}), a_j^\dagger(\vec{k'}) \right] = \delta_{ij}\, \delta^{(3)}(\vec{k} - \vec{k'}) \ . \tag{3.43}$$

In terms of creation and annihilation operators, the pion current is given by

$$j^{\mu(\pi)}(\vec{r}) = -\frac{ie}{2} \sum_{i,j} \epsilon_{ij3} \int \frac{d^3k\, d^3k'}{(2\pi)^3 (\omega_k \omega_{k'})^{1/2}} k^\mu\, S_\pi(\vec{k}_i, \vec{k'}_j; \mu)\, e^{i(\vec{k}-\vec{k'})\cdot\vec{r}} \tag{3.44}$$

where

$$S_\pi(\vec{k}_i, \vec{k'}_j; \mu) = \left[a_j(-\vec{k'}) + a_j^\dagger(\vec{k'}) \right] \left[a_i(\vec{k}) - g^{\mu\mu} a_i^\dagger(-\vec{k}) \right] \tag{3.45}$$

and there is no sum over μ in $g^{\mu\mu}$ (recall that $g^{00} = 1$ and $g^{ii} = -1$ in our conventions).

Now that the pion part of the electromagnetic current has been expressed in terms of operators, Eqs. (3.44) – (3.45), we can calculate the expectation value $\langle B | j^{\mu(\pi)}(\vec{r}) | B \rangle$. This allows the pion contribution to the form factors, $G_X^{(\pi)}(q^2)$, to be determined via Eqs. (3.31) and (3.32). Here we show the steps in this calculation for the nucleon. The calculation is analogous for other baryons. Firstly, the physical nucleon state, $|N\rangle$, must be written in terms of bare bag states as in Eq. (3.30). Secondly, one inserts a complete set of the bare eigenstates between each operator in the expectation value. After making these substitutions, it can be seen [17, 18] that the lowest order processes contributing to the pion part of the form factors are the processes depicted in Fig. 3.3. Evaluating the diagrams Fig. 3.3(a)–(c) leads to the following expressions for the processes where the intermediate baryon is a nucleon,

$$G_E^{(\pi)}(q^2; N) = \frac{1}{36\pi^3} \left(\frac{f^{NN}}{\mu} \right)^2 \int d^3k \frac{u(kR) u(k'R) \vec{k} \cdot \vec{k'}}{\omega_k \omega_{k'} (\omega_k + \omega_{k'})} \langle N | \tau_3 | N \rangle \tag{3.46}$$

$$G_M^{(\pi)}(q^2;N) = \frac{m_N}{36\pi^3}\left(\frac{f^{NN}}{\mu}\right)^2 \int d^3k \frac{u(kR)u(k'R)(\hat{q}\times\vec{k})^2}{(\omega_k\omega_{k'})^2}\langle N|\tau_3|N\rangle \qquad (3.47)$$

where $\vec{k'} = \vec{k} + \vec{q}$, $\omega_k = \sqrt{k^2+m_\pi^2}$, $\mu = 139$ MeV is the physical pion mass, f^{NN} is the renormalized NN coupling constant [17] and $u(kR) = 3j_1(kR)/kR$. Similar expressions are obtained for $G_E^{(\pi)}(q^2;\Delta)$ and $G_M^{(\pi)}(q^2;\Delta)$, where Δ is the intermediate baryon state (Fig. 3.3(d)–(f)). The explicit expressions for $G_E^{(\pi)}(q^2;\Delta)$ and $G_M^{(\pi)}(q^2;\Delta)$ can be found in Refs. [17, 31].

The pion contribution to the form factors gives rise to non-analytic behaviour in the expansions of electric charge radii and magnetic moments. As an example we consider the one-loop pion contribution to the nucleon magnetic form factor. As we will see, this contribution produces the leading non-analytic term in the nucleon magnetic moment expansion. Recall that the pion contribution to the nucleon magnetic moment is given by $G_M^{(\pi)}(0;N) + G_M^{(\pi)}(0;\Delta)$. It can be shown [32] that the leading non-analytic behaviour in the nucleon magnetic moment expansion originates from the $G_M^{(\pi)}(0;N)$ piece of the pion form factor, where the intermediate baryon is a nucleon. From Eq. (3.47) this contribution can be written as

$$\begin{aligned} G_M^{(\pi)}(0;N) &= \frac{m_N}{18\pi^2}\left(\frac{f^{NN}}{\mu}\right)^2 \langle N|\tau_3|N\rangle \int_0^\pi d\theta sin^3\theta \int_0^\infty dk \frac{k^4u^2(kR)}{\omega_k^4} \\ &= \frac{m_N}{18\pi^2}\left(\frac{f^{NN}}{\mu}\right)^2 \frac{4}{3}\langle N|\tau_3|N\rangle \int_0^\infty dk \frac{k^4u^2(kR)}{(k^2+m_\pi^2)^2} \end{aligned}$$

The remaining integral can be evaluated using residue methods, since $u(kR) \equiv 1$ at $k = \pm im_\pi$ by definition. One finds that the leading non-analytic contribution from $G_M^{(\pi)}(0;N)$ is given by

$$\left\{-\frac{m_N}{18\pi}\left(\frac{f^{NN}}{\mu}\right)^2\langle N|\tau_3|N\rangle\right\} m_\pi \ . \qquad (3.48)$$

The coefficient in braces agrees with the coefficient of the $O(m_\pi)$ term in the magnetic moment chiral expansion, Eq. (2.63), which is given by $\mp(F+D)^2 m_N/(8\pi f_\pi^2)$ for $N = p/n$. This can be seen by numerically evaluating each coefficient (using $f^{NN} \approx 3.03$ and $(F+D) = g_A = 1.26$). Thus the one-loop pion contribution to the magnetic moment produces the leading non-analytic term predicted in chiral perturbation theory.

We now briefly consider the quark contribution to the form factors. This contribution is not as interesting as the pion contribution, since it is the pion contribution which gives rise to the leading non-analytic behaviour in the chiral expansions. In terms of creation and annihilation operators the quark contribution to the current is obtained by substituting the MIT bag model wavefunctions, given in Eq. (3.12), into the expression for $j^{\mu(Q)}(x)$, given in Eq. (3.39). The following expressions are obtained

$$j^{0(Q)}(\vec{r}) = \sum_{i=1}^{3} e_i N_i^2 \left[j_0^2\left(\frac{\omega_i r}{R}\right) + j_1^2\left(\frac{\omega_i r}{R}\right)\right] b_i^\dagger b_i \,\theta(R-r) \qquad (3.49)$$

$$\vec{j}^{(Q)}(\vec{r}) = \sum_{i=1}^{3} 2\, e_i N_i^2 \omega_i\, j_0\left(\frac{\omega_i r}{R}\right) j_1\left(\frac{\omega_i r}{R}\right) b_i^\dagger\, \vec{\sigma}\times\hat{r}\, b_i \qquad (3.50)$$

The calculation of $G_E^{(Q)}(q^2)$ is very simple. It involves calculating the following expectation value (where the sum over i is implicit)

$$\left\langle N\left|j^{0(Q)}(\vec{r})\right|N\right\rangle = \left[j_0^2\left(\frac{\omega_i r}{R}\right) + j_1^2\left(\frac{\omega_i r}{R}\right)\right]\theta(R-r)\left\langle N\left|e_i b_i^\dagger b_i\right|N\right\rangle \qquad (3.51)$$

This is simple to calculate since the operator $e_i\, b_i^\dagger\, b_i$ simply counts the quark charge of the baryon state. The explicit expression for $G_E^{(Q)}(q^2)$ can then be obtained by inverting Eq. (3.31). This expression is given in Ref. [17]. The calculation of the quark contribution to the magnetic form factor, $G_M^{(Q)}(q^2)$, is very similar to the calculation of $G_M^{(\pi)}(q^2)$ described above. However, since it is mainly the pionic contribution that we are interested in, we will not go through this calculation. The full calculation can be found in Ref. [17].

3.4 Using the CBM to extrapolate magnetic moments

In this section we show how the CBM can be used to extrapolate lattice QCD results for physical observables. In particular, we consider extrapolating lattice results for nucleon magnetic moments within the CBM. This extrapolation was first performed in Ref. [11]. Here we give a general overview of the extrapolation procedure used in Ref. [11]. In this section we will not discuss how the lattice results were obtained, but simply consider the results as "data" for the nucleon magnetic moments at 6 rather heavy pion masses. Details of the lattice calculations can be found in Ref. [11] and also in Refs. [33] and [34], where the results were originally published.

The aim here is to calculate nucleon magnetic moments in the CBM over a range of different pion masses. As we will see, there are 3 input parameters in this calculation which can be tuned to best accommodate the lattice results. The experimental value ($\mu_p = 2.713\ \mu_N$, $\mu_n = -1.913\ \mu_N$) will also be included in the data set in each extrapolation. This will make it possible to determine whether the lattice results at large m_π are consistent with experimental measurements. Historically the inclusion of the experimental point in the extrapolations is important since previous extrapolations (which used either simple linear fits as a function of m_π^2 or chiral perturbation theory expansions directly) had been unable to make contact with both the lattice results at large m_π and the experimental point at the physical pion mass, $\mu = 139$ MeV.

Recall that the nucleon magnetic moment is given by

$$\mu_N = G_M^{(Q)}(q^2 = 0) + G_M^{(\pi)}(q^2 = 0)\ , \tag{3.52}$$

where the full expressions for the one-loop contributions can be found in Refs. [17, 31]. (In Eq. (3.47) the one-loop pion contribution is given for the case where the intermediate state is a nucleon. As discussed in § 3.3, the full $G_M^{(\pi)}(q^2 = 0)$ includes terms arising from the Δ also.) Note that the magnitude of each contribution in Eq. (3.52) is related to the bag radius, R. When the bag radius is large the contribution from the quark core is enhanced and the pion cloud contribution, $G_M^{(\pi)}(0)$, is suppressed. In this extrapolation we use the following phenomenological form for the form factor, $u(k)$:

$$u(k) = \frac{\Lambda^2 - \mu^2}{\Lambda^2 + k^2} \tag{3.53}$$

where μ is the physical pion mass, k is the loop momentum and Λ is a (constant) cut-off value. Λ is one of the input parameters of this extrapolation and can be adjusted to fit the data.

Before extrapolating the lattice data a number of relationships between parameters of the CBM must be established. In particular, all parameters of the CBM (e.g. the bag radius, R, the ground state frequency, ω_0, the bag constant, B, etc.) must be expressed in terms of the input parameters and/or the changing pion mass. The first relationship to establish is the connection between the quark mass, m_q, and the pion mass, m_π. In the CBM the pion is considered as an elementary field and its underlying quark structure is not included in the model (long wavelength approximation). In particular, this means that the pion mass, m_π, is not directly related to the quark mass, m_q, inside the bag. However, since we are extrapolating lattice results within the CBM as a function of m_π, a relationship between m_π and m_q is essential. In the range of

pion masses considered in this extrapolation, current lattice simulations indicate that $m_\pi^2 \propto m_q$. Therefore, we write

$$m_q = \left(\frac{m_\pi}{\mu}\right)^2 m_q^{(0)} \ , \tag{3.54}$$

where μ is the physical pion mass and $m_q^{(0)}$ is an input parameter which can be tuned to best fit the results. $m_q^{(0)}$ corresponds to the current quark mass at the physical pion mass. It should lie in the range $\approx 5 - 7$ MeV to be consistent with perturbative QCD results.

We now consider finding a relationship between the radius of the confining region, R, and the changing pion mass, m_π. The authors of Ref. [11] used the following relation, Eq. (3.17), to determine the radius of the bag[1]

$$R^4 = \frac{3\omega_0 - Z_0}{4\pi B} \ , \tag{3.55}$$

where the ground state frequency, ω_0, is given by the smallest positive solution of

$$\tan\omega = \frac{\omega}{1 - m_q R - [\omega^2 + (m_q R)^2]^{1/2}} \ . \tag{3.56}$$

Thus we see that the quantities R and ω_0 are intimately connected and both change as the pion (or quark) mass is changed. Therefore the ground state MIT bag model solutions, Eqs. (3.12) and (3.18), depend on the changing pion mass, m_π, through their dependence on R and ω_0. This means that the Sachs form factors, which are evaluated using the MIT bag model solutions, are also dependent on m_π.

At the physical pion mass the ground state frequency, $\omega_0^{(0)}$, may be evaluated in terms of input parameters as follows

$$\tan\omega_0^{(0)} = \frac{\omega_0^{(0)}}{1 - m_q^{(0)} R_0 - [(\omega_0^{(0)})^2 + (m_q^{(0)} R_0)^2]^{1/2}} \ , \tag{3.57}$$

where R_0 is the bag radius at the physical pion mass. By substituting the value obtained for $\omega_0^{(0)}$ from Eq. (3.57) into Eq. (3.55), we produce the following linear equation relating the parameters B and Z_0, which are both assumed to be independent of m_π,

$$4\pi R_0^4 B = 3\omega_0^{(0)} - Z_0 \tag{3.58}$$

To fully determine Z_0 and B we must find a second equation relating these two quantities. Equating the physical nucleon mass, $m_N = 940$ MeV, with the $M(R_0)$ from Eq. (3.15), gives such a relation. Thus B and Z_0 can be fully determined.

Since B and Z_0 can be expressed in terms of the input parameters, it follows from Eqs. (3.55) and (3.56) that the radius of the bag, R, and ground state frequency, ω_0, can be evaluated numerically at each pion mass considered in the extrapolation. This allows the magnetic moments to be determined within the CBM over the range of pion masses. By tuning the input parameters one can fit the lattice data and experimental point with the CBM predictions and obtain the extrapolations shown in Figs. 3.4 and 3.5.

From Figs. 3.4 and 3.5 it is clear that the CBM can accommodate both the lattice results and experimental measurements for the nucleon magnetic moments in smooth extrapolation curves. The reasonable values obtained for the input parameters (see Table 3.4) support the assumptions

[1] A small correction arising from the dependence of ω_0 on R was later found to this relation in Ref. [12], but it did not significantly affect the results.

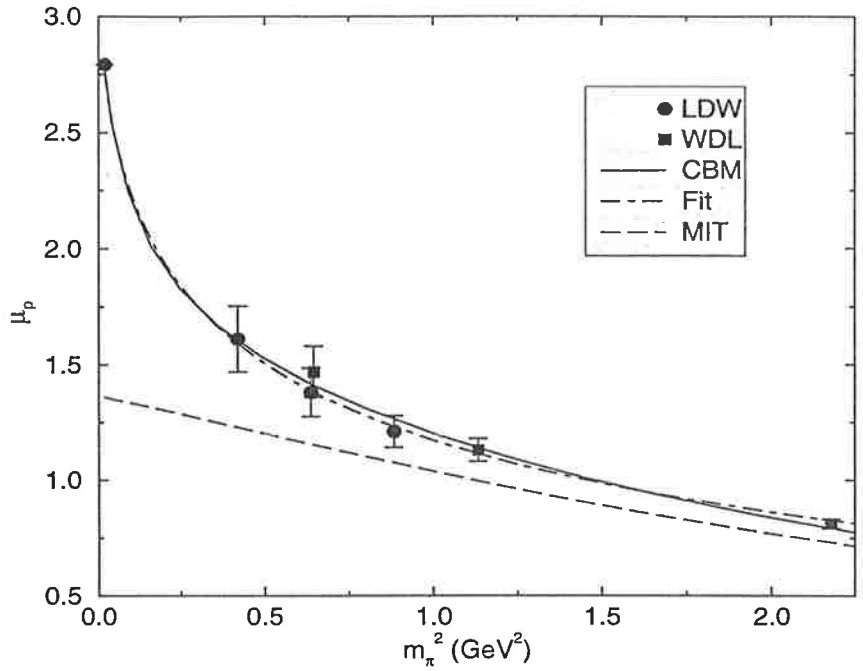

Figure 3.4: Fits of magnetic moment lattice data for the proton using the Cloudy Bag Model (CBM). The input parameters used for the CBM extrapolation are given in Table 3.4. The lattice results from Ref. [33] (LDW) are indicated by circles and the results from Ref. [34] (WDL) by squares. The solid line indicates the CBM fit to the data and the dashed line represents the MIT bag model, where the pion cloud is omitted. The dot-dashed line is the fit using the encapsulating formula, Eq. (3.61). The experimental point is included in each fit.

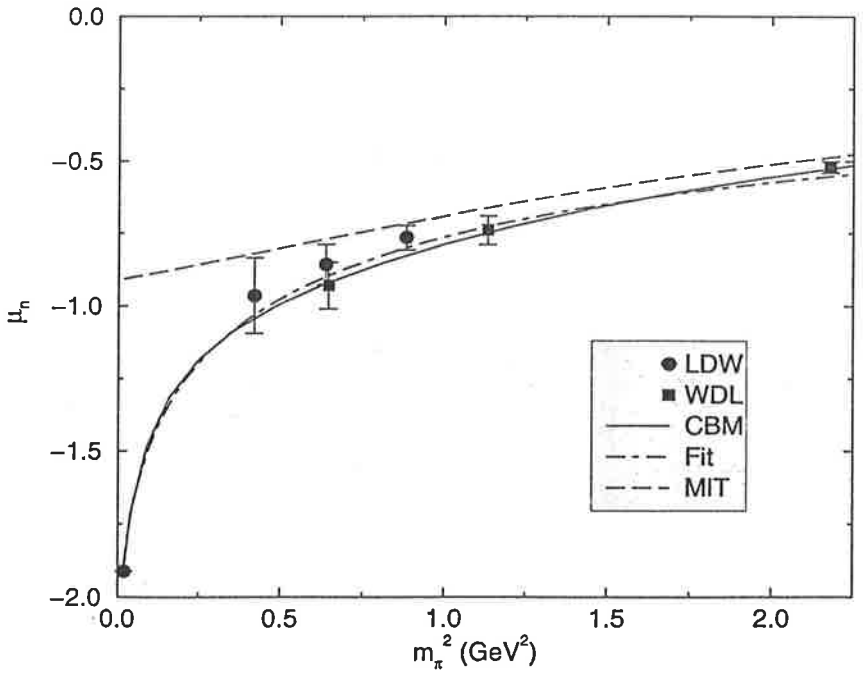

Figure 3.5: Fits of magnetic moment lattice data for the neutron using the Cloudy Bag Model (CBM). The input parameters for the CBM extrapolation are given in Table 3.4. Symbols and line types are defined in the caption of Fig. 3.4 and in the key.

Nucleon	R_0 (fm)	Λ (GeV)	$m_q^{(0)}$ (MeV)
p	1.0	0.68	4.8
n	1.0	0.59	4.8

Table 3.1: Input parameters for the CBM extrapolations shown in Figs. 3.4 and 3.5.

used in the extrapolation procedure (e.g. B was assumed to be independent of m_π). Comparing the CBM extrapolation curves with the corresponding MIT bag model extrapolations, one can clearly see that the meson cloud is very important and accounts for the significant curvature in the fits in the small m_π regime. This indicates that the notion of using chiral expansions to extrapolate the results is not completely unreasonable, since these expansions focus on the meson cloud effects. However, it is simply not appropriate to use chiral expansions to extrapolate lattice results obtained at large pion masses far from the chiral limit. Thus the CBM, which respects chiral symmetry while building in good phenomenology, is a much more suitable tool for extrapolating the results. We now consider encapsulating the CBM extrapolation curves in an analytic formula which may be regarded as an analytic continuation of chiral perturbation theory.

3.5 Encapsulating formula

In § 3.4 we saw that lattice results for nucleon magnetic moments could be smoothly extrapolated to the experimental value within the CBM. However, as we have seen, the algorithm for this extrapolation procedure is very complicated. In this section we wish to encapsulate the CBM extrapolation curves, shown in Figs. 3.4 and 3.5, in a simpler, analytic continuation of chiral perturbation theory.

To construct an analytic extrapolation formula we first note the qualitative features of the CBM fits. In both extrapolations the magnetic moment falls off at large values of m_π. This indicates that an encapsulating formula might take the form m_π^{-n}, for some integer n, in the heavy pion mass regime. In fact we expect that at heavy quark (or pion) masses the magnetic moment should fall off as the Dirac moment:

$$\mu = \frac{e_q}{2m_q} \propto \frac{1}{m_\pi^2} \,. \tag{3.59}$$

We also require that the encapsulating formula matches the CBM predictions in the small m_π regime. In the chiral limit the CBM calculations reproduce predictions from chiral perturbation theory (for example in § 3.3 we saw that the one-loop CBM calculations for nucleon magnetic moments contain the leading non-analytic behaviour predicted in chiral perturbation theory) and thus we expect that a satisfactory encapsulating formula would agree with chiral perturbation theory in the limit $m_\pi \to 0$. Recall from Eq. (2.63) that the chiral expansion for the magnetic moment of an octet baryon is of the form

$$\mu = \gamma + a m_\pi + b m_K + \dots \,, \tag{3.60}$$

where γ, a and b are constant coefficients (see § 2.5). We expect that the chiral limit of the encapsulating form reproduces this expansion.

Since $m_K > m_\pi$, one might conclude that the kaon loop contribution is the dominant term in the magnetic moment expansion, Eq. (3.60). However, kaon loop contributions can be neglected for the following reasons. The CBM calculations (see Eq. (3.47)) indicate that at large pseudoscalar masses the pseudoscalar contribution to the magnetic moment is suppressed by form factors

Nucleon	μ_0	χ	c
p	3.31	−4.54	0.452
n	−2.39	4.42	0.271

Table 3.2: Fit parameters for extrapolations using the encapsulating form, Eq. (3.61), shown in Figs. 3.4 and 3.5 by the dot-dashed curves. The units for the fit parameters are as follows: μ_N for μ_0, $\mu_N \cdot \mathrm{GeV}^{-1}$ for χ and GeV^{-2} for c.

Nucleon	Encapsulating form	Chiral Perturbation Theory
	χ	$\mp\frac{(F+D)^2 m_N}{8\pi f_\pi^2}$
p	−4.54	−4.41
n	4.42	4.41

Table 3.3: Values of the fit parameter, χ, for the encapsulating form extrapolations shown in Figs. (3.4)–(3.5). It is compared with the predicted coefficient from chiral perturbation theory.

which describe the finite size of the baryon. In the case of the pion, this means that the pion loop contributions are suppressed at large pion masses. For the kaon, which has a much larger mass than the pion, this means that kaon loop effects are almost negligible. Despite the model-dependence associated with the form factors, the lattice results themselves do not show a rapid variation with m_K. Thus kaon loop effects are expected to be relatively small and slowly varying as a function of m_q [2]. They can therefore be absorbed in the fit parameters. On the other hand, the rapid variation of m_π with m_q means that the leading non-analytic behaviour in m_π must be treated explicitly. Therefore we require the encapsulating form to reproduce the chiral expansion, Eq. (3.60), only to $\mathcal{O}(m_\pi)$ in the chiral limit.

A natural choice for the encapsulating formula, which builds in the requirements specified above, is given by

$$\mu_N(m_\pi) = \frac{\mu_0}{1 - \frac{\chi}{\mu_0} m_\pi + c m_\pi^2} \quad , \tag{3.61}$$

where μ_0, χ and c are constants chosen to best fit the CBM results. This formula clearly gives the expected Dirac moment behaviour in the heavy pion mass regime. Expanding Eq. (3.61) about $m_\pi = 0$ we find

$$\mu_N = \mu_0 + \chi m_\pi + \left(\frac{\chi^2}{\mu_0} - \mu_0 c\right) m_\pi^2 + \ldots \quad , \tag{3.62}$$

which clearly agrees with the requirements from chiral perturbation theory. Therefore the encapsulating form, Eq. (3.61), is well motivated in the both the chiral limit and heavy quark mass regime.

The results from fitting the CBM extrapolation curves with the encapsulating formula, Eq. (3.61), are shown in Figs. 3.4 and 3.5 by the dot-dashed lines (these fits were published in Ref. [11]). The fit parameters for these curves are given in Table 3.2. In both cases the encapsulating form provides a very good approximation to the CBM results.

To establish the ability of the encapsulating form to match the CBM predictions, we compare the value of χ found by the fitting routine with the value predicted by chiral perturbation theory (given in Eq. (2.63)). This is shown in Table 3.3. In both extrapolations the value of

[2] Note that $m_K^2 \propto m_s + m_q$ and here m_s is fixed and large

χ chosen to best fit the data is remarkably close to the value predicted by chiral perturbation theory. This similarity suggests that the value of χ can indeed be fixed to the value predicted by chiral perturbation theory in the fitting formula, Eq. (3.61), so that the SU(2) chiral expansion is reproduced in full to leading non-analytic order. A two parameter fit can then be performed with the resulting extrapolation formula. We will see the results for two parameter fits of magnetic moment lattice results in Chapter 4, where the formalism will be extended to the entire baryon octet.

Chapter 4

Magnetic Moments

In this chapter we build on the ideas of § 3.5 to propose a simple extrapolation scheme for octet baryon magnetic moments as a function of m_π. In particular, we use a two parameter fitting function, similar to the encapsulating form, Eq. (3.61), to extrapolate the magnetic moment lattice results of Ref. [33]. The results from these extrapolations will be compared with experimental measurements at the physical pion mass. The method and results discussed in this chapter have been published in Ref. [15].

4.1 Extrapolating function

In § 3.5 we saw that the function

$$\mu_N(m_\pi) = \frac{\mu_0}{1 - \frac{\chi}{\mu_0} m_\pi + c m_\pi^2} \tag{4.1}$$

with χ, μ_0 and c chosen to best fit the data, could successfully encapsulate the CBM extrapolations of the nucleon magnetic moment lattice results. In each case we saw that the value obtained for the fit parameter χ agreed well with the value predicted by chiral perturbation theory (see Table 3.3). In this chapter we explore the possibility of fixing the value of χ in Eq. (4.1) to the chiral perturbation theory prediction and then performing a two parameter fit with the resulting formula. For example, in the case of the proton we would set $\chi = -4.41$ and use the following two parameter formula to extrapolate the lattice results

$$\mu_p(m_\pi) = \frac{\mu_0}{1 + \frac{4.41}{\mu_0} m_\pi + c m_\pi^2} , \tag{4.2}$$

where m_π is in GeV and μ_p is in nuclear magnetons (μ_N). In the small m_π limit, this extrapolation formula reproduces the chiral expansion to $\mathcal{O}(m_\pi)$ and the leading non-analytic term has the correct (model-independent) coefficient. (As in § 3.5, we neglect kaon loop contributions.) As before, the extrapolation formula also maintains the expected Dirac moment behaviour in the heavy pion mass regime.

In Ref. [11] the two parameter fit function described above was used to extrapolate lattice results for the proton and neutron magnetic moments. The extrapolated values obtained at the physical pion mass were found to agree very well with experiment. The following results were obtained (where the experimental value is indicated in parentheses): $\mu_p = 2.85(22)\,\mu_N$ $\{2.793\,\mu_N\}$ and $\mu_n = -1.90(15)\,\mu_N$ $\{-1.913\,\mu_N\}$.

Given the sucess of the proton and neutron extrapolations, we now extend the two parameter extrapolation formula to the entire baryon octet. For each baryon "i" we extrapolate the results using the Padé approximant,

$$\mu_i(m_\pi) = \frac{\mu_0}{1 - \frac{\chi_i}{\mu_0} m_\pi + c m_\pi^2} , \tag{4.3}$$

where χ_i is fixed to the value predicted by chiral perturbation theory and the fit parameters, μ_0 and c, are optimized for each baryon. From Eq. (2.63), χ_i is given explicitly by $\chi_i = (\beta_i^{(\pi)} m_N)/(8\pi f_\pi^2)$ and the one-loop corrected estimates of $\beta_i^{(\pi)}$ and χ_i are given in Table 4.1. The Padé approximant gives a simple way of connecting magnetic moment lattice results obtained at large pion masses with the physical world. This extrapolation procedure is clearly well motivated by the excellent phenomenology of the CBM. It also agrees with chiral perturbation theory and heavy quark effective theory in the small and large m_π limits respectively.

4.2 Lattice Calculations

The magnetic moment results used here are extracted from the lattice QCD calculations of Ref. [33]. While these results are now quite old, they continue to be the *only* lattice estimates of the spin-1/2 baryon octet magnetic moments available at the moment. These simulations were performed on a $24 \times 12 \times 12 \times 24$ periodic lattice using standard Wilson actions at $\beta = 5.9$. Dirichlet boundary conditions were used for fermions in the time direction. Twenty-eight quenched gauge configurations were generated by the Cabibbo-Marinari [35] pseudo-heat-bath method. The conserved electromagnetic current was derived from the Wilson fermion action via the Noether procedure. The associated lattice Ward identity protects this vector current from renormalization. The magnetic moments were obtained from the form factors at 0.16 GeV^2 by assuming equivalent q^2 dependences for the electric and magnetic form factors. For each octet baryon, the magnetic moment was calculated at 3 different quark masses, corresponding to rather heavy pion masses, all above 600 MeV. Statistical uncertainties in the results were calculated in a third-order, single elimination jackknife [36, 37]. Further details may be found in Ref. [33].

Since the lattice calculations of Ref. [33] were obtained using the quenched approximation, there are expected to be errors in the results arising from the quark loops neglected in the simulation. A quantitative procedure for eliminating these errors is not known. However, as explained in Ref. [11], the errors due to quenching are expected to be on the scale of the statistical errors. Hence we will assume that the results of Ref. [33] are a fair representation of the full QCD results. Nevertheless, an ideal extrapolation of magnetic moments would use full QCD lattice results which are unavailable at the moment.

4.3 Results

In the following graphs, Figs. 4.1–4.4, lattice calculations of the baryon magnetic moments are fitted as a function of m_π, according to the Padé approximant, Eq. (4.3), with coefficients, χ_i, from Table 4.1. In each case the solid lines are Padé approximant fits to the magnetic moment lattice results. Experimental measurements are indicated at the physical pion mass by an asterisk ($\star$). The magnetic moment predictions from the Padé approximant extrapolations are compared with experimental values in Table 4.1. The fit parameters, μ_0 and c, for the solid lines are also indicated in Table 4.1.

In the case of the nucleon, the fits given here (Figs. 4.1 and 4.2) are slightly different from those given in Ref. [11], as the second set of lattice results have been omitted in order to produce a consistent set of graphs for the entire baryon octet. (The second set of results were extracted from Ref. [34] which dealt with the nucleon only.) However, the nucleon extrapolations shown here still give excellent agreement with the experimental measurements. The magnetic moment predictions for the Σ^+ and Σ^- (see Table 4.1 and Figs. 4.2 – 4.3) are also in good agreement with experiment.

Baryon	$\beta_i^{(\pi)}$	χ_i	μ_0	c	Lattice	Averaged Lattice	Experiment
p	$-(F+D)^2$	-4.41	3.46	0.68	2.90(20)		2.793
n	$(F+D)^2$	4.41	-2.28	0.11	$-1.79(21)$		-1.913
Λ	0	0	-0.38	0.005	$-0.38(3)$		$-0.613(4)$
Σ^+	$-\frac{2}{3}D^2-2F^2$	-2.46	2.71	0.40	2.39(16)	2.53(18)	2.42(5)
Σ^0	0	0	0.54	0.44	0.53(5)	0.58(7)	0.63(4)[1]
Σ^-	$\frac{2}{3}D^2+2F^2$	2.46	-1.64	1.35	$-1.33(8)$	$-1.35(15)$	$-1.157(25)$
Ξ^0	$-(D-F)^2$	-0.19	-0.80	0.29	$-0.82(4)$	$-0.99(10)$	$-1.250(14)$
Ξ^-	$(D-F)^2$	0.19	-0.46	-0.38	$-0.44(2)$	$-0.67(8)$	$-0.69(4)$

Table 4.1: Magnetic moments of the octet baryons (in nuclear magnetons) predicted by lattice QCD compared with experiment. The one-loop corrected estimates of $\beta_i^{(\pi)}$ and χ_i are also reported. The fit parameters μ_0 and c of the Padé approximant are indicated in units of μ_N and GeV^{-2} respectively. The column entitled "Averaged Lattice" reports magnetic moment predictions from extrapolations of lattice calculations averaged to better describe the strange quark mass, as discussed in the text.

Using magnetic moment values predicted by the Padé approximant we can calculate the ratio of the Ξ^- and Λ magnetic moments. The simple quark model predicts that this ratio is given by

$$\frac{\mu_{\Xi^-}}{\mu_\Lambda} = \frac{1}{3}\left(4 - \frac{\mu_d}{\mu_s}\right) \tag{4.4}$$

which becomes

$$\frac{\mu_{\Xi^-}}{\mu_\Lambda} = \frac{1}{3}\left(4 - \frac{m_s}{m_d}\right) \tag{4.5}$$

if we take each quark magnetic moment to be given by the Dirac moment of its constituent mass. In this case the ratio is less than 1 for $m_s > m_d$. This disagrees with the experimentally measured value of 1.13(7). However, using the predictions of the Padé approximant, we obtain a value of 1.15 for this ratio, which is in excellent agreement with the experimental result. This is a good indication that meson cloud effects must be included in extrapolations of lattice results to the physical regime.

The lattice calculations of Ref. [33] were made with a strange quark mass of approximately 250 MeV. This is much heavier than the physical mass of the strange quark of 115 ± 8 MeV at a scale 2 GeV, taken from a careful analysis of QCD sum rules for τ decay [38]. The contribution of the strange quark to the Σ baryon magnetic moments is very small. Lattice QCD calculations indicate that the contribution of a singly represented quark in a baryon is half that anticipated by SU(6) spin-flavour symmetry [13]. Hence the heavy strange quark mass will have a subtle effect on the Σ moments. By contrast, the strange quarks dominate the Λ and Ξ magnetic moments. Thus the heavy strange quark produces a large error in the lattice results for these baryons, which has not yet been taken into account. This is reflected in the predictions of the Λ , Ξ^0 and Ξ^- magnetic moments which are smaller in magnitude than the experimental measurements in all cases.

[1]The experimental value for Σ^0 is taken from the average of Σ^+ and Σ^- experimental results, which is valid in the limit of isospin symmetry.

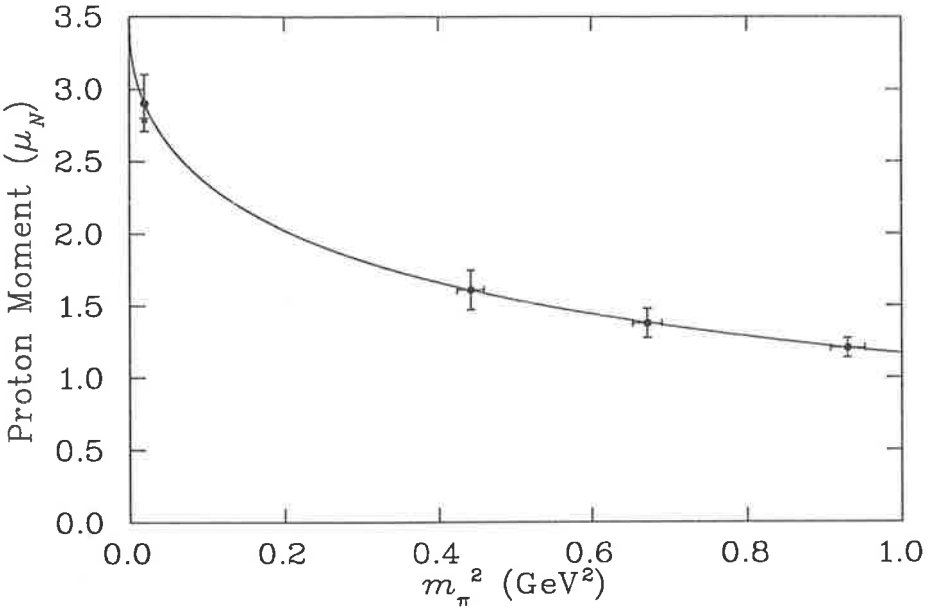

Figure 4.1: Fits to lattice results of the proton magnetic moment. The physical value predicted by the fit is also indicated, as is the experimental value, denoted by an asterisk.

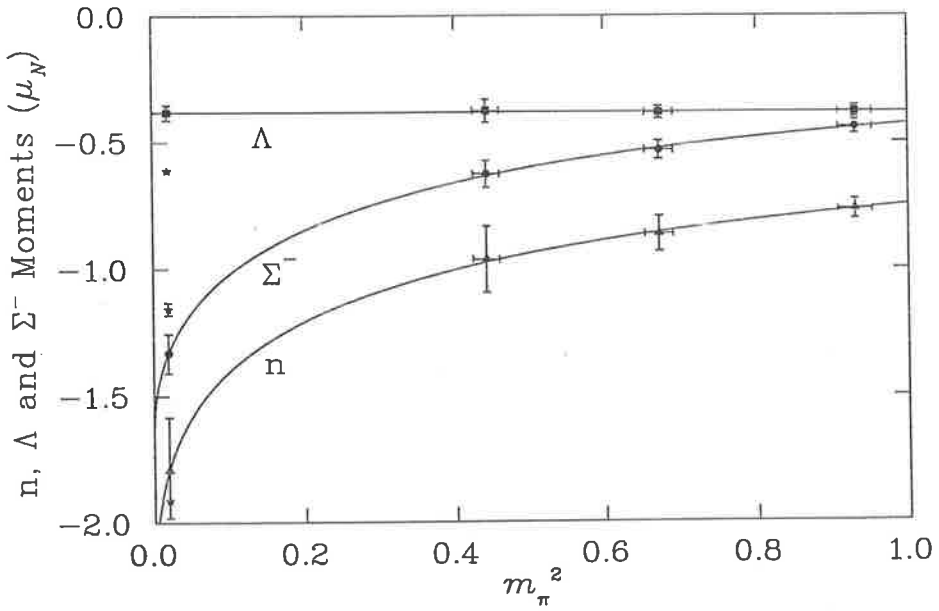

Figure 4.2: Fits to lattice results of the neutron, Λ and Σ^- magnetic moments. The physical values predicted by the fits are indicated, as are the experimental values, which are denoted by asterisks.

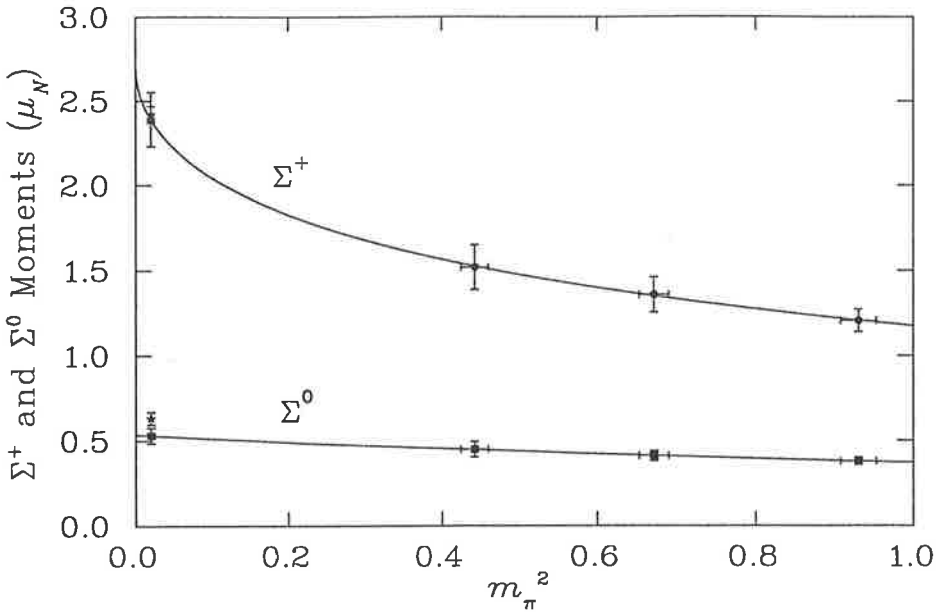

Figure 4.3: Fits to lattice calculations of the Σ^+ and Σ^0 moments. Physical values predicted by the fits are indicated, as are the experimental values which are denoted by asterisks. (The experimental value for Σ^0 is obtained from the isospin average of the Σ^+ and Σ^- measurements.)

In an attempt to correct for the effect of the large strange quark mass considered in the lattice calculations, we average the magnetic moment lattice results of each $S \neq 0$ baryon with magnetic moment results of a light-quark equivalent baryon [2]. This procedure interpolates between magnetic moment lattice results produced with heavy strange quarks and those produced with zero strange quark mass. These averaged results have an effective strange quark mass closer to the physical strange quark mass. The Padé approximant is then used to extrapolate these averaged results. The effect on the Σ moments is subtle (see Table 4.1). However, in the case of Ξ^-, this method is sufficient to reproduce the empirical Ξ^- moment (as shown by the dashed line in Fig. 4.4). There is a remaining discrepancy in the value predicted for the Ξ^0. Clearly the present estimate of the correction for the heavy strange quark mass is somewhat crude. It is therefore very important to have new simulation data with a realistic strange quark mass. At that stage it may also be necessary to include kaon loop effects, because the transition $\Xi^0 \to \Sigma^+ + K^-$ is energetically favoured, and will make a negative contribution to the Ξ^0 magnetic moment.

4.4 Summary

We have seen that the Padé approximant can be used to extrapolate magnetic moment lattice results of the spin-1/2 baryon octet to the physical regime. The magnetic moment values predicted by the fits for the p, n, Σ^+ and Σ^- compare well with experimental measurements. As a first estimate of the correction to be expected if a more realistic strange quark mass were used, the lattice results for the $S \neq 0$ baryons were averaged with the magnetic moments of the corresponding light-quark equivalent baryons. In the case of Ξ^-, the averaging procedure produced good agreement with experiment. Including kaon loop contributions is expected to further improve the Ξ moments, and hopefully reduce the discrepancy in the Ξ^0 result. However, first it is important to apply the Padé approximant to more precise lattice results, calculated with a realistic strange quark mass.

[2] Lattice calculations of a light-quark equivalent Λ are not available.

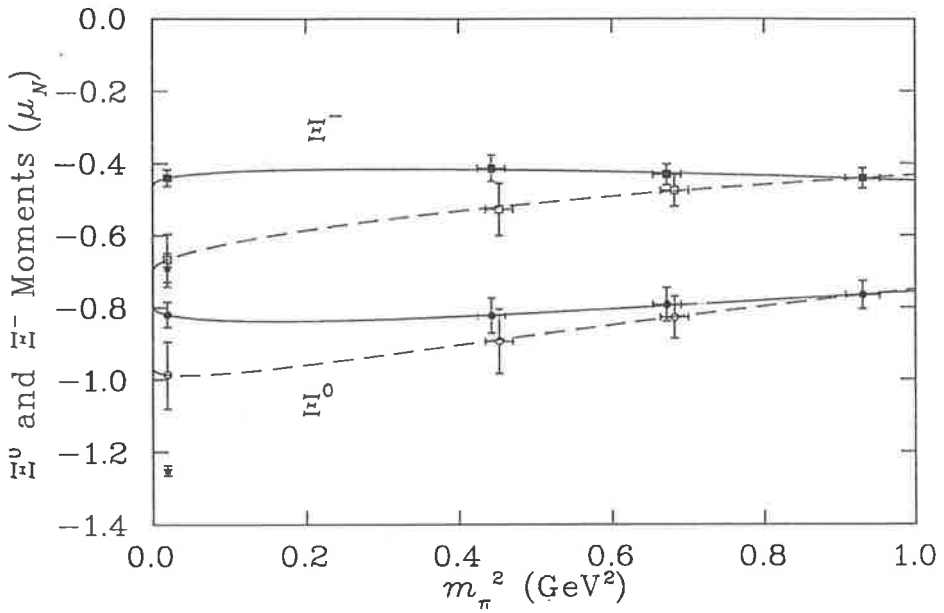

Figure 4.4: Fits to lattice calculations of the Ξ^0 and Ξ^- magnetic moments. The upper two lines are fits for Ξ^- results and the lower two lines for Ξ^0 results. Solid lines represent fits to the original magnetic moment results of Ref. [33], while the dashed lines represent fits to averaged results (denoted by open symbols which are offset for clarity), as described in the text. The physical values predicted by the fits are indicated, as are the experimental values, which are denoted by asterisks.

Chapter 5

Electric Charge Radii

In the previous chapter we found that the Padé approximant, which was an extrapolation formula designed to agree with chiral perturbation theory and heavy quark effective theory in the appropriate limits, gave successful predictions for the octet baryon magnetic moments (see Table 4.1). In this chapter we wish to find an analogous procedure for extrapolating lattice results for octet baryon charge radii. Chiral expansions of electric charge radii contain non-analytic behaviour in the form of logarithmic terms in m_π (see § 2.5). In this chapter we develop extrapolation schemes for octet baryon charge radii which include these logarithmic terms. A similar approach [8] has been successful in explaining why lattice calculations of pion and proton charge radii are similar in size, while experimental measurements reveal a significant difference. In Ref. [8] it was found that dramatic differences in the chiral behaviour of the pion and proton charge radii account for the similarity of the lattice results at moderately heavy pion masses, while allowing good agreement with experiment at the physical pion mass. In this chapter we improve the formalism of the chiral extrapolations used in Ref. [8] by incorporating both chiral symmetry and heavy quark effective theory in our extrapolation formulae. The results given in this chapter have been published in Ref. [16].

5.1 Extrapolations

Recall from § 2.5 that the chiral expansion for the squared electric charge radius, $\langle {r_i}^2 \rangle$, of a spin-1/2 octet baryon (labelled by i) is given by

$$\langle {r_i}^2 \rangle = \gamma_i + \sum_{X=\pi,K} \frac{6\alpha_i^{(X)}}{(4\pi f_\pi)^2} \log\left(\frac{m_X}{\lambda}\right) + \cdots \,, \tag{5.1}$$

where all quantities are defined in § 2.5. The leading non-analytic terms in this expansion are the logarithmic terms which are non-analytic functions of the quark mass, m_q[1]. Thus these terms have model independent coefficients. The logarithmic terms are analogous to the $\mathcal{O}(m_X)$ terms in the magnetic moment chiral expansions, Eq. (2.63). As in the magnetic moment case (see § 3.5), we will not explicitly include kaon loop effects in our extrapolation formulae, since kaon contributions are expected to be strongly suppressed by form factors describing the finite size of the baryon.

To extrapolate the electric charge radius lattice results, we consider two distinct fitting procedures. Like the Padé approximant for magnetic moments, both the extrapolation schemes considered here for charge radii satisfy the constraints of chiral perturbation theory and heavy quark effective theory. The first extrapolation procedure we investigate is given simply by the

[1] Recall that $m_\pi^2 \propto m_q$ and $m_K^2 \propto m_q + m_s$ over a wide range of quark masses.

formula

$$\langle {r_i}^2 \rangle = \frac{c_1 + \chi_i \ln(m_\pi/\Lambda)}{1 + c_2 m_\pi^2} \ , \tag{5.2}$$

where $\langle {r_i}^2 \rangle$ are the lattice QCD results (at several values of m_π) extracted from Ref. [33], c_1 and c_2 are fit parameters which are optimized for each baryon, χ_i (corresponding to the i^{th} baryon) is fixed (model-independently) by chiral perturbation theory and Λ, which is directly correlated with c_1, is fixed at 1 GeV. Note that the lattice results used here were produced by fitting the electric form factor to a dipole form. (In the original paper, Ref. [33], the electric form factor was also fit to a monopole form. However, it is known from experiment that the dipole form is more suitable for parameterizing the electric form factor. Thus we consider only the dipole results here.) Further details of the lattice results may be found in Ref. [33] and also in § 4.2. The extrapolation procedure given in Eq. (5.2) is not feasible for the neutral baryons because in this case $\langle {r_i}^2 \rangle \to 0$ as m_π becomes large and thus sensitivity to the c_2 fit parameter is lost. In order to extrapolate the neutral baryon charge radii results we consider a second extrapolation procedure, focusing on individual quark "sector" (or flavour) contributions, as discussed below.

Clearly the extrapolation formula given in Eq. (5.2) builds in the correct chiral behaviour, since in the limit $m_\pi \to 0$ it can be expanded as follows

$$\langle {r_i}^2 \rangle = c_1 + \chi_i \ln(m_\pi) - c_1 c_2 m_\pi^2 + \ldots \tag{5.3}$$

(Recall that the scale Λ, in Eq. (5.2), has been set to 1 GeV. This choice is also implicit in Eqs. (5.6)–(5.10), below, where m_π in the logarithm must be in GeV.) This agrees with the chiral SU(2) expansion of the squared electric charge radius (see Eq. (5.1)), provided we fix the coefficient χ_i to $6\alpha_i^{(\pi)}/(4\pi f_\pi)^2$. The one loop corrected estimates of the coefficients $\alpha_i^{(\pi)}$ and χ_i are given in Table 5.1.

In the large m_q limit, the quarks are expected to behave non-relativistically, and hence the squared charge radius should fall off as m_q^{-2}, as in non-relativistic quantum mechanics. In the region where m_q is very large, $m_q \propto m_\pi$, and hence we require that

$$\langle {r_i}^2 \rangle \propto \frac{1}{m_\pi^2} \ , \tag{5.4}$$

as m_π becomes extremely large. This is clearly satisfied by the first extrapolation formula, Eq. (5.2), since the logarithm is very slowly varying.

In the second extrapolation procedure the individual quark sector contributions to the baryon charge radii are dealt with individually. For example, in the case of the nucleons, we extrapolate the up and down sector contributions separately. For the hyperons the strange and light sector results are extrapolated individually. This avoids the problem encountered with the neutral baryons which was mentioned previously, because now all the quantities being extrapolated are charged, even if the overall charge on the baryon is zero. This separation is valid since the squared electric charge radius can be decomposed as

$$\langle {r_i}^2 \rangle = \sum_{q=u,d,s} e_q \left\langle r_i^{(q)\,2} \right\rangle \tag{5.5}$$

where $\left\langle r_i^{(q)\,2} \right\rangle$ is the contribution from the q^{th} quark sector and e_q is the charge of this quark sector. Therefore, provided that the extrapolation formulae from each sector add so that the chiral and heavy quark limits of the sum are in agreement with Eqs. (5.1) and (5.4) respectively, this method contains the same physics as the first method, but simply makes use of the extra information contained in the individual quark sector results. Not only does this second extrapolation procedure solve the neutral baryon extrapolation difficulty, it also provides predictions for

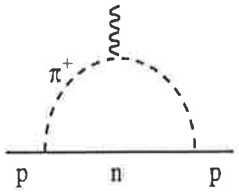

Figure 5.1: Schematic illustration of the pion loop which produces the leading non-analytic contribution to the proton charge radius.

individual quark sector radii, which will be resolved at Jefferson Lab for the nucleon [39], and perhaps future accelerator facilities for hyperons.

Isolation of the individual quark sector contributions to the charge radii is relatively straightforward from the theoretical point of view. For example, to isolate the u-sector contribution to the charge radius of the proton one simply sets the d-quark charge to zero and calculates the proton charge radius as if only the u quark carried charge. In the chiral expansion of the proton charge radius, the coefficient of the logarithm, $\chi_p^{(\pi)}$, originates from the pion loop, $p \to n + \pi^+$ (see Fig. 5.1), and includes the charge of the pion cloud. (For clarity, we employ (π) superscripts on the chiral coefficients.) Therefore, to extrapolate the u-sector contribution to the proton charge radius, the appropriate coefficient of the logarithm is $\frac{2}{3}\chi_p^{(\pi)}$, since the pion now carries charge $+2/3$. Thus we extrapolate the u-sector results of the proton according to

$$2\, e_u \left\langle r_p^{(u)\,2} \right\rangle = \frac{c_1 + \frac{2}{3}\chi_p^{(\pi)} \ln(m_\pi)}{1 + c_2 m_\pi^2} \,, \tag{5.6}$$

where $\chi_p^{(\pi)}$ is the full chiral coefficient of the proton, given in Table 5.1 and $\left\langle r_p^{(u)\,2} \right\rangle$ is the squared charge radius of a single u-quark of unit charge. Similarly, the d-sector results are extrapolated according to

$$e_d \left\langle r_p^{(d)\,2} \right\rangle = \frac{c_1{}' + \frac{1}{3}\chi_p^{(\pi)} \ln(m_\pi)}{1 + c_2{}' m_\pi^2} \,, \tag{5.7}$$

where the factor of $1/3$ originates from the $\bar{d}$ contribution to the pion cloud. Clearly adding the left hand sides of Eqs. (5.6) and (5.7) yields the full expression for $\langle r_p^2 \rangle$. In the chiral limit the right hand sides add so that the correct chiral form for $\langle r_p^2 \rangle$, given in Eq. (5.3), is retained. The sum of Eqs. (5.6) and (5.7) also obeys the correct heavy quark behaviour, given in Eq. (5.4). Since the parameters c_2 and $c_2{}'$ are not necessarily the same, the individual quark sector extrapolation formulae (Eqs. (5.6) and (5.7)) cannot be added directly to give Eq. (5.2). Therefore, in general we do not expect the two extrapolation procedures to give exactly the same results. For the charged baryons this may be used to help quantify the systematic error of the approach. For the neutron, the analogous extrapolation functions are given by

$$e_u \left\langle r_n^{(u)\,2} \right\rangle = \frac{c_1 + \frac{2}{3}\chi_n^{(\pi)} \ln(m_\pi)}{1 + c_2 m_\pi^2} \tag{5.8}$$

for the u-quark sector, and

$$2e_d \left\langle r_n^{(d)\,2} \right\rangle = \frac{c_1{}' + \frac{1}{3}\chi_n^{(\pi)} \ln(m_\pi)}{1 + c_2{}' m_\pi^2} \tag{5.9}$$

for the d-quark sector results, where $\chi_n^{(\pi)}$ is given in Table 5.1.

We now consider extrapolating the hyperon radii using the second extrapolation procedure, i.e., extrapolating the strange and light quark sector results separately. In extrapolating the strange quark sector the charges of the light quarks are set to zero. Since the logarithmic term considered here originates from pionic corrections to the charge radius (and pions do not contain strange quarks), the coefficient of the logarithm in the strange sector extrapolation will be zero. Similarly, for the light sector extrapolation, strange quarks do not carry charge and hence the coefficient of the logarithm in this extrapolation will be the full coefficient, $\chi_i^{(\pi)}$. This results in the following extrapolation formulae for the hyperon quark sector contributions

$$e_l \left\langle r_i^{(l)\,2} \right\rangle = \frac{c_1 + \chi_i^{(\pi)} \ln(m_\pi)}{1 + c_2 m_\pi^2} \tag{5.10}$$

and

$$e_s \left\langle r_i^{(s)\,2} \right\rangle = \frac{c_1{}'}{1 + c_2{}' m_\pi^2} \,, \tag{5.11}$$

where i runs over the hyperons only, and l corresponds to the light-quark (u and/or d) sector. Since the strange quark mass is held fixed in the light quark mass extrapolation, any variation in the strange quark sector is purely an environment effect from the surrounding light quarks. As such, the functional form for the strange quark sector is constrained by neither leading order chiral perturbation theory nor heavy quark effective theory. As we shall see, $c_2{}'$ is small and negative for each hyperon, which suggests that a simple linear ansatz for the strange quark sector extrapolation could also have been used.

Note that the extrapolation procedure of separating the strange and light sector contributions is distinct from the u-d separation which we perform for the nucleon. For example, in the strange-light separation of Σ^+, we extrapolate the sectors according to Eqs. (5.10) and (5.11). However, if we were to make a further separation into u and d sectors, then the light-quark sector results would be extrapolated as u sector results, with chiral coefficient $\frac{2}{3}\chi_{\Sigma^+}$. The d-quark sector contribution (which is purely a sea contribution) could then be inferred from the difference between light and u quark sector extrapolations.

5.2 Results

The extrapolations of the charge radius lattice results of the spin-1/2 baryon octet are shown in Figs. 5.2 – 5.9. Extrapolations of baryon radii performed according to Eq. (5.2), are indicated by the solid lines, where the full circles (•) represent the baryon charge radii from lattice QCD and the extrapolated value at $m_\pi = 139$ MeV. The individual quark sector extrapolations are shown by the dashed and dot-dashed lines, and the baryon charge radius predicted by this method is indicated by a full square(■) in each case. Experimental measurements are indicated at the physical pion mass by an asterisk ($\star$). Note that for the charged baryons, two extrapolation schemes and two corresponding predicted physical values are shown, whereas (for the reasons given in section 5.1) only one extrapolation procedure is shown for each neutral baryon.

In the case of the proton, the two extrapolated values agree very well with the experimental measurement. It can be seen that a traditional linear extrapolation in m_π^2 would significantly underestimate the experimental result. Similarly the predicted charge radius for the neutron (produced by separate extrapolations of the u- and d-sector results) agrees with the experimental measurement significantly better than would a prediction from a simple linear extrapolation in m_π^2. Finally both predicted values for Σ^- agree very well with the two experimental measurements. These baryons are currently the only baryons of the spin-1/2 octet whose electric charge radius has been measured.

Baryon or Quark Sector	$\alpha_i^{(\pi)}$	χ_i	c_1	c_2	$\langle r^2 \rangle$	Experiment
p	$-\frac{1}{6} - \frac{5}{6}(D+F)^2$	-0.174	0.34	0.50	0.68(8)	0.740(15)[40]
u_p	$\frac{2}{3}\left[-\frac{1}{6} - \frac{5}{6}(D+F)^2\right]$	-0.116	0.52	0.73	0.74(11)	
d_p	$\frac{1}{3}\left[-\frac{1}{6} - \frac{5}{6}(D+F)^2\right]$	-0.058	-0.18	1.38	$-0.06(5)$	
$^\star p$					0.68(10)	0.740(15)[40]
n	$\frac{1}{6} + \frac{5}{6}(D+F)^2$	0.174				
u_n	$\frac{2}{3}\left[\frac{1}{6} + \frac{5}{6}(D+F)^2\right]$	0.116	0.35	1.38	0.12(10)	
d_n	$\frac{1}{3}\left[\frac{1}{6} + \frac{5}{6}(D+F)^2\right]$	0.058	-0.26	0.73	$-0.37(6)$	
$^\star n$					$-0.25(8)$	$-0.113(4)$[30]
Λ	0	0				
l_Λ	0	0	0.15	0.97	0.14(3)	
s_Λ	0	0	-0.07	-0.10	$-0.07(1)$	
$^\star\Lambda$					0.07(3)	
Σ^+	$-\frac{1}{3} - \frac{5}{3}\left(\frac{D^2}{3} + F^2\right)$	-0.138	0.68	2.03	0.92(11)	
l_{Σ^+}	$-\frac{1}{3} - \frac{5}{3}\left(\frac{D^2}{3} + F^2\right)$	-0.138	0.58	0.93	0.83(8)	
s_{Σ^+}	0	0	-0.06	-0.17	$-0.06(1)$	
$^\star\Sigma^+$					0.77(8)	
Σ^0	0	0				
l_{Σ^0}	0	0	0.19	1.48	0.18(2)	
s_{Σ^0}	0	0	-0.06	-0.17	$-0.06(1)$	
$^\star\Sigma^0$					0.12(2)	
Σ^-	$\frac{1}{3} + \frac{5}{3}\left(\frac{D^2}{3} + F^2\right)$	0.138	-0.25	0.08	$-0.52(3)$	$-0.60(16)$[41]
						$-0.91(72)$[42]
l_{Σ^-}	$\frac{1}{3} + \frac{5}{3}\left(\frac{D^2}{3} + F^2\right)$	0.138	-0.21	0.37	$-0.47(3)$	
s_{Σ^-}	0	0	-0.06	-0.17	$-0.06(1)$	
$^\star\Sigma^-$					$-0.54(3)$	$-0.60(16)$[41]
						$-0.91(72)$[42]
Ξ^0	$-\frac{1}{6} - \frac{5}{6}(D-F)^2$	-0.035				
l_{Ξ^0}	$-\frac{1}{6} - \frac{5}{6}(D-F)^2$	-0.035	0.29	0.97	0.35(5)	
s_{Ξ^0}	0	0	-0.15	-0.05	$-0.15(1)$	
$^\star\Xi^0$					0.20(5)	
Ξ^-	$\frac{1}{6} + \frac{5}{6}(D-F)^2$	0.035	-0.24	0.07	$-0.32(2)$	
l_{Ξ^-}	$\frac{1}{6} + \frac{5}{6}(D-F)^2$	0.035	-0.12	0.70	$-0.19(2)$	
s_{Ξ^-}	0	0	-0.15	-0.05	$-0.15(1)$	
$^\star\Xi^-$					$-0.34(2)$	

Table 5.1: Baryon electric charge radii and the quark sector contributions. The latter are defined on the left hand sides of Eqs. (5.6)-(5.11). One-loop corrected estimates of $\alpha_i^{(\pi)}$ and χ_i for each octet baryon are indicated. For each extrapolation, the fit parameters, c_1 and c_2, and the predicted value of $\langle r^2 \rangle$ at the physical pion mass are reported. Asterisks denote the squared charge radii reconstructed from the sum of separate quark sector extrapolations. (The units are such that the pion mass is in GeV and the squared charge radius is in fm^2.)

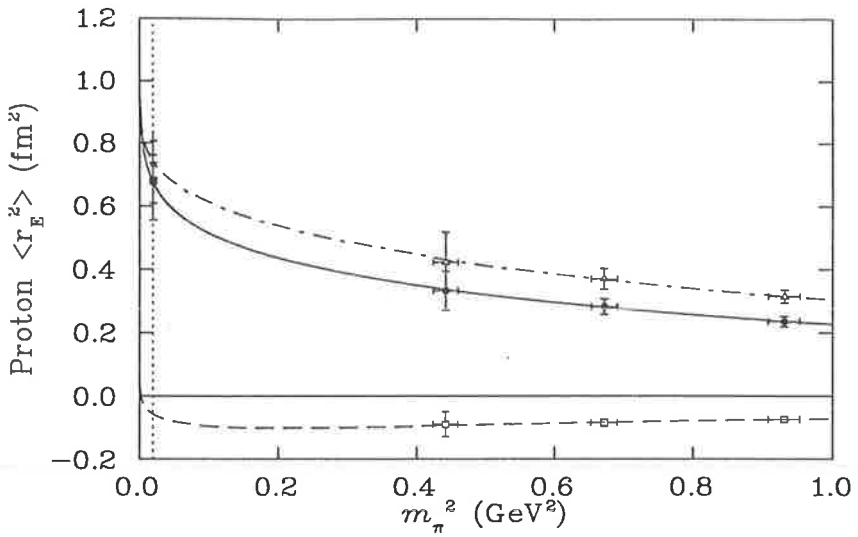

Figure 5.2: Fits to electric charge radius lattice results of the proton. Fits to the individual quark sector results are also shown. The u-quark sector results are indicated by open triangles and the d-quark sector results by open squares. Physical values predicted by the fits are indicated at the physical pion mass, where the full circle denotes the result predicted from the first extrapolation procedure and the full square denotes the baryon radius reconstructed from the quark sector extrapolations (see text). (N.B. The latter values are actually so close as to be indistinguishable on the graph.) The experimental value is denoted by an asterisk.

From simple quark model arguments [33], where the heavier strange quark has a smaller distribution than the light quarks, we expect the hierarchy of electric charge radii of charged octet baryons to be given as follows

$$|\langle r^2_{\Sigma^+}\rangle| \geq |\langle r^2_p\rangle| \geq |\langle r^2_{\Sigma^-}\rangle| \geq |\langle r^2_{\Xi^-}\rangle| \quad . \tag{5.12}$$

From Table 5.1 it is clear that the results of our extrapolations are in qualitative agreement with this expectation. Indeed, in the regime of the actual lattice data ($m_\pi \geq 600$ MeV) the argument is even quantitative. However, as the chiral limit (and physical pion mass) is approached, the simple quark model description is no longer adequate and chiral physics gives rise to dramatic effects. For example, in the extrapolation of the d-quark sector of the proton (Fig. 5.2), chiral effects mean that the d-quark sector can actually make a *positive* contribution to the charge radius, via the $\bar{d}$ contribution in π^+ – even though the total contribution is negative at the physical pion mass. This behaviour is not anticipated by the simple quark model.

As discussed in § 5.1, it is possible to perform a further separation of the light quark sector results for the hyperons into u and d sectors. The u and d sector results can then be extrapolated separately. For the Σ^+ (uus) this separation involves extrapolating the light quark sector results with chiral coefficient $\frac{2}{3}\chi_{\Sigma^+}$. From this procedure we find that the d-quark sector contribution to the Σ^+ is 0.04 fm^2, i.e. small and positive. This indicates that the $\bar{d}$ quark in the pion loop, $\Sigma^+ \to \pi^+ + \Sigma^0\Lambda$, makes a more significant contribution to the Σ^+ radius than the d quark in the $\Sigma^0\Lambda$. This is expected because the π^+ occurs at larger radius. It is encouraging that the d-quark sector contribution is small, as a large result would indicate that the quark loops which are omitted from the lattice simulations produce a significant contribution to the radius.

For the neutral baryons the sign of the squared charge radius is important. In the neutron, the two d quarks are most likely to be found in a spin 1 configuration, where they will undergo hyperfine repulsion. This leads to a small, negative charge radius. However, as one approaches

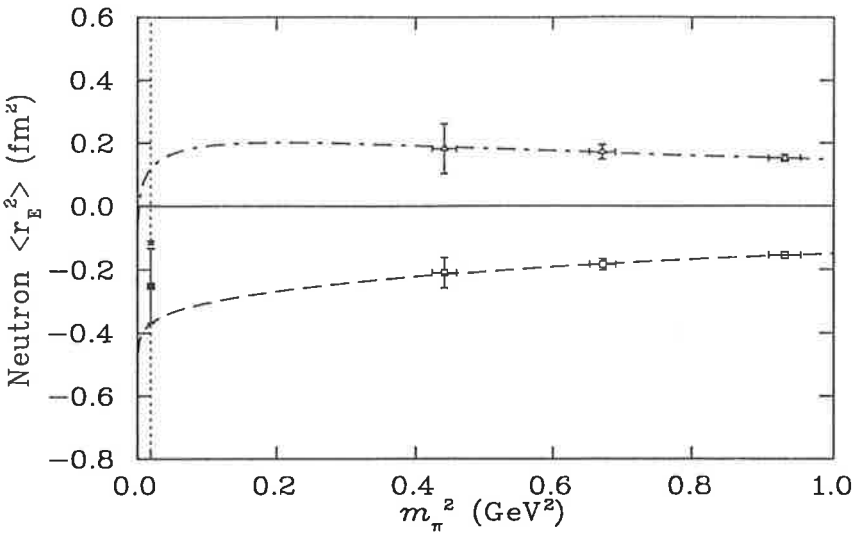

Figure 5.3: Fits to lattice results for the quark sector contributions to the squared electric charge radius of the neutron. All symbols are defined in the caption below Fig. 5.2.

the chiral limit, spontaneous chiral symmetry breaking, in particular the process $n \to p\pi^-$, which carries d-quarks to larger radii and screens the u-quark contribution via the $\overline{u}$ in the π^-, leads to an enhancement of the negative charge radius. The remaining neutral baryons. Σ^0, Λ and Ξ^0, have a positive squared charge radius. This is because in each case the strange quark distribution is more localized than the light quark charge distribution (due to the larger mass of the strange quark). Therefore on average the light quark charge distribution occurs at a larger radius, resulting in a positive charge radius (since the light quark charge is positive in each case).

As we remarked in Chapter 4, the lattice results used here were calculated with a large strange quark mass (approximately 250 MeV, compared with the physical strange quark mass of 115 ± 8 MeV). In the magnetic moment case, we found that the heavy strange quark had a significant effect on the predictions of the Ξ moments. Here we expect that the heavy strange quark will also have some effect on the Ξ charge radii. With a strange quark mass closer to the physical mass the strange quark contribution would be increased. This would result in a lower predicted charge radius for the Ξ^0 and a larger (in magnitude) charge radius for the Ξ^-. In the absence of experimental measurements we will not attempt to correct for the effect of the strange quark mass here.

As we see from Table 5.1, the extrapolated mean square charge radii obtained from both extrapolation procedures agree quite well for each charged octet baryon. For the proton, Σ^- and Ξ^- the reconstructed values completely cover the result from the original extrapolations of Eq. (5.2). In the case of the Σ^+ the two values overlap only on the error bars. This is due to the small variation in the strange quark contribution (which is caused by an environment effect). When this environment effect is included in the baryon charge radius, the magnitude of the slope is increased, resulting in a larger charge radius after extrapolation.

In turning the dimensionless masses calculated on the lattice to physical units, the lattice spacing, a, was set in the traditional manner by fixing the nucleon mass, obtained by a naive linear extrapolation in m_π^2, equal to the observed mass. Of course, such a linear extrapolation is known [12] to be inconsistent with chiral symmetry. Applying a more consistent chiral extrapolation would systematically lower values of $\langle r^2 \rangle$ obtained for the charged octet by of the order 15%. (The effect on neutral baryons is much smaller.) On the other hand, the data which we are forced

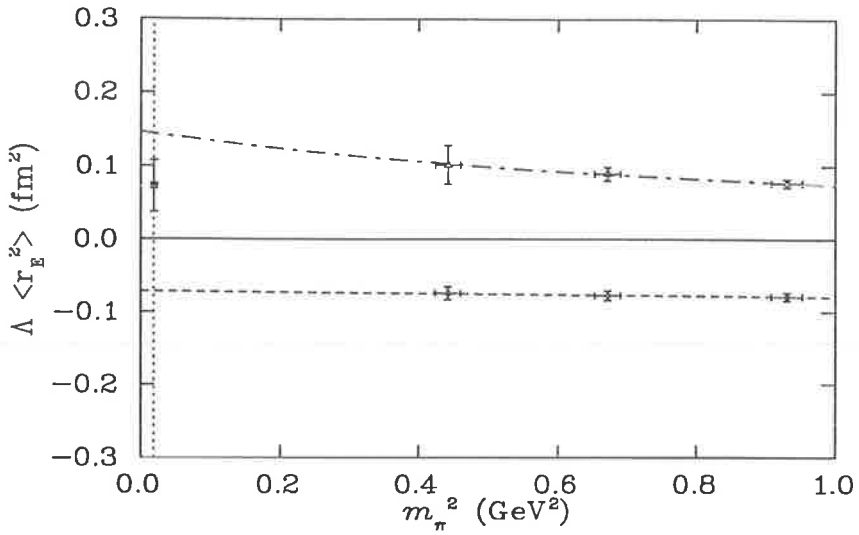

Figure 5.4: Fits to lattice results for the quark sector contributions to the squared electric charge radius of the Λ. The strange quark sector results are indicated by open diamonds. All other symbols are defined in the caption below Fig. 5.2.

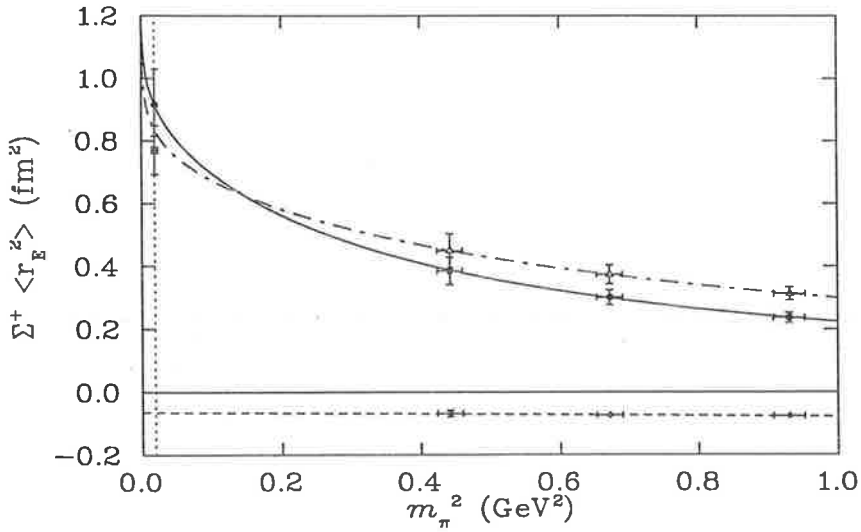

Figure 5.5: Fits to lattice results of the squared electric charge radius of the Σ^+. Fits to the individual quark sector results are also shown. All symbols are defined in the captions below Figs. 5.2 and 5.4.

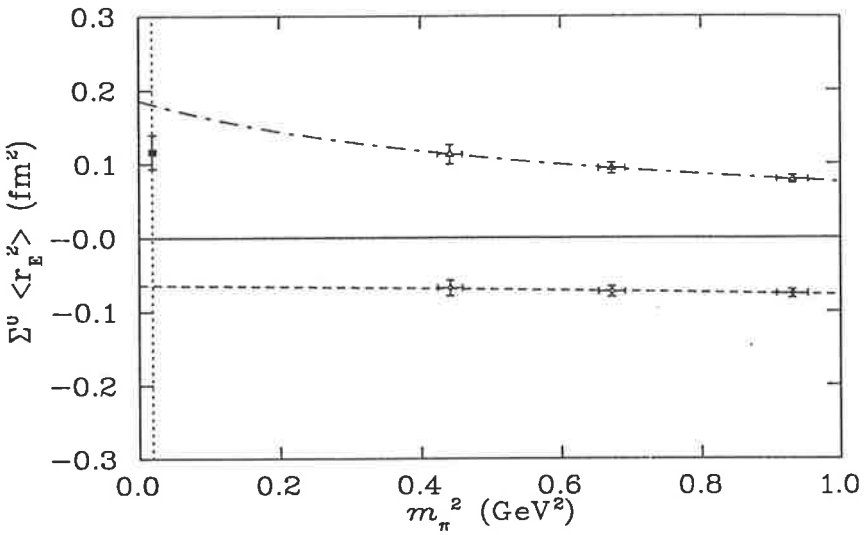

Figure 5.6: Fits to lattice results for the quark sector contributions to the squared electric charge radius of the Σ^0. All symbols are defined in the captions below Figs. 5.2 and 5.4.

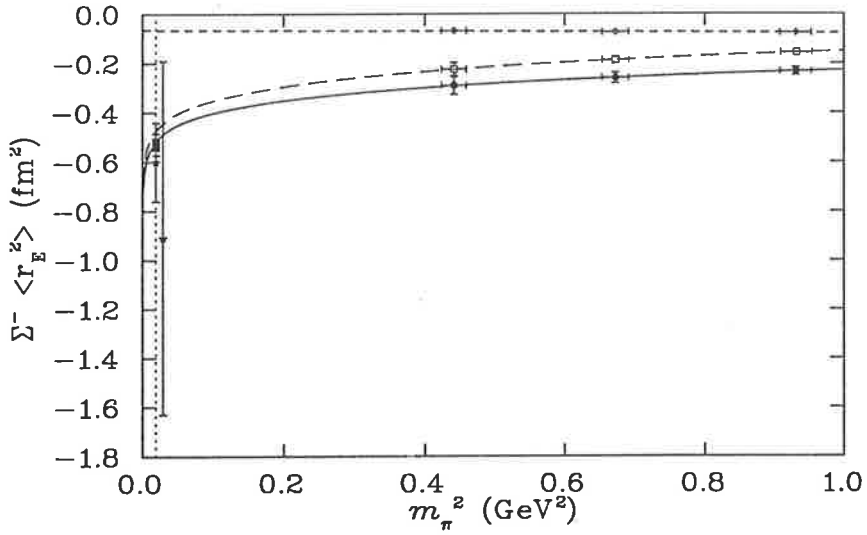

Figure 5.7: Fits to lattice results of the squared electric charge radius of the Σ^-. Fits to the individual quark sector results are also shown. All symbols are defined in the captions below Figs. 5.2 and 5.4.

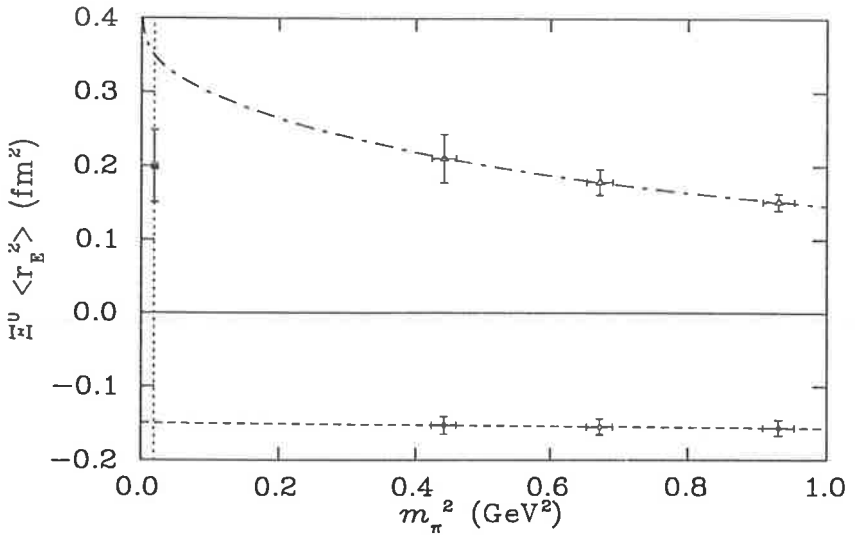

Figure 5.8: Fits to lattice results for the quark sector contributions to the squared electric charge radius of the Ξ^0. All symbols are defined in the captions below Figs. 5.2 and 5.4.

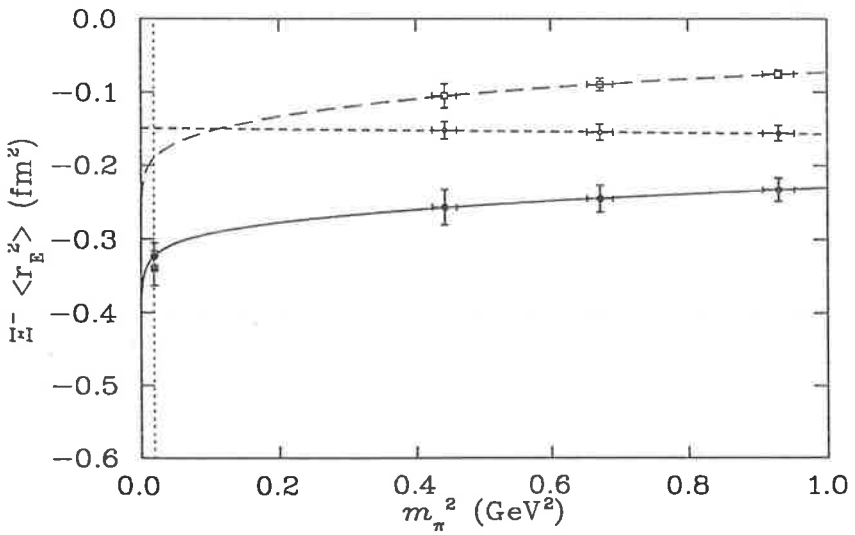

Figure 5.9: Fits to lattice results of the squared electric charge radius of the Ξ^-. Fits to the individual quark sector results are also shown. All symbols are defined in the captions below Figs. 5.2 and 5.4.

to use is quenched data which omits some pion corrections. Although these are expected to be suppressed at the large values of m_π^2 for which the data is available (c.f. Ref.[11]), the associated systematic error would tend to increase the calculated values of $\langle r^2 \rangle$, perhaps by 5-10%. Rather than attempt to repair these deficiencies in the present data, it is more reasonable to simply accept that there is an additional systematic error of the order 15% associated with the extrapolated values shown in Table 5.1. Adding this systematic in quadrature means that the values in Table 5.1 would become, for example, $\langle r_{*p}^2 \rangle = 0.68 \pm 0.14$ fm^2, $\langle r_{*\Sigma^-}^2 \rangle = -0.54 \pm 0.09$ fm^2, $\langle r_{*\Sigma^+}^2 \rangle = 0.77 \pm 0.14$ fm^2. It will be interesting to repeat the analysis in this chapter with unquenched data at lower quark mass when these results become available. In the meantime, we await further experimental measurements of baryon charge radii to test our predictions.

Chapter 6

Conclusion

In this thesis we have explored methods of extrapolating lattice QCD results to the physical regime. In particular, we have considered the extrapolation of lattice results for octet baryon magnetic moments and electric charge radii as functions of the pion mass, m_π. At this point the only available lattice results for these observables are obtained at quite large pion masses, all above 600 MeV. Since chiral perturbation theory is not applicable in this regime, chiral expansions cannot be used directly to extrapolate the lattice results. However, the chiral expansions contain important non-analytic terms arising from Goldstone boson loops which must be included in extrapolations to the physical regime.

To guide extrapolations of the lattice results we first considered the predictions of a successful chiral quark model, the Cloudy Bag Model (CBM). The CBM is a relativistic quark model of baryons which builds in the phenomena of quark confinement and pion emission. The pion loop contributions to observables calculated in the CBM match the leading non-analytic behaviour predicted by chiral perturbation theory in the chiral limit. However, as larger pion masses are approached, these non-analytic terms are suppressed by form factors which regulate the pion loops. Therefore, by extrapolating the results using the CBM, the leading non-analytic behaviour at small m_π is included, while the expected behaviour at large m_π is also maintained. CBM extrapolations were performed for the magnetic moment lattice results of the proton and neutron [11]. It was found that the CBM extrapolations could be reproduced by a simple extrapolation formula, the Padé approximant. This approximant manifestly builds in the leading non-analytic chiral behaviour at small m_π and the expected Dirac moment behaviour at large m_π. The Padé approximant was used to extrapolate the magnetic moment lattice results of the entire baryon octet.

The Padé approximant extrapolations of the magnetic moment lattice results of Ref. [33] produced some very successful predictions. In particular, we obtained the following results for the nucleons and Σ baryons (where experimental measurements are indicated in the square brackets and all magnetic moments are in units of nuclear magnetons, μ_N): $\mu_p = 2.90(20)$ [2.793], $\mu_n = -1.79(21)$ [-1.913], $\mu_{\Sigma^+} = 2.39(16)$ [2.42(5)], $\mu_{\Sigma^0} = 0.53(5)$ [0.63(4)[1]] and $\mu_{\Sigma^-} = -1.33(8)$ [$-1.157(25)$]. The predictions for the Ξ baryon magnetic moments did not agree so well with experiment. However, this problem is thought to originate from the lattice results themselves. The lattice results we were forced to use were produced with a very large strange quark mass, which has the greatest effect in the doubly strange Ξ baryon results. By averaging the Ξ results with light quark equivalent lattice results we were able to reduce the effect of the heavy strange quark, and obtain better results. However, the best solution to this problem is to repeat the analysis with lattice results produced with a more realistic strange quark mass when these results become available.

[1]The experimental value for the Σ^0 magnetic moment is taken from the isospin average of Σ^+ and Σ^- experimental results.

The success of the Padé approximant extrapolations motivated the proposal of similar extrapolation procedures for the electric charge radius results. Like the magnetic moment case, our extrapolation formulae for the charge radii were designed to reproduce the leading non-analytic logarithmic terms predicted by chiral perturbation theory in the chiral limit while maintaining the correct heavy quark behaviour. We obtained the following predictions for the charge radii of the nucleons and the Σ^- (where experimental measurements are indicated in square brackets and all charge radii are in units of fm^2): $\langle r_p^2 \rangle = 0.68(10)$ [0.740(15)], $\langle r_n^2 \rangle = -0.25(8)$ [$-0.113(4)$] and $\langle r_{\Sigma^-}^2 \rangle = -0.54(3)$ [$-0.60(16)$, $-0.91(72)$]. Predictions were also made for the remaining octet baryon charge radii, which have not yet been measured experimentally (see Table 5.1). There is an additional systematic error of the order 15% in the charge radii predictions. This error arises from problems in setting the lattice spacing and from the fact that the lattice simulations are quenched. To remove this systematic error the best solution is to repeat the extrapolations with lattice data produced at lower quark masses in full QCD.

In the future we hope to apply both extrapolation procedures to more accurate lattice data, produced with a more realistic strange quark mass. It will be interesting to resolve the extent to which further refinements are required. For example, it may be necessary to include kaon loop contributions in the extrapolation formulae. However, these contributions are expected to produce a fairly subtle effect due to the form factor suppression of the kaon loops. The effect is most likely to be observed for the doubly strange Ξ baryons which couple most strongly to kaons. We defer this treatment until more accurate lattice results are available. We also await future experimental measurements, particularly for the charge radii of the spin-1/2 baryon octet, so that our predictions can be compared with experiment.

Bibliography

[1] M. Gell-Mann, Phys. Lett. **8**, 214 (1964).

[2] G. Zweig, CERN preprint (1964) unpublished.

[3] O. W. Greenburg and C. A. Nelson, Phys. Rep. 32C, 69 (1977).

[4] H. Fritzsch, M. Gell-Mann and H. Leutwyler, Phys. Lett. **B47**, 365 (1973).

[5] M. Binger, C. Ji and D. G. Robertson, Phys. Rev. **D61**, 114011 (2000), hep-ph/9912241.

[6] A. V. Berezhnoy, V. V. Kiselev and A. K. Likhoded, hep-ph/9901333.

[7] M. E. Peskin and D. V. Schroeder, "An Introduction to Quantum Field Theory", Perseus Books (1995).

[8] D. B. Leinweber and T. D. Cohen, Phys. Rev. **D47**, 2147 (1993), hep-lat/9211058.

[9] J. N. Labrenz and S. R. Sharpe, Phys. Rev. **D54**, 4595 (1996), hep-lat/9605034.

[10] M. F. L. Golterman and K. C. Leung, Phys. Rev. **D58**, 097503 (1998), hep-lat/9805032.

[11] D. B. Leinweber, D. H. Lu and A. W. Thomas, Phys. Rev. **D60**, 034014 (1999), hep-lat/9810005.

[12] D. B. Leinweber, A. W. Thomas, K. Tsushima and S. V. Wright, Phys. Rev. **D61**, 074502 (2000), hep-lat/9906027.

[13] D. B. Leinweber and A. W. Thomas, Phys. Rev. **D62**, 074505 (2000), hep-lat/9912052.

[14] D. B. Leinweber, A. W. Thomas and S. V. Wright, Phys. Lett. **B482**, 109 (2000), hep-lat/0001007.

[15] E. J. Hackett-Jones, D. B. Leinweber and A. W. Thomas, Phys. Lett. **B489**, 143 (2000), hep-lat/0004006.

[16] E. J. Hackett-Jones, D. B. Leinweber and A. W. Thomas, Phys. Lett. **B494**, 89 (2000), hep-lat/0008018.

[17] S. Theberge, Ph.D. Thesis, The University of British Columbia (1982).

[18] S. Theberge and A. W. Thomas, Nucl. Phys. **A393**, 252 (1983); Adv. Nucl. Phys. **13**, 1 (1984).

[19] D. E. Groom *et al.*, The European Physical Journal **C15**, 1 (2000).

[20] V. Bernard, N. Kaiser and U. Meissner, Int. J. Mod. Phys. E4, 193 (1995), hep-ph/9501384.

[21] A. Pich, CERN-TH.6978/93, hep-ph/9308351

[22] B. R. Holstein, hep-ph/9911449.

[23] J. F. Donoghue, E. Golowich and B. R. Holstein, "Dynamics of the Standard Model", Cambridge University Press (1992).

[24] E. Jenkins, M. Luke, A. V. Manohar and M. J. Savage, Phys. Lett. **B302**, 482 (1993); **388**, 866(E) (1996), hep-ph/9212226.

[25] B. Kubis, T. R. Hemmert and U. Meissner, Phys. Lett. **B456**, 240 (1999), hep-ph/9903285.

[26] V. Bernard, N. Kaiser and U. Meissner, Int. J. Mod. Phys. **E4**, 193 (1995).

[27] L. Durand and P. Ha, Phys. Rev. **D58**, 013010 (1998), hep-ph/9712492.

[28] E. Jenkins and A. V. Manohar, Phys. Lett. **B255**, 558 (1991).

[29] D. G. Caldi and H. Pagels, Phys. Rev. **D10**, 3739(1974).

[30] S. Kopecky *et al.*, Phys. Rev. Lett. **74**, 2427 (1995).

[31] D. H. Lu, A. W. Thomas and A. G. Williams, Phys. Rev. **C57**, 2628 (1998), nucl-th/9706019.

[32] A. W. Thomas and G. Krein, Phys. Lett. **B481**, 21 (2000).

[33] D. B. Leinweber, R. M. Woloshyn and T. Draper, Phys. Rev. **D43**, 1659 (1991).

[34] W. Wilcox, T. Draper and K. F. Liu, Phys. Rev. **D46**, 1109 (1992), hep-lat/9205015.

[35] N. Cabibbo and E. Marinari, Phys. Rev. Lett. **119B**, 387 (1982).

[36] B. Efron, SIAM Rev. **21**, 460 (1979).

[37] S. Gottlieb, P. B. MacKenzie, H. B. Thacker, and D. Weingarten, Nucl. Phys. **B263**, 704 (1986).

[38] K. Maltman, Phys. Lett. **B462**, 195 (1999), hep-ph/9904370.

[39] K. A. Aniol *et al.* [HAPPEX Collaboration], Phys. Rev. Lett. **82**, 1096 (1999), nucl-ex/9810012.

[40] P. Mergell, U. Meissner and D. Drechsel, Nucl. Phys. **A596**, 367 (1996), hep-ph/9506375.

[41] I. Eschrich (for the SELEX collaboration), hep-ex/9811003.

[42] M. I. Adamovich *et al.* (for the WA89 Collaboration), Eur. Phys. J. **C8**, 59 (1999).

Appendix A

List of Publications

E. J. Hackett-Jones, D. B. Leinweber and A. W. Thomas,
Incorporating Chiral Symmetry in Extrapolations of Octet Baryon Magnetic Moments,
Phys. Lett. **B489**, 143 (2000), hep-lat/0004006.

E. J. Hackett-Jones, D. B. Leinweber and A. W. Thomas,
Incorporating Chiral Symmetry and Heavy Quark Theory in Extrapolations of Octet Baryon Charge Radii,
Phys. Lett. **B494**, 89 (2000), hep-lat/0008018.

ELSEVIER

14 September 2000

Physics Letters B 489 (2000) 143–147

PHYSICS LETTERS B

www.elsevier.nl/locate/npe

Incorporating chiral symmetry in extrapolations of octet baryon magnetic moments

E.J. Hackett-Jones, D.B. Leinweber, A.W. Thomas

Department of Physics and Mathematical Physics, and Special Research Centre for the Subatomic Structure of Matter, University of Adelaide, Australia 5005

Received 13 April 2000; received in revised form 19 July 2000; accepted 8 August 2000
Editor: W. Haxton

Abstract

We explore methods of extrapolating lattice calculations of hadronic observables to the physical regime, while respecting the constraints of chiral symmetry and heavy quark effective theory. In particular, we extrapolate lattice results for magnetic moments of the spin-1/2 baryon octet to the physical pion mass and compare with experimental measurements. The success previously reported for extrapolations of the nucleon magnetic moments carries over to the Σ baryons. A study of the residual discrepancies in the Ξ baryon moments suggests that it is important to have new simulation data with a more realistic strange quark mass.

1. Introduction

One of the key goals of lattice QCD is to confront experimental data with the predictions of QCD. However, computational limitations mean that hadronic observables, such as masses and magnetic moments, are calculated at quark masses much larger than their physical values. Although improvements in algorithms and computer speed will allow lattice calculations of hadronic observables to be performed much closer to the physical regime, these improvements will proceed over many years. In the meantime it is imperative that one has an understanding of how to extrapolate lattice results, obtained at large quark masses, to the physical world.

A difficult problem encountered in calculating hadronic observables at heavy quark masses on the lattice is that chiral perturbation theory is not applicable in this heavy quark mass regime. Nevertheless, chiral symmetry does require certain model-independent, non-analytic behaviour as a function of the quark mass, m_q (or equivalently of m_π^2, as $m_q \propto m_\pi^2$ in this range). This non-analytic behaviour must be taken into account in *any* extrapolation to the physical regime. In our earlier work we studied the quark mass dependence of the nucleon magnetic moments within a particular chiral quark model which guaranteed the correct leading and next-to-leading non-analytic behavior in m_q [1]. It turned out that the complete dependence on m_q could be described very well by a simple Padé approximant (cf. Eq. (1) below), even though the usual perturbative chiral expansion deviated quite badly from the Padé for pion masses less than twice the physical pion mass – well below any existing lattice data.

E-mail addresses: ehackett@physics.adelaide.edu.au (E.J. Hackett-Jones), dleinweb@physics.adelaide.edu.au (D.B. Leinweber), athomas@physics.adelaide.edu.au (A.W. Thomas).

0370-2693/00/$ - see front matter
PII: S0370-2693(00)00899-6

In view of these earlier results, our extrapolations here will also be based on Padé approximants which ensure the correct leading non-analytic behavior as well as the correct heavy quark behaviour. In the case of the nucleon, this extrapolation procedure led to very reasonable values for the proton and neutron magnetic moments at the physical pion mass, $\mu_p = 2.85(22)\,\mu_N$ and $\mu_n = -1.90(15)\,\mu_N$ (see Figure 5 of Ref. [1]). These values agree well with the experimental measurements, namely $\mu_p = 2.793\,\mu_N$ and $\mu_n = -1.913\,\mu_N$. Here we explore the application of this procedure to octet baryons in general.

The magnetic moment results used here are extracted from the lattice QCD calculations of Ref. [2]. While the results are now quite old, they continue to be the *only* lattice estimates of the spin-1/2 baryon octet magnetic moments available at the moment. These results were all obtained at pion masses above 600 MeV. We extrapolate these results as functions of the pion mass, m_π, to the physical pion mass of 140 MeV, to obtain the physical magnetic moment predictions. Because the lattice calculations are quenched, we expect that there are errors in the lattice data which we have been unable to take into account. However, as explained in Ref. [1], these errors are expected to be on the scale of the statistical errors. Nevertheless, an ideal extrapolation of magnetic moments would use full QCD lattice results which are unavailable at the moment.

2. Extrapolations

To extrapolate the lattice calculations of the magnetic moments we use the Padé approximant:

$$\mu_i(m_\pi) = \frac{\mu_0}{1 - \dfrac{\chi_i}{\mu_0} m_\pi + c\, m_\pi^2} \tag{1}$$

where χ_i, corresponding to the i^{th} baryon, is fixed model-independently by chiral perturbation theory and μ_0 and c are allowed to vary to best fit the data [1]. This formula builds in the chiral behaviour at small m_π, governed by χ_i, as well as the correct heavy quark behaviour, as discussed in the following.

The Goldstone boson loops resulting from dynamical chiral symmetry breaking mean that the baryon magnetic moments exhibit certain model independent, non-analytic behaviour in the quark masses. Using an expansion about the chiral SU(3) limit, one finds that the magnetic moments of the octet baryons (in nuclear magnetons, μ_N) are given by

$$\mu_i = \gamma_i + \sum_{X=\pi,K} \beta_i^{(X)} \frac{m_N}{8\pi f^2} m_X + \ldots \tag{2}$$

where the ellipses represent higher order terms, including logarithms [3]. Here f is the pion decay constant in the chiral limit (93 MeV) and m_N is the nucleon mass. For our purposes, namely extrapolating lattice data at fixed strange quark mass (m_s) as a function of the light quark mass (m_q), it is preferable to expand about the SU(2) chiral limit. The cloudy bag calculations in Ref. [1] showed that Goldstone boson loops are suppressed like m_X^{-4} at large m_X (comparable to m_K). Although this result is model dependent, the lattice simulations themselves do not show a rapid variation with m_X at values of order m_K or higher, thus supporting the general conclusion. One therefore expects that the kaon loops should be relatively small and slowly varying as a function of m_q[1]. They can therefore be absorbed in the fit parameters μ_0 and c. On the other hand, the rapid variation of m_π with m_q means that the leading non-analytic behaviour in m_π must be treated explicitly.

It is simple to see that the Padé approximant, Eq. (1), guarantees the correct behaviour of the magnetic moments in the chiral SU(2) limit. Expanding Eq. (1) about $m_\pi = 0$ we find

$$\mu_i = \mu_0 + \chi_i m_\pi + \left(\frac{\chi_i^2}{\mu_0} - \mu_0 c \right) m_\pi^2 + \ldots \tag{3}$$

In order to reproduce the leading non-analytic behaviour of the chiral expansion in our fit we fix χ_i to the value $\beta_i^{(\pi)}\left(m_N/8\pi f^2\right)$ for the i^{th} octet baryon. The one-loop corrected estimates [3] of the coefficients $\beta_i^{(\pi)}$ and χ_i are given in Table 1.

[1] Recall that $m_K^2 \propto m_s + m_q$ and m_s is fixed and large.

Table 1
One-loop corrected estimates of $\beta_i^{(\pi)}$ (in Eq. (2)) and $\chi_i = \beta_i^{(\pi)}\left(m_N/8\pi f^2\right)$

	p	n	Λ	Σ^+	Σ^0	Σ^-	Ξ^0	Ξ^-
$\beta_i^{(\pi)}$	$-(F+D)^2$	$(F+D)^2$	0	$-\frac{2}{3}D^2-2F^2$	0	$\frac{2}{3}D^2+2F^2$	$-(D-F)^2$	$(D-F)^2$
$\beta_i^{(\pi)}$	-1.02	1.02	0	-0.57	0	0.57	-0.04	0.04
χ_i	-4.41	4.41	0	-2.46	0	2.46	-1.91	1.91

The Padé approximant, Eq. (1), also builds in the expected behaviour at large m_π. At heavy quark masses we expect that the magnetic moment should fall off as the Dirac moment

$$\mu = \frac{e_q}{2m_q} \propto \frac{1}{m_\pi^2} \tag{4}$$

as m_π becomes moderately large. This is clearly the case in the Padé approximant. Therefore, the Padé approximant has been chosen to reproduce physical phenomena at the small and large m_π scales. It also succinctly describes the excellent phenomenology of the Cloudy Bag Model [1,4]. The Padé approximant has already been used successfully in the extrapolation of lattice results of magnetic moments of the nucleon, which we include here for completeness [1].

3. Results

In the following graphs, Figs. 1, 2, 3, 4, lattice calculations of the baryon magnetic moments are fitted as a function of m_π, according to the Padé approximant given in Eq. (1), with coefficients, χ_i, from Table 1. In each case the solid lines are Padé approximant fits to the magnetic moment lattice results. Experimental measurements are indicated at the physical pion mass by an asterisk (★). The magnetic moment predictions of the Padé approximant are compared with experimental values in Table 2. The fit parameters, μ_0 and c, for the solid lines are also indicated.

In the case of the nucleon, the fits given here (Figs. 1 and 2) are slightly different from those given in Ref. [1], as we omit the second set of lattice results (these were extracted from Ref. [6] which dealt with the nucleon only) in order to produce a consistent set of graphs for the entire baryon octet. However, the nucleon fits shown here still give excellent agreement with experimental data. The physical magnetic moment predictions for the Σ^+ and Σ^- are also in good agreement with experiment.

Using magnetic moment values predicted by the Padé approximant we can calculate the ratio of the

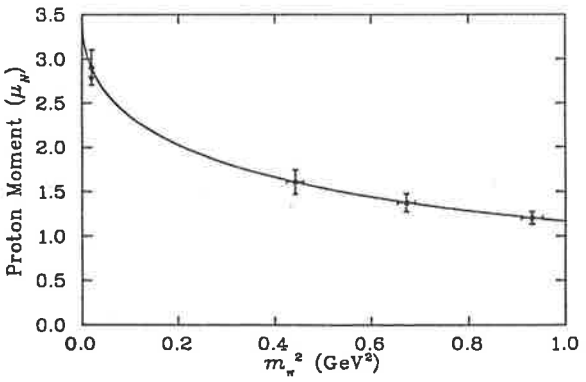

Fig. 1. Fits to lattice results of the proton magnetic moment. The physical value predicted by the fit is also indicated, as is the experimental value, denoted by an asterisk.

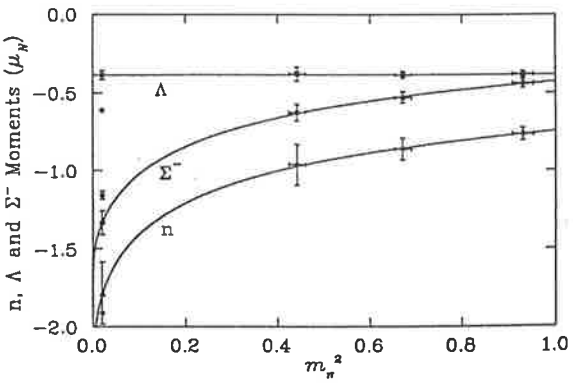

Fig. 2. Fits to lattice results of the neutron, Λ and Σ^- magnetic moments. The physical values predicted by the fits are indicated, as are the experimental values, which are denoted by asterisks.

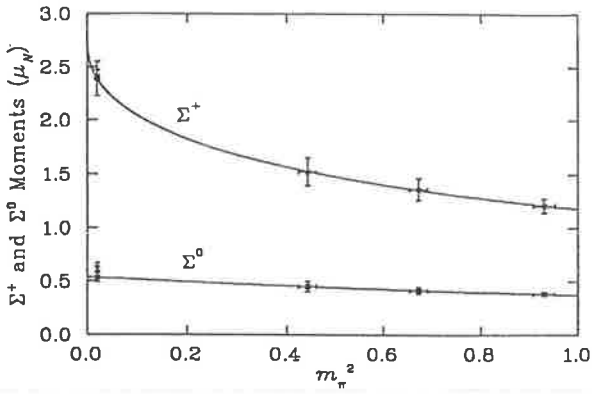

Fig. 3. Fits to lattice calculations of the Σ^+ and Σ^0 magnetic moments. The physical values predicted by the fits are indicated, as are the experimental values (see text), which are denoted by asterisks.

Ξ^- and Λ magnetic moments. The simple quark model predicts that this ratio is given by

$$\frac{\mu_{\Xi^-}}{\mu_\Lambda} = \frac{1}{3}\left(4 - \frac{\mu_d}{\mu_s}\right) \tag{5}$$

which becomes

$$\frac{\mu_{\Xi^-}}{\mu_\Lambda} = \frac{1}{3}\left(4 - \frac{m_s}{m_d}\right) \tag{6}$$

if we take each quark magnetic moment to be given by the Dirac moment of its constituent mass. In this case the ratio is less than 1 for $m_s > m_d$. This disagrees with the experimentally measured value of 1.13(7). However, using the predictions of the Padé approximant, we obtain a value of 1.15 for this ratio, which is in excellent agreement with the experimental data. This is a good indication that meson cloud effects must be included in an extrapolation of lattice results to the physical regime.

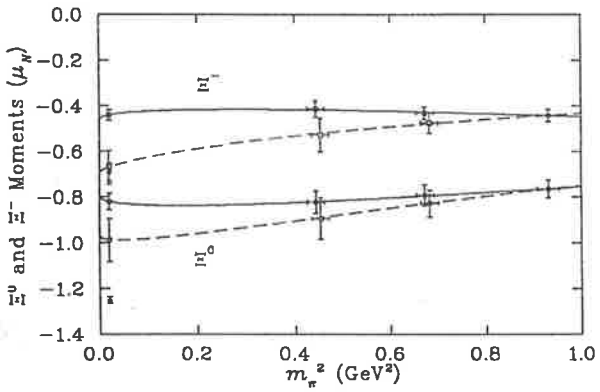

Fig. 4. Fits to lattice calculations of the Ξ^0 and Ξ^- magnetic moments. The upper two lines are fits for Ξ^- results and the lower two lines for Ξ^0 results. Solid lines represent fits to the magnetic moment results, whereas dashed lines represent fits to averaged results (denoted by open symbols which are offset for clarity), as described in the text. The physical values predicted by the fits are indicated, as are the experimental values, which are denoted by asterisks.

Table 2
Magnetic moments of the octet baryons (in nuclear magnetons) predicted by lattice QCD compared with experiment. (The experimental value for Σ^0 is taken from the average of Σ^+ and Σ^- experimental results, which is valid in the limit of isospin symmetry.) The fit parameters μ_0 and c of the Padé approximant are also indicated in units of μ_N and GeV^{-2} respectively. The column entitled 'Averaged Lattice' reports magnetic moments from extrapolations of lattice calculations averaged to better describe the strange quark mass, as discussed in the text

Baryon	μ_0	c	Lattice	Averaged Lattice	Experiment
p	3.46	0.68	2.90(20)		2.793
n	−2.28	0.11	−1.79(21)		−1.913
Λ	−0.38	0.005	−0.38(3)		−0.613(4)
Σ^+	2.71	0.40	2.39(16)	2.53(18)	2.42(5)
Σ^0	0.54	0.44	0.53(5)	0.58(7)	0.63(4)
Σ^-	−1.64	1.35	−1.33(8)	−1.35(15)	−1.157(25)
Ξ^0	−0.80	0.29	−0.82(4)	−0.99(10)	−1.250(14)
Ξ^-	−0.46	−0.38	−0.44(2)	−0.67(8)	−0.69(4)

The lattice calculations of baryon magnetic moments used in this letter were made with a strange quark mass of approximately 250 MeV [2]. This is much heavier than the physical mass of the strange quark of 115 ± 8 MeV at a scale 2 GeV, taken from a careful analysis of QCD sum rules for τ decay [5]. The contribution of the strange quark to the Σ baryon magnetic moments is very small. Lattice QCD calculations indicate that the contribution of a singly represented quark in a baryon is half that anticipated by SU(6) spin-flavour symmetry [7]. Hence the heavy strange quark mass will have a subtle effect on the Σ moments. By contrast, the strange quarks dominate the Λ and Ξ magnetic moments. Thus the heavy strange quark produces a large error in the lattice data for these baryons, which so far we have not taken into account. This is reflected in the predictions of the Λ, Ξ^0 and Ξ^- magnetic moments which are smaller in magnitude than the experimental measurements in all cases.

In an attempt to correct for the effect of the large strange quark mass considered in the lattice calculations, we average the magnetic moment lattice results of each $S \neq 0$ baryon with magnetic moment results of a light-quark equivalent baryon[2]. This procedure interpolates between magnetic moment lattice results produced with heavy strange quarks and those produced with zero strange quark mass. These averaged results have an effective strange quark mass closer to the physical strange quark mass. We have also used the Padé approximant to extrapolate the averaged results. The effect on the Σ moments is subtle (see Table 2). However, in the case of Ξ^-, this method is sufficient to reproduce the empirical Ξ^- moment (as shown by the dashed line in Fig. 4). There is a remaining discrepancy in the value predicted for the Ξ^0. Clearly the present estimate of the correction for the heavy strange quark mass is somewhat crude. We therefore regard it as very important to have new simulation data with a realistic strange quark mass. At that stage it may also be necessary to include kaon loop effects, because the transition $\Xi^0 \to \Sigma^+ + K^-$ is energetically favoured, and will make a negative contribution to the Ξ^0 magnetic moment.

4. Conclusion

We have shown that the Padé approximant which was introduced to extrapolate lattice results for the magnetic moments of the nucleon, is also successful in predicting magnetic moments for the spin-1/2 baryon octet. The magnetic moment values predicted by the fits for the p, n, Σ^+ and Σ^- compare well with experimental data. As a first estimate of the correction to be expected if a more realistic strange quark mass were used, we averaged lattice results for the $S \neq 0$ baryons with the magnetic moments of the corresponding light-quark baryons. This had a small effect on the predictions for the Σ baryon magnetic moments, but significantly improved the Ξ baryon results. In the case of Ξ^-, the averaging procedure produced good agreement with the experimental results. In the future we hope to perform a similar extrapolation procedure using more precise magnetic moment lattice data, calculated with realistic strange quark masses. At that stage it may also be necessary to include the kaon loop corrections, especially for the doubly strange Ξ hyperons.

[2] Lattice calculations of a light-quark equivalent Λ are not available.

Acknowledgements

This work was supported by the Australian research Council and the University of Adelaide.

References

[1] D.B. Leinweber, D.H. Lu, A.W. Thomas, Phys. Rev. D 60 (1999) 034014, hep-lat/9810005.
[2] D.B. Leinweber, R.M. Woloshyn, T. Draper, Phys. Rev. D 43 (1991) 1659.
[3] E. Jenkins, M. Luke, A.V. Manohar, M.J. Savage, Phys. Lett. B 302 (1993) 482; Phys. Lett. B 388 (1996) 866 (E), hep-ph/9212226.
[4] S. Theberge, A.W. Thomas, Nucl. Phys. A 393 (1983) 252; A.W. Thomas, Adv. Nucl. Phys. 13 (1984) 1.
[5] K. Maltman, Phys. Lett. B 462 (1999) 195, hep-ph/9904370.
[6] W. Wilcox, T. Draper, K.F. Liu, Phys. Rev. D 46 (1992) 1109, hep-lat/9205015.
[7] D.B. Leinweber, A.W. Thomas, ADP-99-52/T388, hep-lat/9912052.

ELSEVIER

23 November 2000

PHYSICS LETTERS B

Physics Letters B 494 (2000) 89–99

www.elsevier.nl/locate/npe

Incorporating chiral symmetry and heavy quark theory in extrapolations of octet baryon charge radii

E.J. Hackett-Jones, D.B. Leinweber *, A.W. Thomas

Special Research Centre for the Subatomic Structure of Matter and Department of Physics and Mathematical Physics, University of Adelaide, Adelaide, Australia 5005

Received 30 June 2000; received in revised form 9 August 2000; accepted 18 August 2000
Editor: W. Haxton

Abstract

We extrapolate lattice calculations of electric charge radii of the spin-1/2 baryon octet to the physical regime. The extrapolation procedure incorporates chiral perturbation theory and heavy quark effective theory in the appropriate limits. In particular, this procedure includes the non-analytic, logarithmic terms from pion loops. The electric charge radii of the nucleons and Σ^- obtained from the chiral extrapolations agree well with experimental data. We make predictions for the charge radii of the remaining baryons in anticipation of future experimental measurements. © 2000 Elsevier Science B.V. All rights reserved.

1. Introduction

Lattice QCD is so far the most successful method of calculating hadronic observables from the theory of QCD. However, computational limitations mean that hadronic observables are calculated on the lattice at quark masses larger than their physical values. Hence results from lattice simulations cannot be directly compared with experimental data. Although, with improvements in actions, algorithms and computer speed, future lattice calculations will be performed much closer to the physical regime, these improvements will proceed over many years. Therefore, to make sense of any lattice results produced to date, and to compare them with experiment, one must understand how to extrapolate lattice results, obtained at large quark masses, to the physical world.

One of the difficulties with calculating hadronic observables at heavy quark masses on the lattice is that chiral perturbation theory cannot be applied in this quark mass regime. However, chiral expansions of hadronic observables contain important non-analytic terms as a function of the quark mass, m_q (or equivalently of m_π^2, as $m_q \propto m_\pi^2$ in this range). It is vital that this non-analytic behaviour is included in *any* extrapolation to the physical regime [1–8].

The chiral expansion of the squared electric charge radius of a spin-1/2 octet baryon includes non-analytic behaviour in the form of logarithmic terms in m_π (or m_q). To extrapolate the lattice results for electric charge radii we incorporate these logarithmic terms in our extrapolation formulae, while ensuring that the correct heavy quark behaviour is also maintained. A similar approach [1] has been successful in explaining why lattice simulations of pion and proton charge radii are similar in size, while experimental measure-

* Corresponding author.
E-mail addresses: ehackett@physics.adelaide.edu.au (E.J. Hackett-Jones), dleinweb@physics.adelaide.edu.au (D.B. Leinweber), athomas@physics.adelaide.edu.au (A.W. Thomas).

0370-2693/00/$ – see front matter
PII: S0370-2693(00)01115-1

ments reveal a significant difference. The dramatic differences in the chiral behaviour of the pion and proton charge radii account for the similarity of the lattice results at moderately heavy pion masses, while allowing good agreement with experiment at the physical pion mass. This illustrates the importance of including meson cloud effects in extrapolations of lattice results to the physical regime. In this paper, we improve the formalism of chiral extrapolations by incorporating both chiral symmetry and heavy quark effective theory.

Our lattice "data" for the electric charge radii is taken from the calculations of Ref. [9]. The contributions to the charge radii from individual quark flavours are also given there. These results are the only available lattice calculations of the electric charge radii of spin-1/2 octet baryons. For each baryon, the electric charge radius was calculated at three different quark masses, corresponding to rather heavy pion masses (all exceeding 600 MeV). Here we extrapolate these results as functions of the squared pion mass, m_π^2, to obtain predictions for the charge radii at the physical pion mass (139 MeV). Because the lattice calculations are quenched, we expect that there are errors in the lattice data which we have been unable to take into account. However, we expect that errors from the quenching approximation will be rather small. At the quark masses considered on the lattice, the dominant effect is a simple renormalization of the strong coupling constant, accounted for in setting the lattice spacing scale. When results from unquenched simulations become available, the formalism presented here may be readily applied.

2. Extrapolations

Dynamical breaking of chiral symmetry in the QCD lagrangian results in the formation of an octet of (pseudo-) Goldstone bosons. Goldstone boson loops give rise to significant non-analytic behaviour in hadronic observables, such as $\langle r_i^2\rangle$ and magnetic moments, as a function of the quark mass, m_q. Using an expansion about the chiral SU(3) limit gives the following expression for the squared electric charge radius, $\langle r_i^2\rangle$, of a spin-1/2 octet baryon (labelled by i) [10]

$$\langle r_i^2\rangle = \gamma_i + \sum_{X=\pi,K} \frac{6\alpha_i^{(X)}}{(4\pi f_\pi)^2} \ln\left(\frac{m_X}{\lambda}\right) + \cdots. \tag{1}$$

Here f_π is the pion decay constant (93 MeV) and λ is the scale of the dimensional regularization. (The value of γ_i is clearly correlated with the choice of λ.) Unlike SU(2)-flavour symmetry, SU(3) is significantly broken in the physical world, with the strange quark mass the same order of magnitude as $\Lambda_{\rm QCD}$ for low-energy phenomenology. The squared kaon mass exceeds the squared pion mass by over an order of magnitude. Given that the source of the meson cloud associated with a baryon is of a finite size, one might anticipate that the role of the kaon cloud will be suppressed away from the SU(3) chiral limit [11]. The form factor describing the finite size of the kaon source will act to suppress kaon loop effects like m_X^{-4} at large m_X (comparable to m_K). This was demonstrated within a particular chiral quark model for the nucleon magnetic moments in Ref. [4]. Despite the model-dependence associated with the form factors, the lattice results themselves are very slowly varying functions of m_X at values of the order m_K or higher, thus supporting the general conclusion. Therefore kaon loop effects are expected to be small and slowly varying as a function of m_q. Hence we do not explicitly include kaon contributions in our extrapolation formulae. Conversely, since m_π varies rapidly with m_q, the leading non-analytic behaviour in m_π must be included explicitly in an extrapolation to the chiral regime.

To extrapolate the lattice calculations of the electric charge radii of the spin-1/2 octet baryons, we consider two distinct fitting procedures. Both these extrapolation schemes satisfy the constraints of chiral perturbation theory and heavy quark effective theory. The first extrapolation procedure we investigate is given simply by the formula

$$\langle r_i^2\rangle = \frac{c_1 + \chi_i \ln(m_\pi/\Lambda)}{1 + c_2 m_\pi^2}, \tag{2}$$

where $\langle r_i^2\rangle$ are the lattice QCD results (at several values of m_π) extracted from Ref. [9], c_1 and c_2 are fit parameters chosen to best fit these results, χ_i (corresponding to the ith baryon) is fixed (model-independently) by chiral perturbation theory and Λ, which is directly correlated with c_1, is fixed at 1 GeV.

This extrapolation procedure is not feasible for the neutral baryons because $\langle r_i^2 \rangle \to 0$ as m_π becomes large and thus sensitivity to the c_2 fit parameter is lost. In order to extrapolate the neutral baryon charge radii results we consider a second extrapolation procedure, focusing on individual quark "sector" (or quark flavour) contributions, as discussed below.

Clearly the extrapolation formula given in Eq. (2) builds in the correct chiral behaviour in the SU(2) limit, since in the limit $m_\pi \to 0$ it can be expanded as follows

$$\langle r_i^2 \rangle = c_1 + \chi_i \ln(m_\pi) - c_2 m_\pi^2 + \cdots . \tag{3}$$

(Recall that the scale Λ, in Eq. (2), has been set to 1 GeV. This choice is also implicit in Eqs. (6)–(10), below, where m_π in the logarithm must be in GeV.) This agrees with the chiral SU(2) expansion of the squared electric charge radius (see Eq. (1)), provided we fix the coefficient χ_i to $6\alpha_i^{(\pi)}/(4\pi f_\pi)^2$ for the ith baryon. The coefficients $\alpha_i^{(\pi)}$ and χ_i are given in Table 1.

In the large m_q limit, we expect that the quarks behave non-relativistically, and the squared charge radius falls off as m_q^{-2}, as it does in non-relativistic quantum mechanics. In the region where m_q is very large, $m_q \propto m_\pi$, and hence we require that

$$\langle r_i^2 \rangle \propto \frac{1}{m_\pi^2}, \tag{4}$$

as m_π becomes extremely large. This is clearly satisfied by our first extrapolation formula, Eq. (2), since the logarithm is very slowly varying.

In the second extrapolation procedure we deal separately with the individual quark sector contributions to the baryon charge radii. For example, in the case of the nucleons, we extrapolate the up and down sector contributions separately. For the hyperons the strange and light sector results are extrapolated separately. This avoids the problem encountered with the neutral baryons which was mentioned previously, because now all the quantities being extrapolated are charged, even if the overall charge on the baryon is zero. This separation is valid because the squared electric charge radius can be decomposed as

$$\langle r_i^2 \rangle = \sum_{q=u,d,s} e_q \langle r_i^{(q)2} \rangle, \tag{5}$$

where $\langle r_i^{(q)2} \rangle$ is the contribution from the qth quark sector and e_q is the charge of this quark sector. Therefore, provided that the extrapolation formulae from each sector add so that the chiral and heavy quark limits of the sum are in agreement with Eqs. (1) and (4), respectively, this method contains the same physics as the first method, but simply makes use of the extra information contained in the individual quark sector results. Not only does this second extrapolation procedure solve the neutral baryon extrapolation difficulty, it also provides predictions for individual quark sector radii, which will be resolved at Jefferson Lab for the nucleon [12], and perhaps future accelerator facilities for hyperons.

Isolation of the individual quark sector contributions to the charge radii is relatively straightforward from the theoretical point of view. For example, to isolate the u-sector contribution to the charge radius of the proton one simply sets the d-quark charge to zero and calculates the proton charge radius as if only the u quark carried charge. In the chiral expansion of the proton charge radius, the coefficient of the logarithm, $\chi_p^{(\pi)}$, originates from the pion loop, $p \to n + \pi^+$ (see Fig. 1), and includes the charge of the pion cloud. Therefore, to extrapolate the u-sector contribution to the proton charge radius, the appropriate coefficient of the logarithm is $\frac{2}{3}\chi_p^{(\pi)}$, since the pion now carries charge $+2/3$. Thus we extrapolate the u-sector results of the proton according to

$$2e_u \langle r_p^{(u)2} \rangle = \frac{c_1 + \frac{2}{3}\chi_p^{(\pi)} \ln(m_\pi)}{1 + c_2 m_\pi^2}, \tag{6}$$

where $\chi_p^{(\pi)}$ is the full chiral coefficient of the proton, given in Table 1 and $\langle r_p^{(u)2} \rangle$ is the squared charge

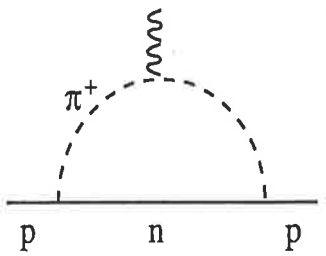

Fig. 1. Schematic illustration of the pion loop which produces the leading non-analytic contribution to the proton charge radius.

radius of a single u-quark of unit charge. Similarly, the d-sector results are extrapolated according to

$$e_d\langle r_p^{(d)2}\rangle = \frac{c_1' + \frac{1}{3}\chi_p \ln(m_\pi)}{1 + c_2' m_\pi^2}, \tag{7}$$

where the factor of $1/3$ originates from the $\bar{d}$ contribution to the pion cloud. Clearly adding the left-hand sides of Eqs. (6) and (7) yields the full expression for $\langle r_p^2\rangle$. In the chiral limit the right-hand sides add so that the correct chiral form for $\langle r_p^2\rangle$, given in Eq. (3), is retained. The sum of Eqs. (6) and (7) also obeys the correct heavy quark behaviour, given in Eq. (4). Since the parameters c_2 and c_2' are not necessarily the same, the individual quark sector extrapolation formulae (Eqs. (6) and (7)) cannot be added directly to give Eq. (2). Therefore, in general we do not expect the two extrapolation procedures to give exactly the same results. For the charged baryons this may be used to help quantify the systematic error of the approach. For the neutron, the analogous extrapolation functions are given by

$$e_u\langle r_n^{(u)2}\rangle = \frac{c_1 + \frac{2}{3}\chi_n^{(\pi)} \ln(m_\pi)}{1 + c_2 m_\pi^2}, \tag{8}$$

for the u-quark sector, and

$$2e_d\langle r_n^{(d)2}\rangle = \frac{c_1' + \frac{1}{3}\chi_n^{(\pi)} \ln(m_\pi)}{1 + c_2' m_\pi^2}, \tag{9}$$

for the d-quark sector results, where $\chi_n^{(\pi)}$ is given in Table 1.

We now consider extrapolating the hyperon charge radii results using the second extrapolation procedure, i.e., extrapolating the strange and light quark sector results separately. In extrapolating the strange quark sector the charges of the light quarks are set to zero. Since the logarithmic term considered here originates from pionic corrections to the charge radius (and pions do not contain strange quarks), the coefficient of the logarithm in the strange sector extrapolation will be zero. Similarly, for the light sector extrapolation, strange quarks do not carry charge and hence the coefficient of the logarithm in this extrapolation will be the full coefficient, $\chi_i^{(\pi)}$. This results in the following extrapolation formulae for the hyperon quark sector contributions

$$e_l\langle r_i^{(l)2}\rangle = \frac{c_1 + \chi_i \ln(m_\pi)}{1 + c_2 m_\pi^2} \tag{10}$$

and

$$e_s\langle r_i^{(s)2}\rangle = \frac{c_1'}{1 + c_2' m_\pi^2}, \tag{11}$$

where i runs over the hyperons only, and l corresponds to the light-quark (u and/or d) sector. Since the strange quark mass is held fixed in the light quark mass extrapolation, any variation in the strange quark sector is purely an environment effect from the surrounding light quarks. As such, the functional form for the strange quark sector is constrained by neither leading order chiral perturbation theory nor heavy quark effective theory. As we shall see, c_2' is small and negative for each hyperon, which suggests that a simple linear ansatz for the strange quark sector extrapolation could also have been used.

3. Results

The lattice QCD simulations were performed on a $24 \times 12 \times 12 \times 24$ periodic lattice using standard Wilson actions at $\beta = 5.9$. Dirichlet boundary conditions were used for fermions in the time direction. Twenty-eight quenched gauge configurations were generated by the Cabibbo–Marinari [18] pseudo-heatbath method. The conserved vector current was derived from the Wilson fermion action via the Noether procedure. The associated lattice Ward identity protects this vector current from renormalization. The radii were produced by fitting the electric form factor to dipole and monopole forms, allowing a charge radius to be extracted in each case. Since it is known from experiment that the dipole form is more suitable for parameterizing the electric form factor, we consider only the dipole results here. Statistical uncertainties in the lattice simulation results are calculated in a third-order, single elimination jackknife [19,20]. Further details may be found in Ref. [9].

The extrapolations of lattice calculations for the charge radii of the spin-1/2 baryon octet are shown in Figs. 2–7. Extrapolations of baryon charge radii results, performed according to Eq. (2), are indicated by the solid lines, where the full circles (•) represent the baryon charge radii from lattice QCD and the extrapolated value at $m_\pi = 139$ MeV. The individual quark sector extrapolations are shown by the dashed and dot-dashed lines, and the baryon charge radius

Table 1
Baryon electric charge radii and the quark sector contributions. The latter are defined on the left-hand sides of Eqs. (6)–(11). One-loop corrected estimates of $\alpha_i^{(\pi)}$ (in Eq. (1)) and χ_i (in units of fm^2) for each octet baryon are indicated. For each extrapolation, the fit parameters, c_1 and c_2, and the predicted value of $\langle r^2\rangle$ at the physical pion mass are reported. Asterisks denote the squared charge radii reconstructed from the sum of separate quark sector extrapolations. (The units are such that the pion mass is in GeV and the squared charge radius in fm^2)

Baryon or quark sector	$\alpha_i^{(\pi)}$	χ_i	c_1	c_2	$\langle r^2\rangle$	Experiment
p	$-\frac{1}{6}-\frac{5}{6}(D+F)^2$	−0.174	0.34	0.50	0.68(8)	0.740(15) [14]
u_p	$\frac{2}{3}\left[-\frac{1}{6}-\frac{5}{6}(D+F)^2\right]$	−0.116	0.52	0.73	0.74(11)	
d_p	$\frac{1}{3}\left[-\frac{1}{6}-\frac{5}{6}(D+F)^2\right]$	−0.058	−0.18	1.38	−0.06(5)	
$^*p$					0.68(10)	0.740(15) [14]
n	$\frac{1}{6}+\frac{5}{6}(D+F)^2$	0.174				
u_n	$\frac{2}{3}\left[\frac{1}{6}+\frac{5}{6}(D+F)^2\right]$	0.116	0.35	1.38	0.12(10)	
d_n	$\frac{1}{3}\left[\frac{1}{6}+\frac{5}{6}(D+F)^2\right]$	0.058	−0.26	0.73	−0.37(6)	
$^*n$					−0.25(8)	−0.113(4) [15]
Λ	0	0				
l_Λ	0	0	0.15	0.97	0.14(3)	
s_Λ	0	0	−0.07	−0.10	−0.07(1)	
$^*\Lambda$					0.07(3)	
Σ^+	$-\frac{1}{3}-\frac{5}{3}\left(\frac{D^2}{3}+F^2\right)$	−0.138	0.68	2.03	0.92(11)	
l_{Σ^+}	$-\frac{1}{3}-\frac{5}{3}\left(\frac{D^2}{3}+F^2\right)$	−0.138	0.58	0.93	0.83(8)	
s_{Σ^+}	0	0	−0.06	−0.17	−0.06(1)	
$^*\Sigma^+$					0.77(8)	
Σ^0	0	0				
l_{Σ^0}	0	0	0.19	1.48	0.18(2)	
s_{Σ^0}	0	0	−0.06	−0.17	−0.06(1)	
$^*\Sigma^0$					0.12(2)	
Σ^-	$\frac{1}{3}+\frac{5}{3}\left(\frac{D^2}{3}+F^2\right)$	0.138	−0.25	0.08	−0.52(3)	−0.60(16) [16]
						−0.91(72) [17]
l_{Σ^-}	$\frac{1}{3}+\frac{5}{3}\left(\frac{D^2}{3}+F^2\right)$	0.138	−0.21	0.37	−0.47(3)	
s_{Σ^-}	0	0	−0.06	−0.17	−0.06(1)	
$^*\Sigma^-$					−0.54(3)	−0.60(16) [16]
						−0.91(72) [17]

(*continued on next page*)

Table 1 (*continued*)

Baryon or quark sector	$\alpha_i^{(\pi)}$	χ_i	c_1	c_2	$\langle r^2 \rangle$	Experiment
Ξ^0	$-\frac{1}{6} - \frac{5}{6}(D-F)^2$	-0.035				
l_{Ξ^0}	$-\frac{1}{6} - \frac{5}{6}(D-F)^2$	-0.035	0.29	0.97	0.35(5)	
s_{Ξ^0}	0	0	-0.15	-0.05	$-0.15(1)$	
$^\star\Xi^0$					0.20(5)	
Ξ^-	$\frac{1}{6} + \frac{5}{6}(D-F)^2$	0.035	-0.24	0.07	$-0.32(2)$	
l_{Ξ^-}	$\frac{1}{6} + \frac{5}{6}(D-F)^2$	0.035	-0.12	0.70	$-0.19(2)$	
s_{Ξ^-}	0	0	-0.15	-0.05	$-0.15(1)$	
$^\star\Xi^-$					$-0.34(2)$	

predicted by this method is indicated by a full square (■). Experimental measurements are indicated at the physical pion mass by an asterisk (⋆). Note that for the charged baryons, two extrapolation schemes and two corresponding predicted physical values are shown, whereas (for the reasons explained in Section 2) only one extrapolation procedure is shown for each neutral baryon.

In the case of the proton, the two extrapolated results agree very well with the experimental measurement. It can be seen that a traditional linear extrapolation in m_π^2 would significantly underestimate the experimental result. Similarly the predicted charge radius for the neutron (produced by separate extrapolations of the u- and d-sector results) agrees with the experimental data significantly better than the prediction from a conventional linear extrapolation in m_π^2. Both predicted values for Σ^- also agree very well with the two experimental measurements. These baryons are currently the only baryons of the spin-1/2 octet whose electric charge radius has been measured.

From simple quark model arguments [9], where the heavier strange quark has a smaller distribution than the light quarks, we expect the hierarchy of electric charge radii of charged octet baryons to be given as follows

$$|\langle r^2_{\Sigma^+}\rangle| \geqslant |\langle r^2_p\rangle| \geqslant |\langle r^2_{\Sigma^-}\rangle| \geqslant |\langle r^2_{\Xi^-}\rangle|. \tag{12}$$

Clearly the results of the lattice extrapolations shown in Table 1 are in qualitative agreement with this expectation. Indeed, in the regime of the actual lattice data ($m_\pi \geqslant 600$ MeV) the argument is even quantitative. However, as the chiral limit (and physical pion mass) is approached, the simple quark model description is no longer adequate and chiral physics gives rise to dramatic effects. For example, in the extrapolation of the d-quark sector of the proton (Fig. 2), chiral effects mean that the d-quark sector can actually make a *positive* contribution to the charge radius, via the $\bar{d}$ contribution in π^+ — even though the total contribution is negative at the physical pion mass. This behaviour is not anticipated by the simple quark model.

For the neutral baryons the sign of the squared charge radius is important. In the neutron, the two d quarks are most likely to be found in a spin-1 configuration, where they will undergo hyperfine repulsion. This leads to a small, negative charge radius squared. However, as one approaches the chiral limit, spontaneous chiral symmetry breaking, in particular the process $n \to p\pi^-$, which carries d-quarks to larger radii and screens the u-quark contribution via the $\bar{u}$ in the π^-, leads to an enhancement of the negative charge radius. The remaining neutral baryons, Σ^0, Λ and Ξ^0, have a positive squared charge radius. This is because in each case the strange quark distribution is more localized than the light quark charge distribution (due to the larger mass of the strange quark). Therefore on average the light quark charge distribution occurs at a larger radius, resulting in a positive charge radius (since the light quark charge is positive in each case).

The lattice results used here were calculated with a strange quark mass of approximately 250 MeV [9]. This is much larger than the physical strange quark

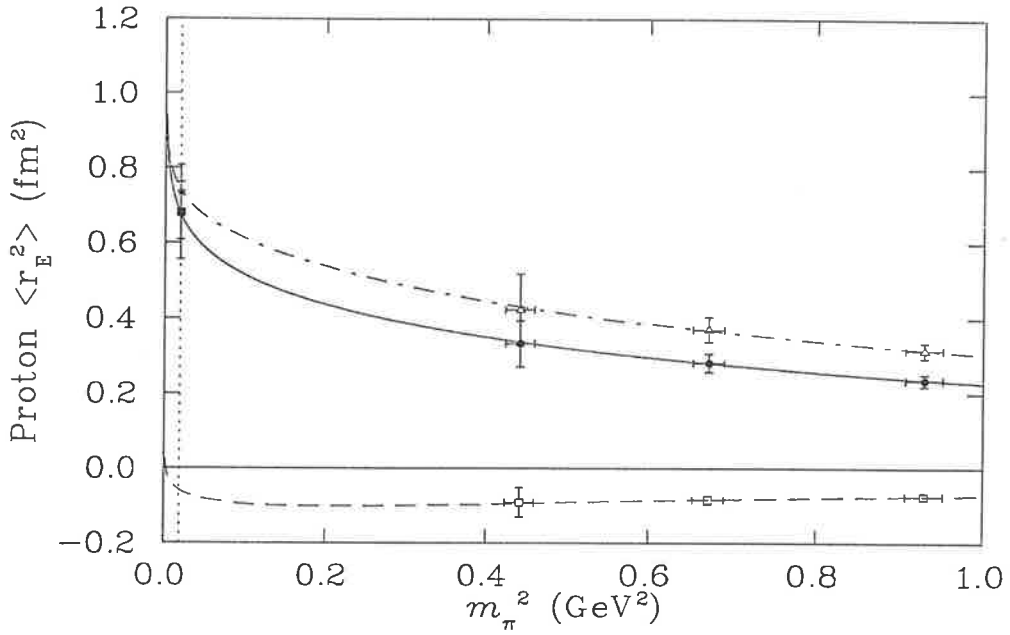

Fig. 2. Fits to lattice results for the squared electric charge radius of the proton. Fits to the individual quark sector results are also shown. The u-quark sector results are indicated by open triangles and the d-quark sector results by open squares. Physical values predicted by the fits are indicated at the physical pion mass, where the full circle denotes the result predicted from the first extrapolation procedure and the full square denotes the baryon radius reconstructed from the quark sector extrapolations (see text). (N.B. The latter values are actually so close as to be indistinguishable on the graph.) The experimental value is denoted by an asterisk.

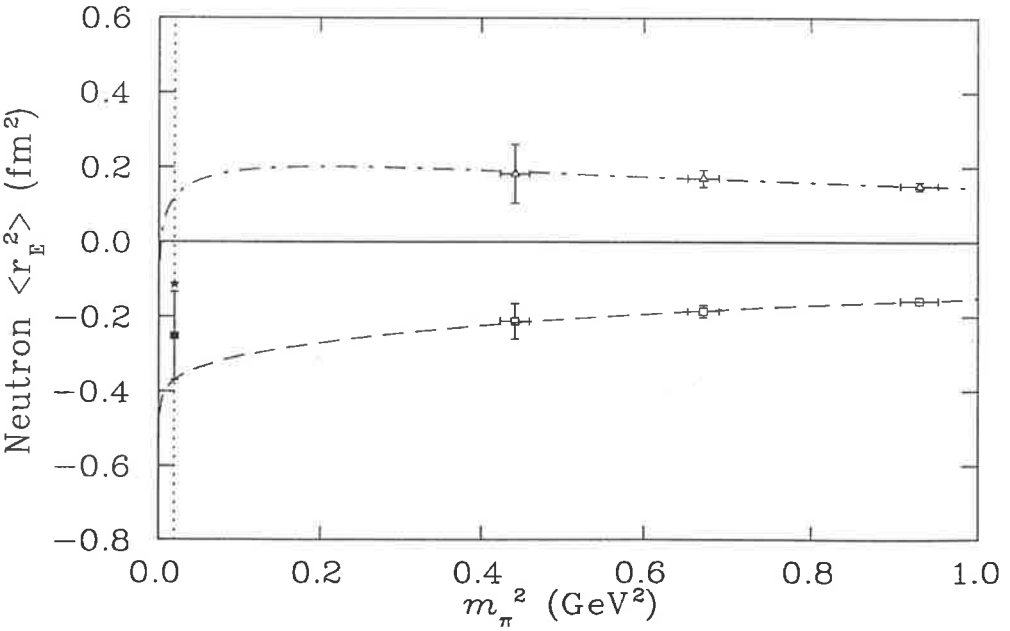

Fig. 3. Fits to lattice results for the quark sector contributions to the squared electric charge radius of the neutron. All symbols are defined in the caption of Fig. 2.

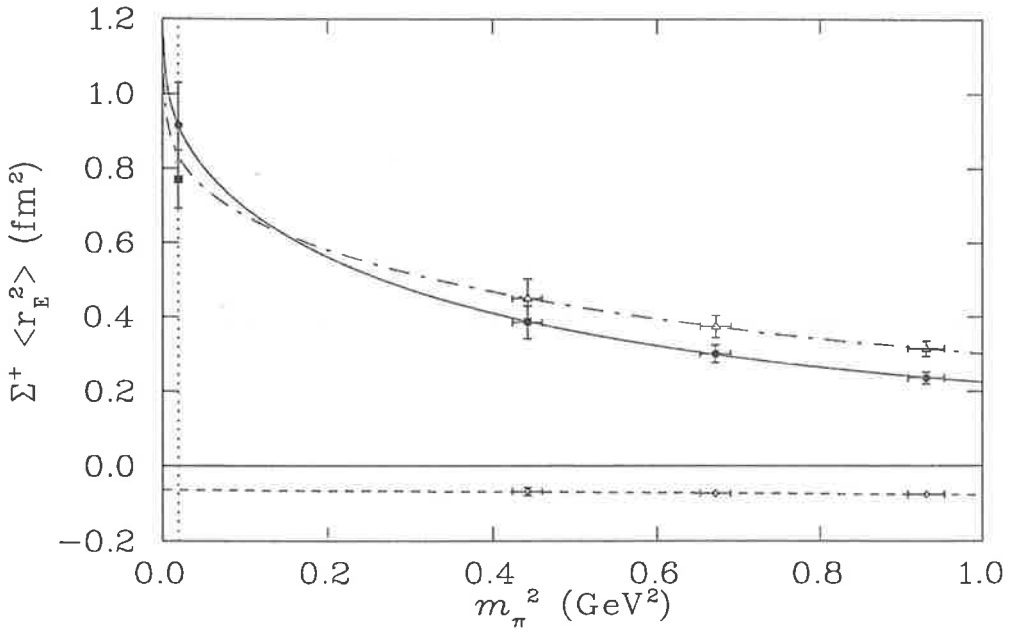

Fig. 4. Fits to lattice results of the squared electric charge radius of the Σ^+. Fits to the individual quark sector results are also shown. The strange quark sector results are indicated by open diamonds. All other symbols are defined in the caption of Fig. 2.

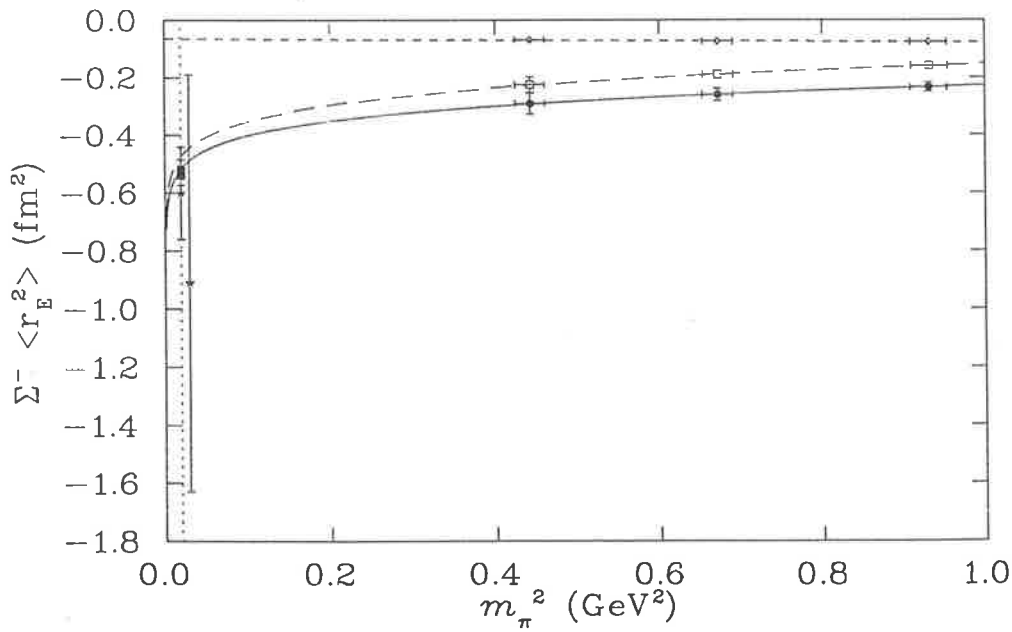

Fig. 5. Fits to lattice results of the squared electric charge radius of the Σ^-. Fits to the individual quark sector results are also shown. All symbols are defined in the captions of Figs. 2 and 4.

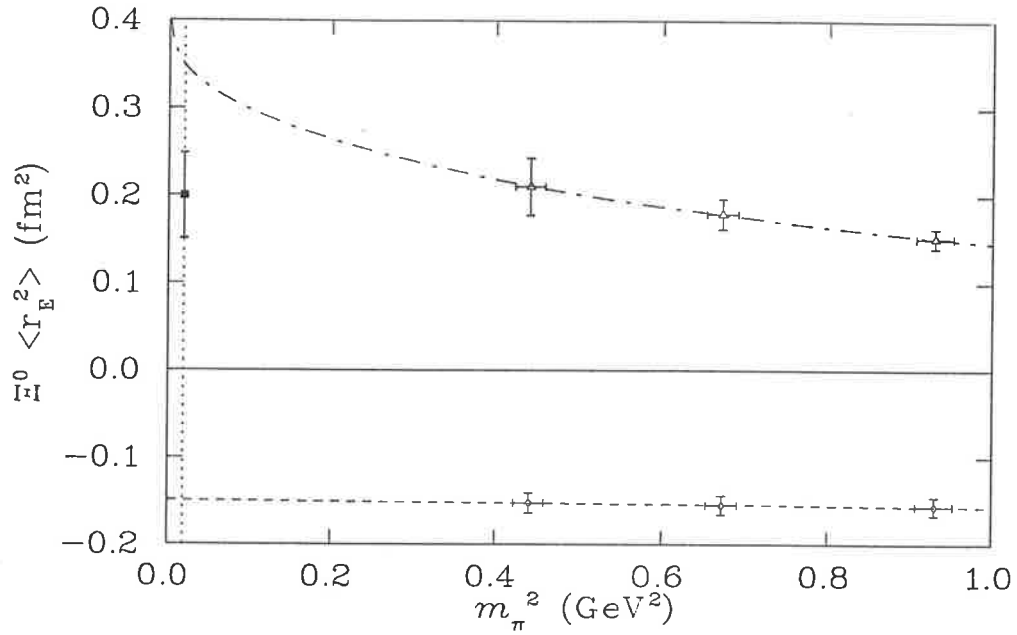

Fig. 6. Fits to lattice results for the quark sector contributions to the squared electric charge radius of the Ξ^0. All symbols are defined in the captions of Figs. 2 and 4.

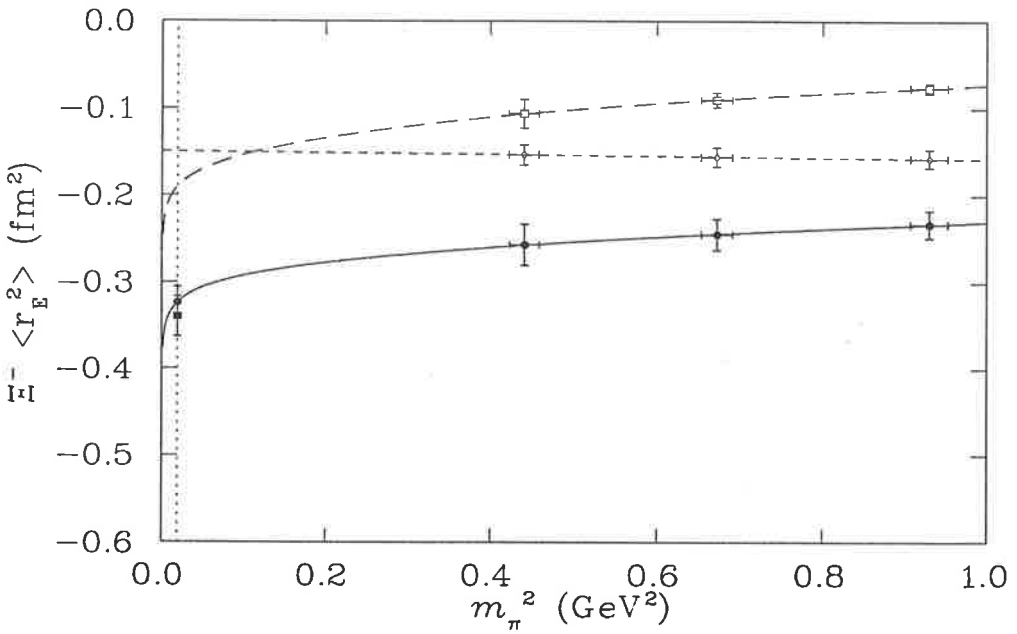

Fig. 7. Fits to lattice results of the squared electric charge radius of the Ξ^-. Fits to the individual quark sector results are also shown. All symbols are defined in the captions below Figs. 2 and 4.

mass of 115 ± 8 MeV at a scale 2 GeV, taken from a careful analysis of QCD sum rules for τ decay [13]. In an earlier study of lattice results for octet baryon magnetic moments [8] (where the results were extracted from the same lattice simulation [9]), it was found that the heavy strange quark had a significant effect on the predictions of the Ξ moments. Here we expect that the heavy strange quark should also have some effect on the Ξ charge radii. With a strange quark mass closer to the physical mass the strange quark contribution would be increased. This would result in a lower predicted charge radius for the Ξ^0 and a larger (in magnitude) charge radius for the Ξ^-. In the absence of experimental measurements we will not attempt to correct for the effect of the strange quark mass here.

As we see from Table 1, the extrapolated mean square charge radii obtained from both extrapolation procedures agree quite well for each charged octet baryon. For the proton, Σ^- and Ξ^- the reconstructed values completely cover the result from the original extrapolations of Eq. (2). In the case of the Σ^+ the two values overlap only on the error bars. This is due to the small variation in the strange quark contribution (which is caused by an environment effect). When this environment effect is included in the baryon charge radius, the magnitude of the slope is increased, resulting in a larger charge radius after extrapolation.

In turning the dimensionless masses calculated on the lattice to physical units, the lattice spacing, a, was set in the traditional manner by fixing the nucleon mass, obtained by a naive linear extrapolation in m_π^2, equal to the observed mass. Of course, such a linear extrapolation is known [5] to be inconsistent with chiral symmetry. We have checked that applying a more consistent chiral extrapolation would systematically lower values of $\langle r^2 \rangle$ obtained for the charged octet by of the order 15%. (The effect on neutral baryons is much smaller.) On the other hand, the data which we are forced to use is quenched data which omits some pion corrections. Although these are expected to be suppressed at the large values of m_π^2 for which the data is available (cf. Ref. [4]), the associated systematic error would tend to increase the calculated values of $\langle r^2 \rangle$, perhaps by 5–10%. Rather than attempt to repair these deficiencies in the present data, we feel it would be more reasonable to simply accept that there is an additional systematic error of the order 15% associated with the extrapolated values shown in Table 1. Adding this systematic in quadrature means that the values in Table 1 would become, for example, $\langle r^2_{\star_p} \rangle = 0.68 \pm 0.14$ fm^2, $\langle r^2_{\star_\Sigma^-} \rangle = -0.54 \pm 0.09$ fm^2, $\langle r^2_{\star_\Sigma^+} \rangle = 0.77 \pm 0.14$ fm^2. We look forward to repeating our analysis with unquenched data at lower quark mass, which is the best way to overcome these problems.

4. Conclusion

In this Letter we have investigated two methods of extrapolating lattice results for the electric charge radii of octet baryons to the physical regime. These procedures build in the correct leading non-analytic behaviour of the electric charge radii in the chiral limit, as well as the correct heavy quark behaviour. Both extrapolation procedures were performed for the charged octet baryons, with the predicted values agreeing very well. The extrapolation formulae seem to be very successful, as good agreement with experiment was obtained for the nucleons and the Σ^-. We await further experimental measurements of the baryon charge radii in order to test our predictions. In the future we hope to perform similar extrapolations of electric charge radius lattice results calculated with a more realistic strange quark mass and eventually with lighter, dynamical u- and d-quarks.

Acknowledgements

This work was supported by the Australian Research Council and the University of Adelaide. D.B.L. would like to thank Frank Lee and the Center for Nuclear Studies at George Washington University for their kind hospitality during which some of this research was carried out. We would also like to thank Pierre Guichon for helpful comments on the manuscript.

References

[1] D.B. Leinweber, T.D. Cohen, Phys. Rev. D 47 (1993) 2147, hep-lat/9211058.
[2] J.N. Labrenz, S.R. Sharpe, Phys. Rev. D 54 (1996) 4595, hep-lat/9605034.

[3] M.F.L. Golterman, K.C. Leung, Phys. Rev. D 58 (1998) 097503, hep-lat/9805032.
[4] D.B. Leinweber, D.H. Lu, A.W. Thomas, Phys. Rev. D 60 (1999) 034014, hep-lat/9810005.
[5] D.B. Leinweber, A.W. Thomas, K. Tsushima, S.V. Wright, Phys. Rev. D 61 (2000) 074502, hep-lat/9906027.
[6] D.B. Leinweber, A.W. Thomas, hep-lat/9912052.
[7] D.B. Leinweber, A.W. Thomas, S.V. Wright, hep-lat/0001007.
[8] E.J. Hackett-Jones, D.B. Leinweber, A.W. Thomas, hep-lat/0004006.
[9] D.B. Leinweber, R.M. Woloshyn, T. Draper, Phys. Rev. D 43 (1991) 1659.
[10] B. Kubis, T.R. Hemmert, U. Meissner, Phys. Lett. B 456 (1999) 240, hep-ph/9903285.
[11] M. Bae, J.A. McGovern, J. Phys. G 22 (1996) 199, hep-ph/9509366.
[12] K.A. Aniol et al., HAPPEX Collaboration, Phys. Rev. Lett. 82 (1999) 1096, nucl-ex/9810012.
[13] K. Maltman, Phys. Lett. B 462 (1999) 195, hep-ph/9904370.
[14] P. Mergell, U. Meissner, D. Drechsel, Nucl. Phys. A 596 (1996) 367, hep-ph/9506375.
[15] S. Kopecky et al., Phys. Rev. Lett. 74 (1995) 2427.
[16] I. Eschrich, (for the SELEX Collaboration), hep-ex/9811003.
[17] M.I. Adamovich et al. (for the WA89 Collaboration), Eur. Phys. J. C 8 (1999) 59.
[18] N. Cabibbo, E. Marinari, Phys. Rev. Lett. 119B (1982) 387.
[19] B. Efron, SIAM Rev. 21 (1979) 460.
[20] S. Gottlieb, P.B. MacKenzie, H.B. Thacker, D. Weingarten, Nucl. Phys. B 263 (1986) 704.